MARTIN MARIETTA ENERGY SYSTEMS LIBRARIES
3 4456 0060347 0

CENTRAL RESEARCH LIBRARY
DOCUMENT COLLECTION

ORNL-3611
UC-25 – Metals, Ceramics, and Materials
TID-4500 (41st ed.)

STATUS AND PROGRESS REPORT FOR THORIUM FUEL CYCLE DEVELOPMENT FOR PERIOD ENDING DECEMBER 31, 1963

OAK RIDGE NATIONAL LABORATORY
operated by
UNION CARBIDE CORPORATION
for the
U.S. ATOMIC ENERGY COMMISSION

Printed in USA. Price $5.00. Available from the Clearinghouse for Federal Scientific and Technical Information, National Bureau of Standards, U.S. Department of Commerce, Springfield, Virginia

LEGAL NOTICE

This report was prepared as an account of Government sponsored work. Neither the United States, nor the Commission, nor any person acting on behalf of the Commission:

A. Makes any warranty or representation, expressed or implied, with respect to the accuracy, completeness, or usefulness of the information contained in this report, or that the use of any information, apparatus, method, or process disclosed in this report may not infringe privately owned rights; or

B. Assumes any liabilities with respect to the use of, or for damages resulting from the use of any information, apparatus, method, or process disclosed in this report.

As used in the above, "person acting on behalf of the Commission" includes any employee or contractor of the Commission, or employee of such contractor, to the extent that such employee or contractor of the Commission, or employee of such contractor prepares, disseminates, or provides access to, any information pursuant to his employment or contract with the Commission, or his employment with such contractor.

ORNL-3611

CHEMICAL TECHNOLOGY DIVISION
METALS AND CERAMICS DIVISION

STATUS AND PROGRESS REPORT FOR THORIUM FUEL CYCLE DEVELOPMENT FOR PERIOD ENDING DECEMBER 31, 1963

Compiled by
R. G. Wymer and D. A. Douglas, Jr.

Contract No. W-7405-eng-26

JULY 1965

OAK RIDGE NATIONAL LABORATORY
Oak Ridge, Tennessee
operated by
UNION CARBIDE CORPORATION
for the
U. S. ATOMIC ENERGY COMMISSION

MARTIN MARIETTA ENERGY SYSTEMS LIBRARIES

3 4456 0060347 0

The following Technical Personnel have contributed to the work reported here:

Chemical Technology Division

R. E. Brooksbank
J. M. Chandler
S. D. Clinton
O. C. Dean
D. E. Ferguson
P. A. Haas
C. C. Haws
A. R. Irvine
J. L. Kelly
A. T. Kleinsteuber
J. L. Matherne
K. H. McCorkle
F. W. Miles
F. C. Moncrief
R. J. Shannon
W. A. Shannon
J. W. Snider
J. W. Ullmann
R. G. Wymer

Plant and Equipment Division

J. W. Anderson
F. C. Davis

Metals and Ceramics Division

J. A. Burka
D. A. Douglas, Jr.
W. S. Ernst, Jr.
R. B. Fitts
A. L. Lotts
C. S. Morgan
S. A. Rabin
J. D. Sease
A. J. Taylor
J. E. Van Cleve, Jr.

Reactor Chemistry Division

E. L. Compere
J. C. Griess
M. J. Kelly
A. J. Shor

Guest Scientists

M. G. Baillie - Australia
F. W. Davis - Babcock and Wilcox
L. J. Hirth - Auburn University
J. R. May - Australia
T. Koizumi - Japan

CONTENTS

	Page
1. Process Demonstration	1
1.1 Introduction	1
1.2 Solvent Extraction	1
1.3 The Sol-Gel Process	8
1.3.1 Process and Facility	8
1.3.2 Construction and Plant Startup	11
1.3.3 Facility	16
Denitration	16
1.3.4 Sol-Gel Operations	16
1.3.5 Radiation-Measurement Program	20
1.4 Rod Fabrication (Kilorod)	23
1.4.1 Installation of Equipment and Preliminary Evaluation	23
1.4.2 Operating Experience with Standin Oxide	26
1.4.3 Operation with ^{233}U	28
2. Thorium-Uranium Fuel Cycle Development Facility	31
2.1 Building Design	31
2.2 Preparation of Thoria-Base Solids	35
2.2.1 Description of Sol-Gel Process	37
2.2.2 Sol-Gel Process Equipment	39
2.3 Oxide-Fabrication Equipment	41
2.3.1 The Process	43
2.3.2 Equipment	45
Operations in the Contaminated-Fabrication Cell	47
Operations in the Clean-Fabrication Cell	50
3. Process Development and Evaluation	51
3.1 Extensions of the Sol-Gel Process	51

CONTENTS (Continued)

		Page
3.1.1	Particle Sizing	52
3.1.2	Formation of Gelled Microspheres from Oxide and Oxide-Carbon Sols	60
	Laboratory Studies	62
	Engineering Studies	63
3.1.3	Preparation of Thorium and Uranium-Thorium Carbide	79
3.2	Effects of Irradiation on Thorium Oxide Fuels	81
3.2.1	Fuel Tubes, Containing Powdered Fuels, Vibratorily Packed	81
	NRX and MTR	81
	ORR Pressurized-Water Loop	89
	Instrumented ORR Poolside Capsules	93
3.2.2	Sol-Gel-Derived ThO_2-UO_2	96
	Current Irradiation Program	102
3.2.3	Fuel Rods Containing Pelleted Oxide Fuel	102
3.2.4	Thorium-Base Alloy Fuel	109
3.3	Development of Vibratory-Compaction Method	112
3.3.1	Results of Experiments	113
3.3.2	Method Adopted	117
3.4	Permeability of Vibratorily Compacted Fuels: Waterlogging	117
3.4.1	Results of Experiments	118
3.4.2	Conclusions	124
3.5	Pellet Fabrication	124
3.6	Thorium Metal Fuels	125
4.	Basic Studies	129
4.1	Preparation of Thorium Carbide and Uranium-Thorium Carbide by the Sol-Gel Process	129
4.1.1	First Step: Preparation of Thoria and Thoria-Urania-Carbon Sols	129

CONTENTS (Continued)

		Page
	Properties of Carbons Used for Preparing Sols	129
	Interaction Between Surfaces of Colloidal Thoria and Carbon	131
	Stability of Thoria-Carbon and Thorium-Uranium Oxide-Carbon Sols	133
4.1.2	Second Step: Preparation of Gel Microspheres from Thoria-Carbon and Thorium-Uranium Oxide-Carbon Sols	137
	Optimization of Extractant	139
	Selection of Surfactants	140
4.1.3	Materials and Experimental Equipment	141
4.1.4	Properties of the Carbide Products	147
4.2	Rates and Mechanisms of Fission-Gas Release from Thoria-Urania Fuels	152
4.3	Volatilization of Protactinium from Irradiated Thoria Fuels: Use of Chloride Melts	153
4.3.1	Materials and Experimental Equipment	154
4.3.2	Experimental Observations	155
	$AlCl_3$-$ZrCl_4$ Systems	156
	$ThCl_4$-$ZrCl_4$	157
Appendix		158

1. PROCESS DEMONSTRATION

1.1 Introduction

A successful demonstration of the Thorium Fuel Cycle process during the past year consisted of an intermediate-scale demonstration of the remote fabrication of ThO_2-$^{233}UO_2$ fuel elements by the ORNL sol-gel vibratory-compaction procedure. This demonstration, dubbed the Kilorod Program, is being conducted during the fulfillment of the request to ORNL to prepare 1000 fuel rods containing 3 wt % $^{233}UO_2$–97 wt % ThO_2 for zero-power criticality experiments at Brookhaven National Laboratory. The design capacity of the Kilorod Facility is 10 kg of calcined oxide per day.

The program is about 75% complete: 720 specification-grade fuel elements have been made, and this section of the report presents the significant results obtained during the demonstration.

The procedure consists in (1) solvent extraction purification of the ^{233}U to remove ^{232}U daughters; (2) production of easily dispersible thoria by hydrothermal denitration of thorium nitrate; (3) preparation of the mixed thoria-urania oxides by the sol-gel process; (4) sizing the mixed oxides and loading the sized oxide into tubes by vibratory compaction; (5) remotely welding the end closure of the tube, cleaning the finished rods, and inspecting and testing them for homogeneity and integrity.

1.2 Solvent Extraction

The ^{233}U for the Kilorod Program was produced under reactor conditions such that its ^{232}U content is 38 ppm. It is this impurity, with its resultant decay products and associated gamma activity, which necessitates the purification by solvent extraction. The efficiency of the purification influences the cost of subsequent refabrication of the ^{233}U.

The uranium to be purified consists of chunks of metal and of uranyl nitrate solutions of varying concentrations. Dissolution of the metal is accomplished with boiling 1.4 M $Th(NO_3)_4$--4 M HNO_3 solution (Fig. 1). Four kilograms of ^{233}U metal is charged to the batch dissolver vessel during one dissolution cycle. Criticality control in the dissolver is assured by the presence of thorium, which will give a $^{233}U/Th$ ratio of 0.025, and by maintaining the volume in the dissolver vessel such that the eversafe concentration of ^{233}U in light water may never be exceeded. The solution from the dissolver is adjusted to meet feed conditions by dilution with water. The procedure employed when uranyl nitrate solution is used as feed consists in blending this solution in small increments with a thorium nitrate solution whose concentration is 400 g/liter.

The solvent extraction equipment selected for the uranium purification program (Fig. 2) uses two pulsed columns in series. Feed from the feed-adjustment tank is pumped into the middle of the extraction column, which is a 38-ft by 5-in.-diam pulsed column. The extractant is a 2.5 vol % solution of di-sec-butyl phenylphosphonate (DSBPP) in diethylbenzene. The pregnant organic extractant is scrubbed in the upper section of the column with an 0.8 M solution of aluminum nitrate, which is 0.4 N acid deficient in order to remove thorium and ionic contamination. The scrubbed organic is then routed to the second pulsed column, which is a strip column wherein the uranium is removed from the organic phase with demineralized water. The uranium product solution, containing 10 g of ^{233}U per liter, is then transferred through a static diluent wash column for the removal of trace quantities of organic extractant prior to boildown of the solution. Final concentration to 100 g/liter is accomplished in a critically safe evaporator. The product is withdrawn from the evaporator-product storage tank as required for fabrication of elements. Spent solvent leaving the process is collected batchwise, treated with 0.2 M Na_2CO_3, and reused.

The majority of the vessels used for chemical processing are not of critically safe configuration; consequently, several important operational and equipment modifications have been made. The total mass of uranium within the facility does not

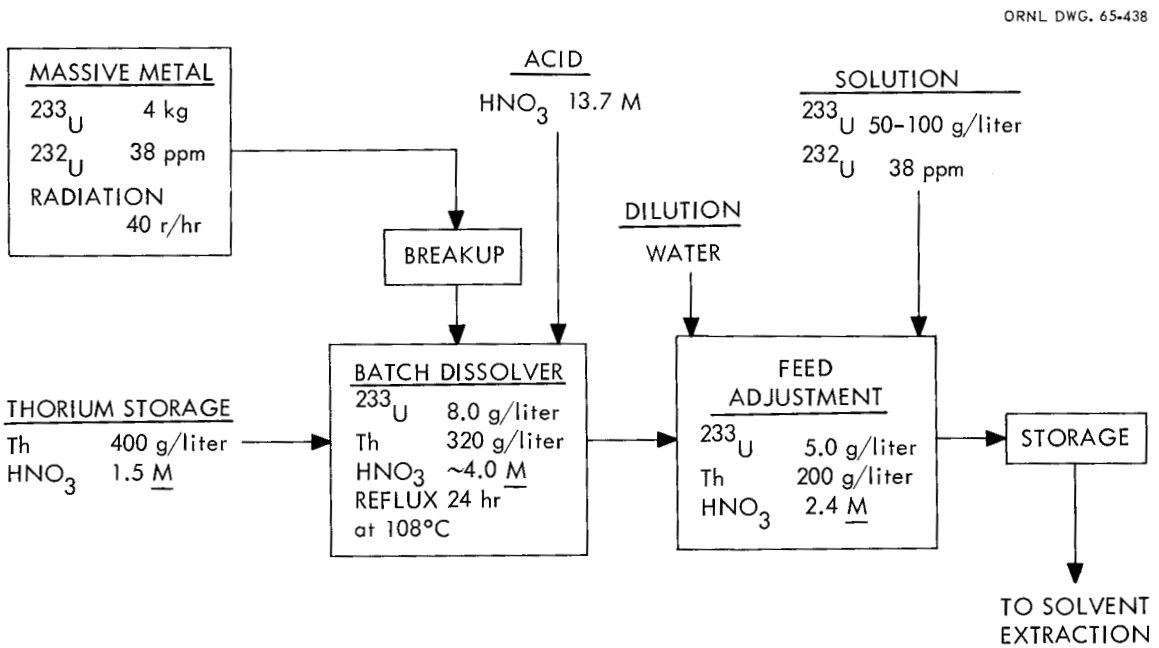

Fig. 1. Flowsheet for Preparation of Feed Solution for the Kilorod Program. This feed solution mixture of ^{233}U and thorium nitrates is then purified by solvent extraction (see Fig. 2).

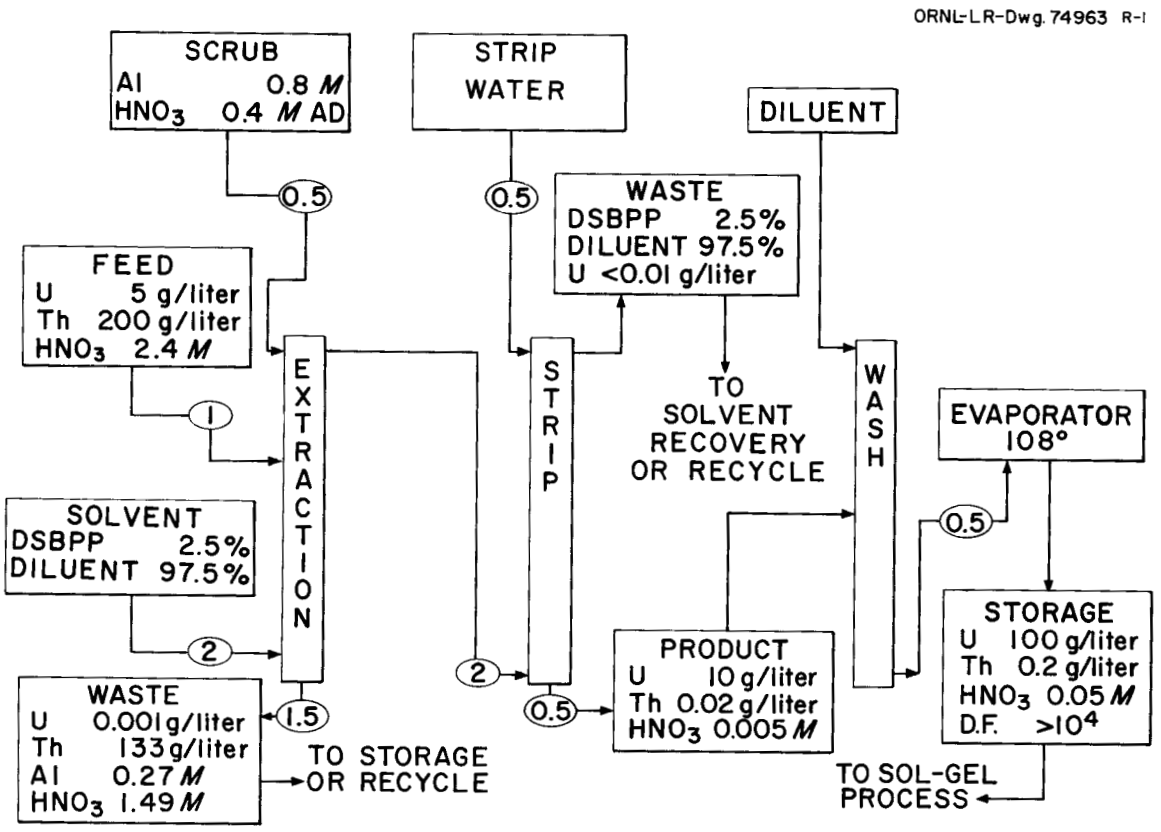

Fig. 2. Flowsheet for Purification of ^{233}U for Kilorod Program. The removal of the daughter products of ^{232}U is the main objective.

exceed 8 ± 0.5 kg. Solution concentrations are maintained below the recommended safe maximum value of 10 g of ^{233}U per liter by flowrate adjustments for aqueous streams and by chemical saturation of organic streams. The only stream that exceeds this value is the product stream (100 g/liter), which is obtained by boildown in a critically safe evaporator consisting of a 5-in.-diam pipe surrounded by a 6-in.-diam steam jacket.

In addition to mass and concentration control, the feed extraction column and raffinate catch tanks contain sufficient thorium to yield a $^{233}U/Th$ ratio of 0.025, which provides adequate poisoning to prevent criticality. The thorium also serves as a salting agent for the extraction process.

As an additional safety measure, Pyrex-glass rings containing 4% boron have been placed in strategic process vessels. Potential nuclear hazards exist in the expanded 8- to 16-in. sections of the disengaging sections of the pulsed columns, and in large-diameter vessels. These sections and vessels were packed with boron-containing rings, and an x-ray procedure was developed to ascertain periodically their location and condition.

To date, about 43 kg of ^{233}U has been purified. Thirty kilograms was for the Kilorod Project, and 13 for other AEC-sponsored projects. A summary of the product quality obtained by this method of purification is presented in Table 1, together with the feed specifications imposed by the Kilorod Program. The product met specifications in all instances. Of particular significance are the results on the measurable ionic impurities in the uranium product; there has been a steady decrease in the total impurities. In each instance, the major impurities have been sodium, calcium, magnesium, and lithium. Analyses of the demineralized water used as strip solution indicates that more than 90% of these impurities originates in the water.

The gross-gamma decontamination factor presented in Table 1 is that obtained from the gamma activity of the concentrated product. Figure 3 shows, for five runs, the change in gamma activity (expressed as counts per min per mg of

Table 1. Kilorod Program: Summary of Solvent Extraction Results

Run No.	^{233}U Recovered (g)	Decontamination Factor		NO_3^-/U Ratio	Measurable Ionic Impurities (ppm in terms of ^{233}U)		
		Gross γ	Thorium		Al	Na, Ca, Mg, Li	Total
HJ-1	4622	230	3×10^3	2.42	2490	2201.86	4744
HJ-2	4527	380	5×10^3	2.25	52	<360.22	193
HJ-3	3784	416	3×10^3	2.16	37	220.10	271
HJ-4	5034	194	3×10^3	2.14	12	227.68	269
DC-1	4358	185	2×10^3	2.12	28	296.46	310
DC-2	7793	310	5.5×10^3	2.12	23	165.05	207
DC-3	7918	258	5.5×10^3	2.12	16	75.59	113
DC-4	5030	300	3.1×10	2.20	26	112.88	172
SPEC.	4-8 kg	$\gtrsim 100$	$\gtrsim 1 \times 10^3$	2.50	<30	-	-

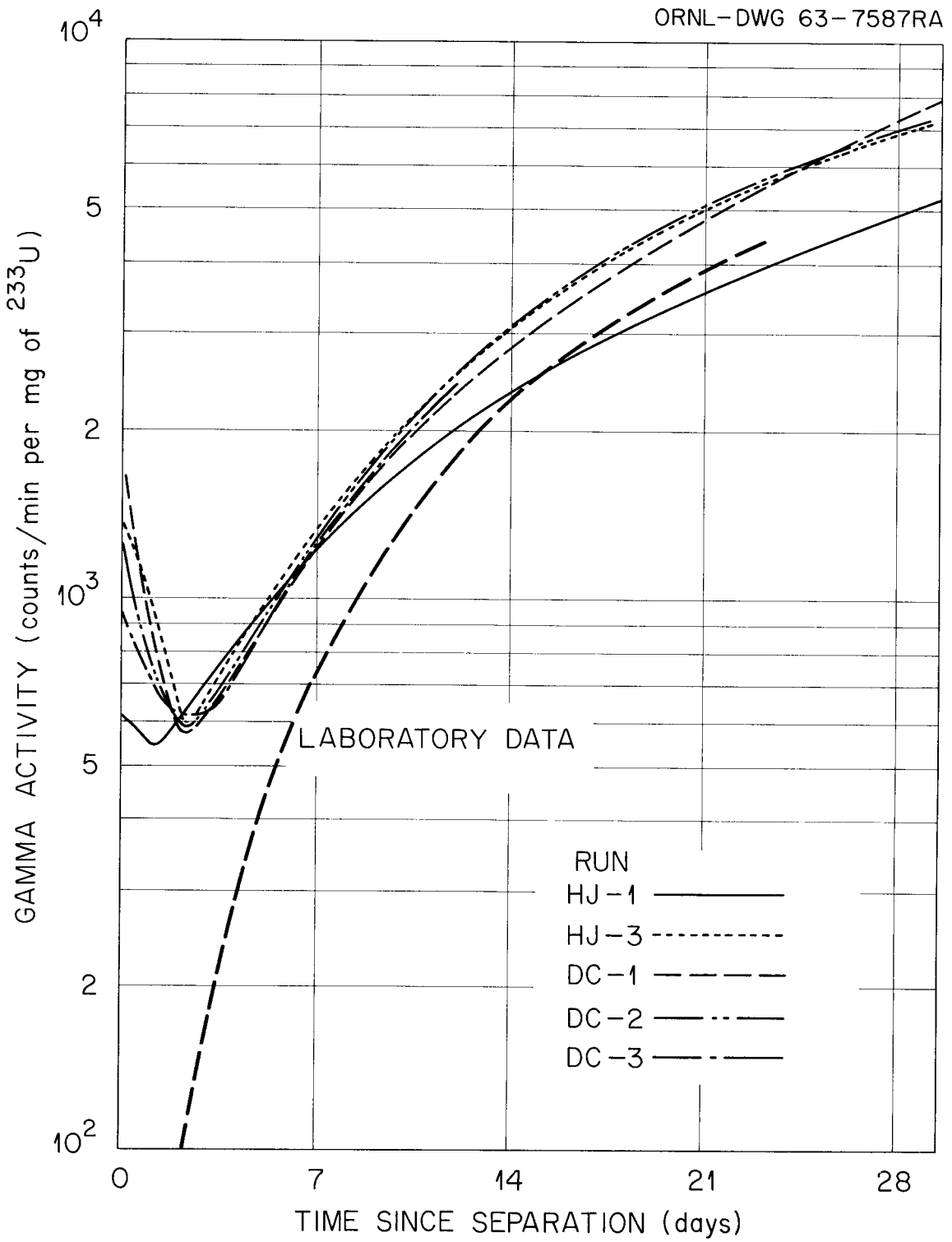

Fig. 3. Growth of Gamma Activity in Purified ^{233}U.

^{233}U) with time after purification. The initial drop in activity is due to the decay of the short-lived daughters, which were not completely removed. After this initial decay, the activity increases as the long-lived daughters grow in. Also presented for comparison is a curve derived from data obtained by R. H. Rainey, ORNL, in laboratory studies of solvent extraction. Rainey's data indicate more complete removal of the short-lived daughters than was achieved in the Kilorod work. However, after a few days, the gamma activities are comparable.

In summary, the solvent extraction process being used to purify ^{233}U has been very successful, producing material that meets all specifications imposed by the sol-gel process, discussed next.

1.3 The Sol-Gel Process

1.3.1 Process and Facility

Four operations make up the sol-gel process. These are: denitration, blending, drying (gelation), and calcination-reduction (Fig. 4). In the Kilorod Program, each of these steps is performed as a batch operation. The blending, drying, and calcination are highly radioactive (alpha) operations, so the equipment used in these steps is housed in a sealed carbon-steel cubicle about 9 ft long, 7 ft wide, and 7 ft high, having eight windows, ten glove ports, and three transfer ports. This cubicle is located on the third floor of the facility (Fig. 5). Biological shielding is provided on the sides by 8 in. of barytes concrete or 4-1/2 in. of steel, and on the floor by a 4-1/2-in.-thick steel slab. The top and back of the sol-gel cubicle abuts a 4-ft-thick concrete slab. Means are provided in the cubicle to permit the maintenance of vulnerable mechanical parts without entering the operating cubicle.

The denitration operation is carried out in a rotary-drum denitrator as an unshielded operation, located at another site at the Laboratory. The equipment was constructed during the pre-Kilorod development effort but was built large in anticipation of requirements of the program.

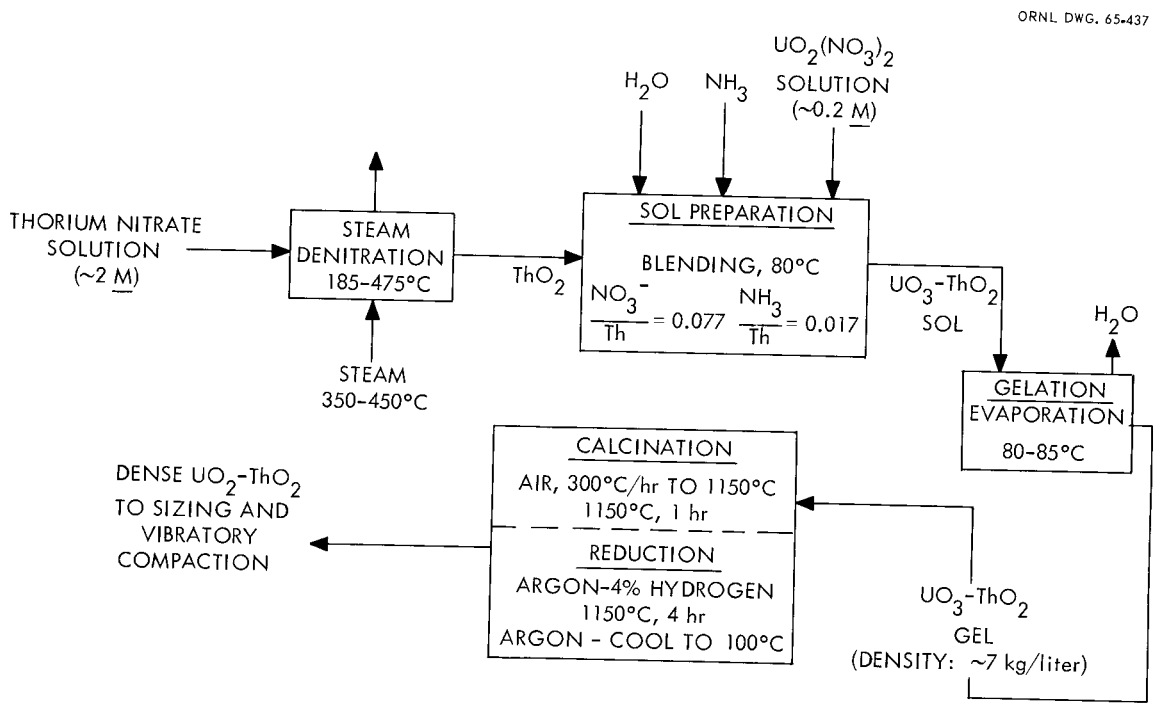

Fig. 4. Flowsheet for the Sol-Gel Process.

ORNL-LR-DWG. 76196

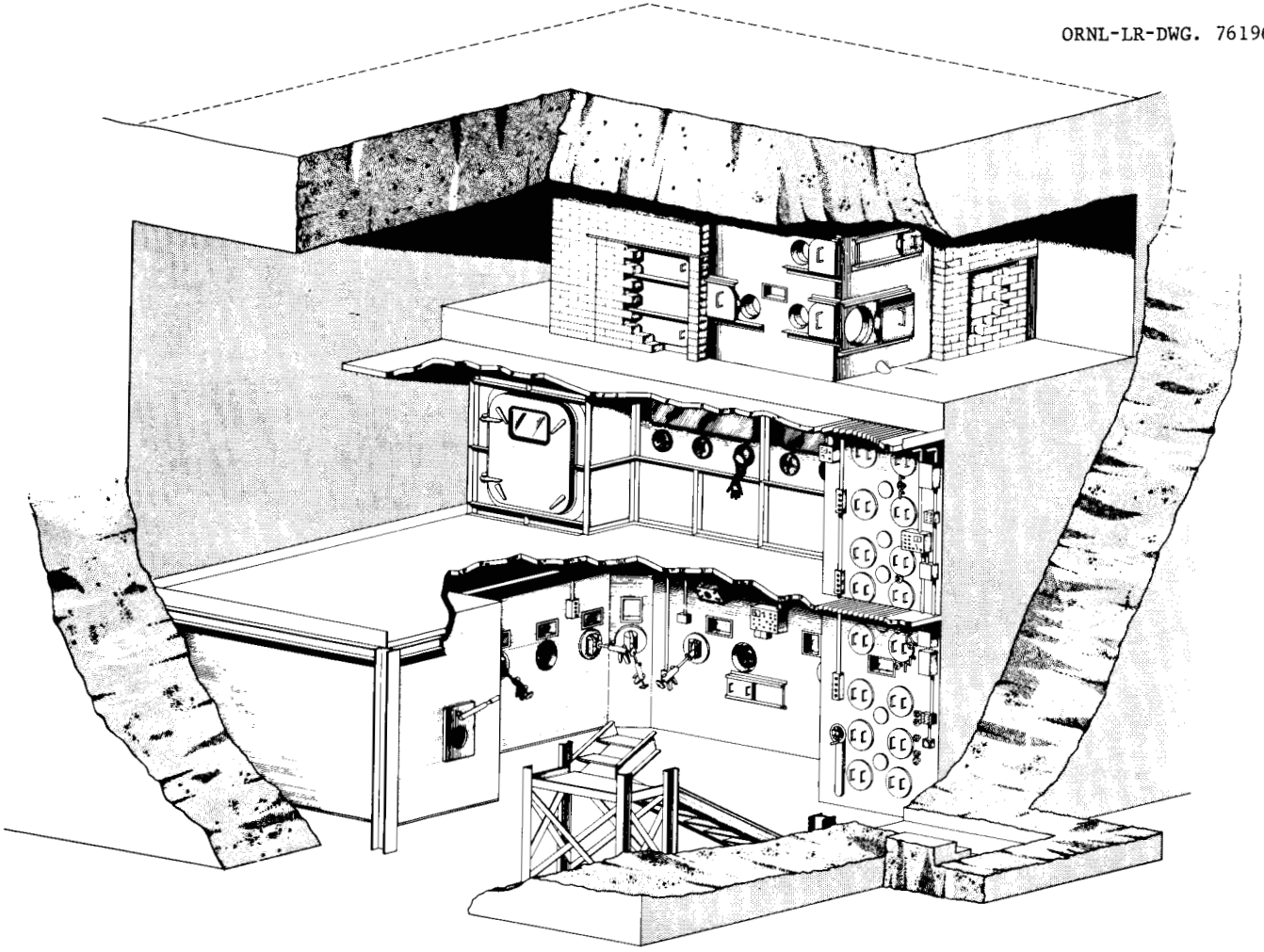

Fig. 5. Solids-Preparation and Rod-Fabrication Facility. The flow of material is from the top where the sol is blended and the gel formed to the bottom where the finished rods are tested and loaded into shipping casks.

The sol-gel equipment operates at the design rate of 10 kg of calcined oxide per day, as follows: Thirty-kilogram batches of thorium nitrate tetrahydrate crystals are charged to the rotary drum denitrator and denitrated under a superheated steam atmosphere (Fig. 6). The 13.5-kg batch of denitrator product (ThO_2) is used in the sol-gel process. To smooth out possible batch-to-batch variations in the denitrated product, 70 kg of the product is charged to a powder blender. After blending, the thoria powder is carefully weighed into 10-kg portions for charging to the blending operation in the sol-gel facility. In the criticality proof (slab geometry) blend tank, the thoria is blended with a precisely measured quantity of ^{233}U, introduced as a uranyl nitrate solution (Fig. 7). At the completion of the blending step, the batch is pumped to a tray dryer (Fig. 8). The sol is dried to a gel in about 30 hr and is then transferred from the trays to Alundum crucibles. The crucibles are placed in the calciner, and the temperature raised to 1150°C under an air purge (Fig. 9). When 1150°C is reached, a 96% Ar--4% H_2 atmosphere is maintained in the furnace for 4 hr. The calciner is then turned off and allowed to cool to 350°C. An argon atmosphere is maintained during the cooling portion of the cycle. The product is removed and placed under argon until cool (less than 100°C). The batch is then weighed and transferred to the rod fabricators.

1.3.2 Construction and Plant Startup

The denitration reactor was placed in operation in January 1963 without difficulty.

Construction of the sol-gel unit of the Kilorod Facility was completed, and testing of individual equipment pieces started March 1. Equipment shakedown and cold testing of individual operations was completed May 3. A sustained five-day operating demonstration was then conducted. Depleted uranium was used as a standin for ^{233}U. This demonstration showed that the plant was operable as an integrated unit, that the design production rate could be maintained, and that the product quality standards could be met.

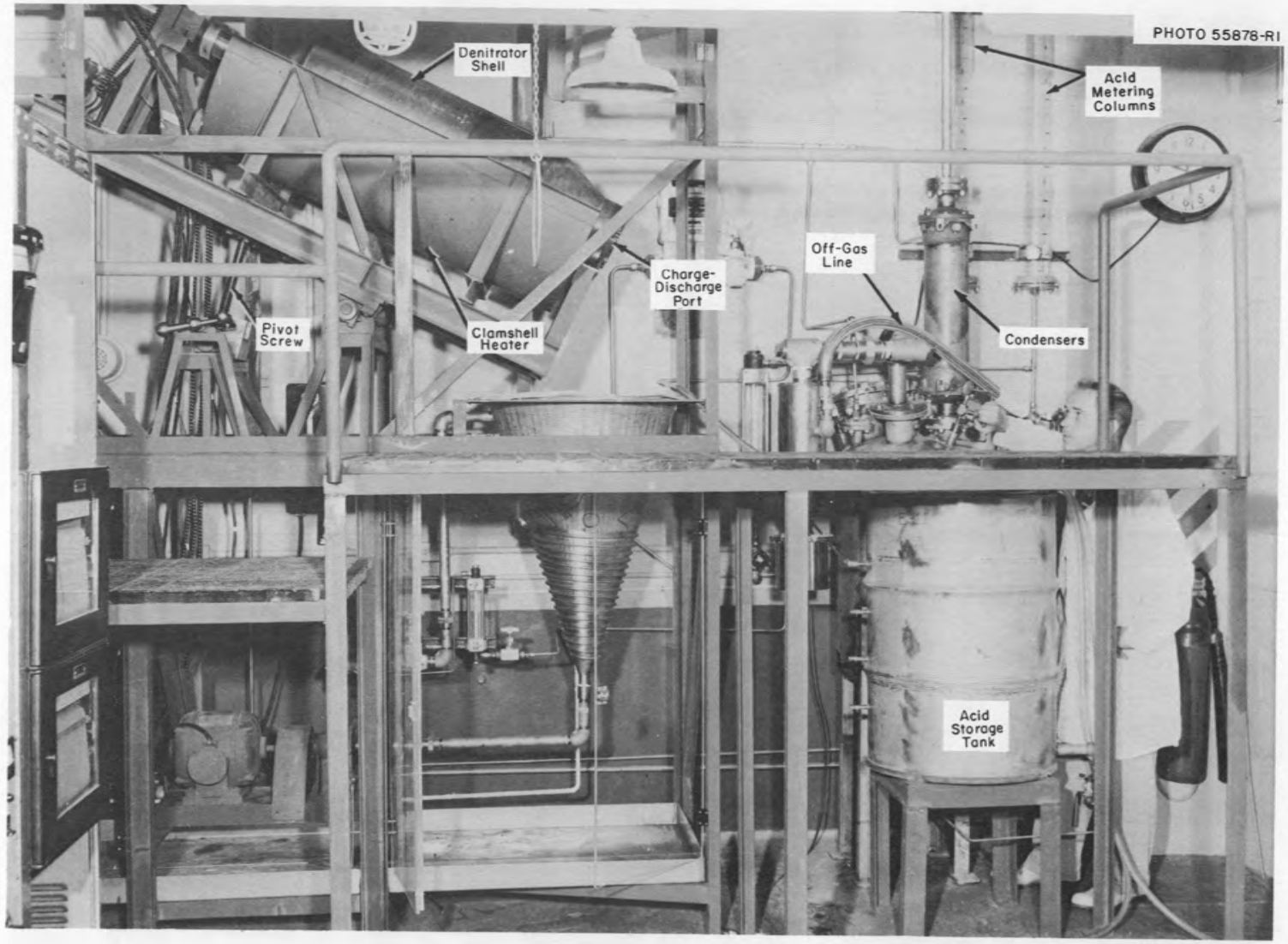

Fig. 6. Rotary Denitrator in the Unloading Position.

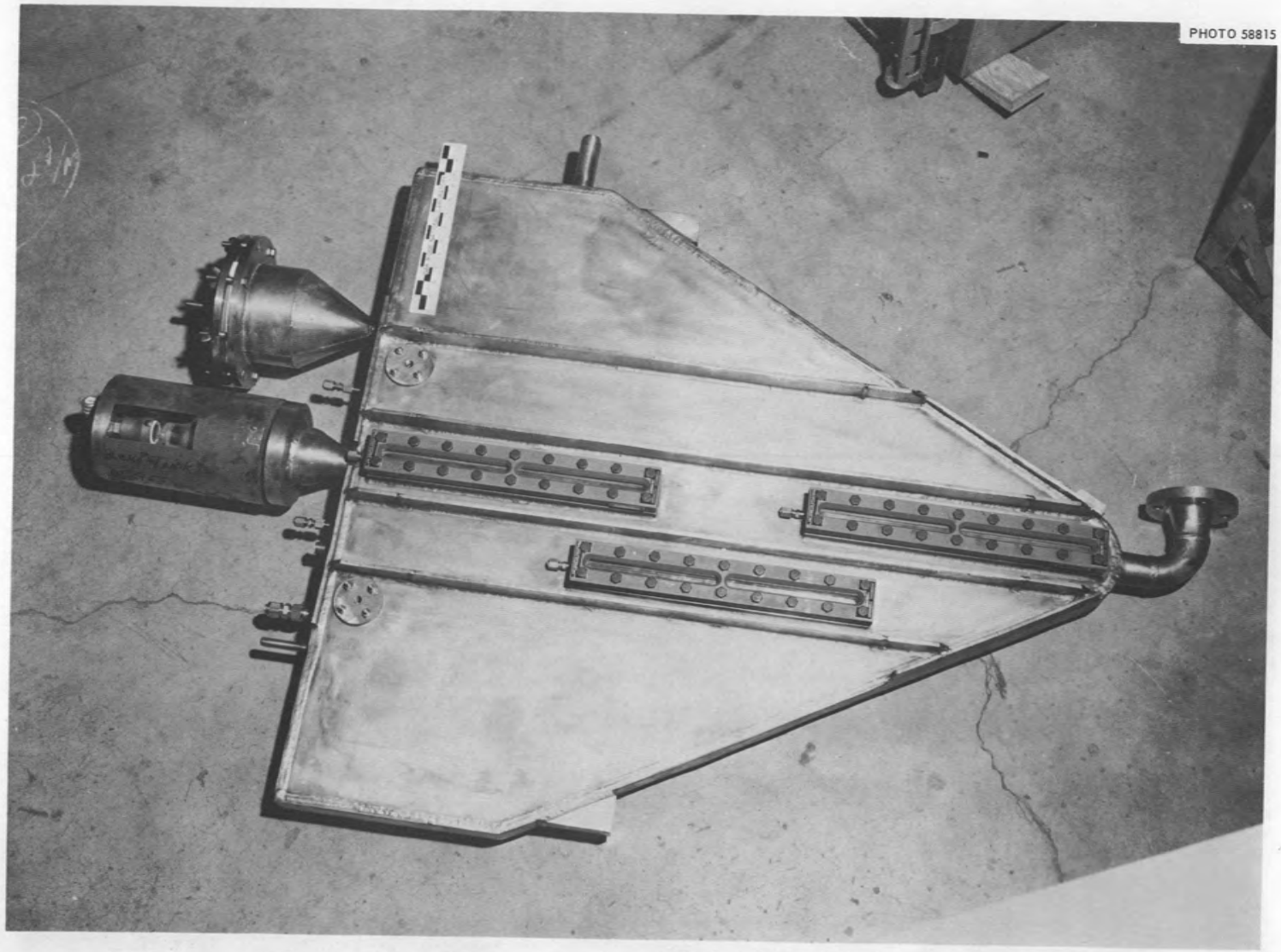

Fig. 7. Critically Safe Slab Blend Tank for Preparing Sol.

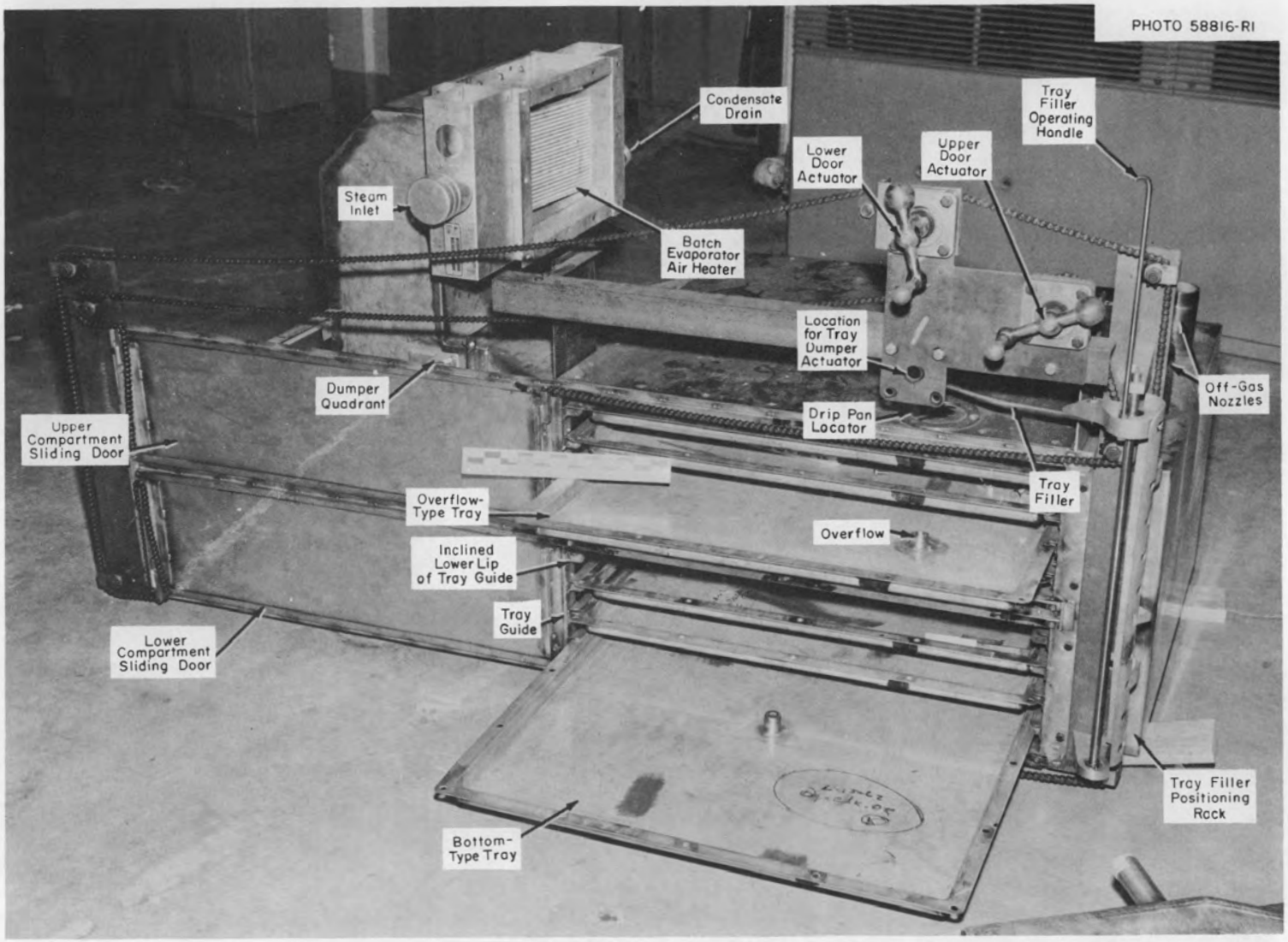

Fig. 8. Tray Dryer for Converting Sol to Gel.

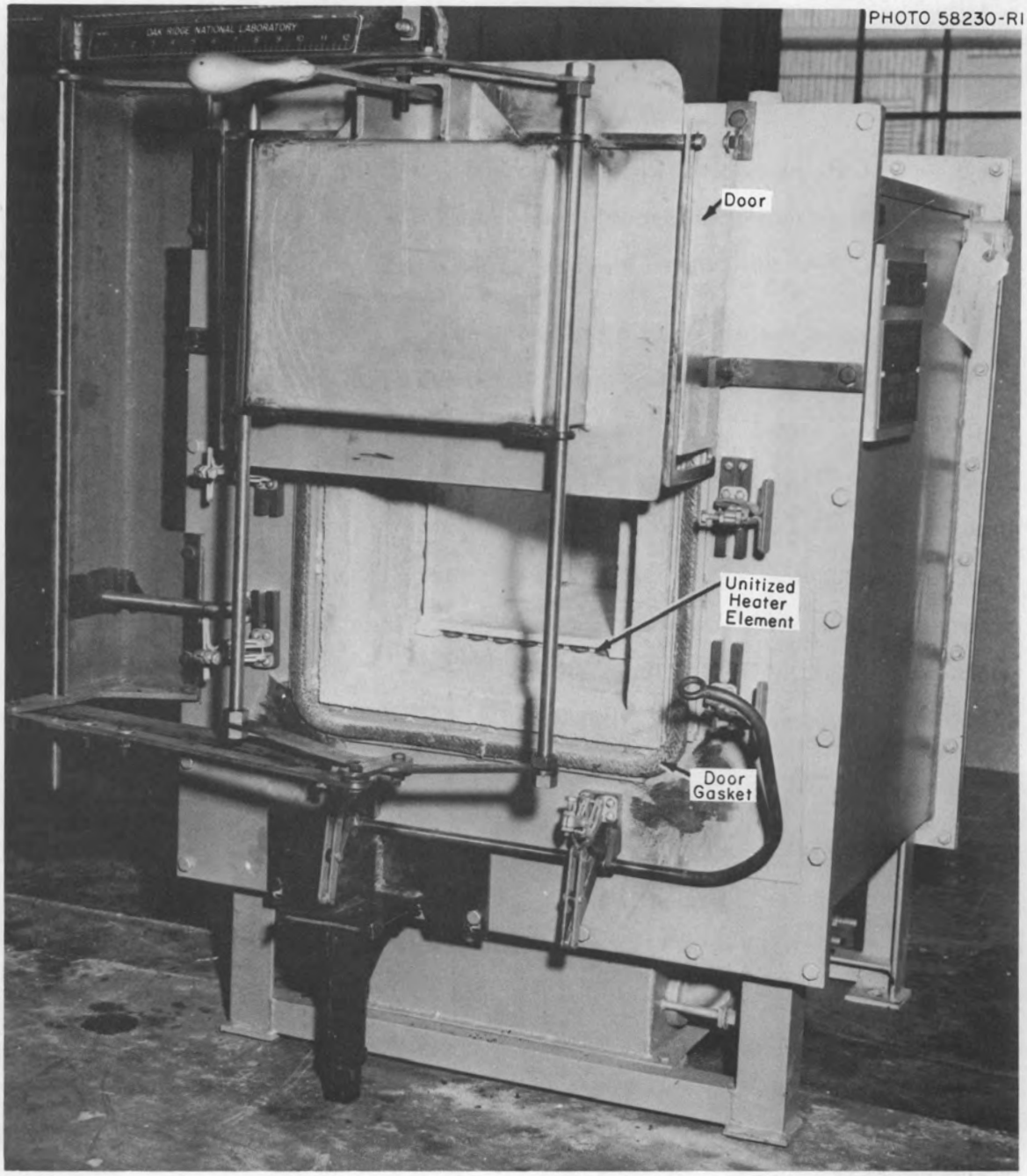

Fig. 9. Controlled Atmosphere Furnace for Converting Gel to Calcined and Reduced ThO_2-UO_2.

Following cold testing, the plant was cleaned thoroughly, and final equipment adjustments made. The facility was ready for hot operation on June 5, 1963.

1.3.3 Facility Operation

Denitration. — The denitrator was operated through November 10, 1963, without a significant mechanical failure. On this date, a failure of the steam supply caused the steam superheater to burn out. More than enough ThO_2 had been accumulated to complete the Kilorod Program, so operation was discontinued.

During this operating period, 99 batches of ThO_2 were processed. Five batches were rejected, two as a result of the superheater failure, and the other three as a result of operator error. The 94 acceptable batches amounted to a total of 1272 kg. An additional 111 kg was prepared for development use. Test dispersions and analytical results showed all this material to be satisfactory for feed. Process control was excellent throughout the period, and no batch rejections were made for lack of proper process control. Denitrator product was uniform, as shown by the percentage thorium values in the ThO_2 (Table 2). The range in N/Th atom ratio (from 0.02 to 0.06) was also expected from earlier work.

1.3.4 Sol-Gel Operations

Seventy-six sol-gel batches were prepared and calcined. Only one batch (No. 10) did not meet all specifications. It was used, however, with BNL permission; thus, all the sol-gel product was accepted for rod fabrication. The total calcined product transferred to the rod-loading operation was 753.5 kg (Table 3). The total ^{233}U used in the process was 20.1 kg, while the total thorium (expressed as metal) used was 650 kg. These quantities of solids were processed in five operating campaigns. Appendix A is a summary of operating and control data for these campaigns.

The control of the $^{233}U/(^{233}U + Th)$ ratio was poor for campaign 1 but excellent for campaigns 2 through 5. The poor operating control for campaign 1 was the result of an inadequate storage facility for the uranyl nitrate feed solution; an

Table 2. Product Quality Control Data for Denitrator Operation

Identification of Materials	ThO_2 Prepared (kg)		% Th	% NO_3^-	N/Th Atom Ratio
1-12[a]	162.380		86.0	0.90	0.037
		Ranges:	85.3-86.4	0.5-1.3	0.02-0.06
BB-1[b]	67.985		86.0	0.73	0.030
BB-2	67.270		86.2	0.66	0.030
BB-3	68.450		86.1	0.73	0.030
BB-4	68.110		85.9	0.80	0.034
BB-5	71.085		85.0	0.88	0.037
BB-6	70.197		85.9	0.89	0.037
BB-7	71.895		85.3	0.89	0.037
BB-8	71.415		84.8	0.80	0.034
BB-9	70.343		85.9	1.00	0.045
BB-10	82.350		85.3	0.93	0.041
BB-11	70.003		84.6	0.84	0.037
BB-12	69.850		86.0	1.06	0.045
BB-13	68.340		85.4	0.93	0.041
BB-14	68.530		85.9	0.84	0.037
BB-15	68.800		85.9	0.80	0.034
BB-16	68.400		85.6	0.80	0.034
BB-17	68.250		86.0	0.58	0.026
		Averages	85.6	0.83	0.036

[a]This represents the first 12 denitrator batches, which were analyzed individually to amass process control data on the denitrator.

[b]The BB designation represents a batch obtained by mixing five rotary denitrator batches in the batch blender.

Table 3. Quantities of ^{233}U and Thorium Charged, and Product Removed from the Sol-Gel Process

Campaign No.	^{233}U Input (kg)	Th Input (kg)	$^{233}U + Th$ Input (kg)	$^{233}U/^{233}U + Th$ X100	$UO_2 + ThO_2$ Output (kg)
1	3.196	104.693	107.889	2.969	118.562
2	4.255	137.162	141.417	3.009	160.940
3	3.166	102.468	105.634	2.997	118.468
4	3.450	110.724	114.174	3.022	128.740
5	6.056	195.530	201.586	3.004	226.845
Totals	20.123	650.577	670.700		753.555

Table 4. Gases Released[a] by Solid Products

	Gas	Calcined Product[b] Average	Calcined Product[b] Range	Crushed Oxide[c] Average	Crushed Oxide[c] Range
Quantity of gases released, std cc/g		0.022	0.004-0.06	0.11	0.05-0.28
Analysis of gases released, vol %					
	H_2	7.6	0.7-16	21	4-33
	CH_4	1.5	0.7-2	0.5	0.3-1
	H_2O	7.8	0.4-25	2.7	0.1-18
	N_2 or CO	36.9	7-71	39	7-59
	O_2	12.7	0.3-56	0.6	0.1-3
	A	0.4	0.2-0.7	0.1	0.1-0.2
	CO_2	41.8	15-73	40	6-83

[a]Obtained by heating to 1200°C under vacuum.

[b]Results represent first 28 calciner batches.

[c]Results represent first 150 rods.

air purge through the storage vessel steadily concentrated the stored solution. The vessel was also wide and was packed with borated-glass Raschig rings, which made agitation and sampling difficult. The problem was solved by installing a geometrically safe feed tank before the startup of campaign 2.

In examining the run-by-run ratios (Table 3) for the last four campaigns, it should be noted that the target value was 3.00 ± .05 wt % ^{233}U for each batch, as well as for the overall campaign ratio. Thus, if a batch was made outside these limits early in a campaign, a matching high- (or low-) ratio batch was made later for pairing with the given batch.

Paired batches were mixed after calcining but before transferring to the rod-fabrication facility. In this way, the ratio for all material entering that facility was held to within the desired 3.00 ± .05 wt % specification. Only the first batch of any pair should be considered to have fallen outside the more rigorous limits. Also, it should be noted that the given campaign ratios are calculated from precisely measured quantities of materials entering the process, and not from analyses of individual batches.

The gas released by the calciner product was not expected to exceed 0.05 std cc/g. Of the first 76 calciner batches, three exceeded this value. These exceptions were 0.056 std cc/g for batch 62, and 0.057 std cc/g for batches 59 and 71. The average value for all calcined products was 0.02 std cc/g (Table 4).

The gas-release values for the powder put into the fuel rods were not expected to exceed 0.3 std cc/g, and, through the first 15 samples, there were no exceptions.

The composition of the gases released was also as expected. Hydrogen, the gas of greatest interest, was not expected to exceed 50 vol %. The highest value of the early runs was 33%.

Mechanical reliability of the equipment has been excellent. Plant on-stream time has exceeded 90%, and operation has been free of minor equipment failures. The only breakdowns experienced were the failures of two calciner heating elements;

each failure required cubicle entry. The first heating element burned out after 54 cycles, including "cold" startup operations. The second heating element was apparently improperly made, since it failed by fracture during the fourth heating cycle. The third heating element was installed and continued to perform satisfactorily after 34 cycles. The average number of service cycles demonstrated by the calciner heating elements to date is at least 25, compared with an expected 20 indicated by pre-Kilorod experience.

In the design of the sol-gel unit, a throughput of 10 kg per day was recognized and accepted as both the normal and the maximum capacity of the plant. This limitation was the result of an unalterable 24-hr cycle for the calciner, imposed by the necessity for returning the calciner to 350°C before removing the charge. The 10-kg-per-day design throughput for the unit has been demonstrated repeatedly over periods of sustained operation, and expectations for capacity have been met.

1.3.5 Radiation-Measurement Program

Radiation exposures of workers have been consistently well below permissible levels, and the accumulation of radioactivity in the equipment has also been low (Table 5). Individual hand and forearm exposures average about 100 millirems per man-week, contrasted to the 1500-millirem permissible value. The highest rate recorded in surveying any equipment to date is 50 mr/hr, found inside the calcining chamber. During one entry for calciner repairs, a complete radiation survey was made with a cutie pie. The maximum radioactivity level in contact with the outside of any piece of equipment was 35 mr/hr. This level was found at the bottom of the tray dumper. Cell entries for furnace repairs resulted in whole-body doses $\leq$ 15 millirems over two 4-hr periods.

Radiation levels of process materials were monitored, and the highest levels obtained are shown in Table 6. Detailed data, in addition, have been fitted to the calculated buildup curve, as shown in Fig. 10.

Table 5. Worker Radiation Exposures and Accumulated Radioactivity in Process Equipment

Operation	Max. Accumulated Weekly Exposure[a] (millirems)	Present Background[c]
Blending	7	6(*)
Dryer	7	7(*)
Calciner	15	50(**)
Total exposure to individual	< 200[b]	

[a]Exposure taken by a finger ring that is used only at the given work station.

[b]This reading taken from finger ring that accumulates dose for all duties.

[c]Readings taken with G-M survey meter (*) and ion chamber (**). About a third of the program had been completed and all equipment pieces had been given normal cleaning.

Table 6. Radiation Levels of Process Materials

Material	Max. Readings Taken (millirems/hr)	Days Since Extraction
Crucible of dried gel (5 kg)[a]	< 200	50
Crucible of fired shards (5 kg)[a]	< 200	50
Finished rods[b]	77	78
	96	98
	118	121
	146	189
	160	226

[a]G-M survey meter used. Probe held in contact with and across top of crucible.

[b]G-M survey meter used. Probe held in contact with rod and with axis of rod and probe parallel.

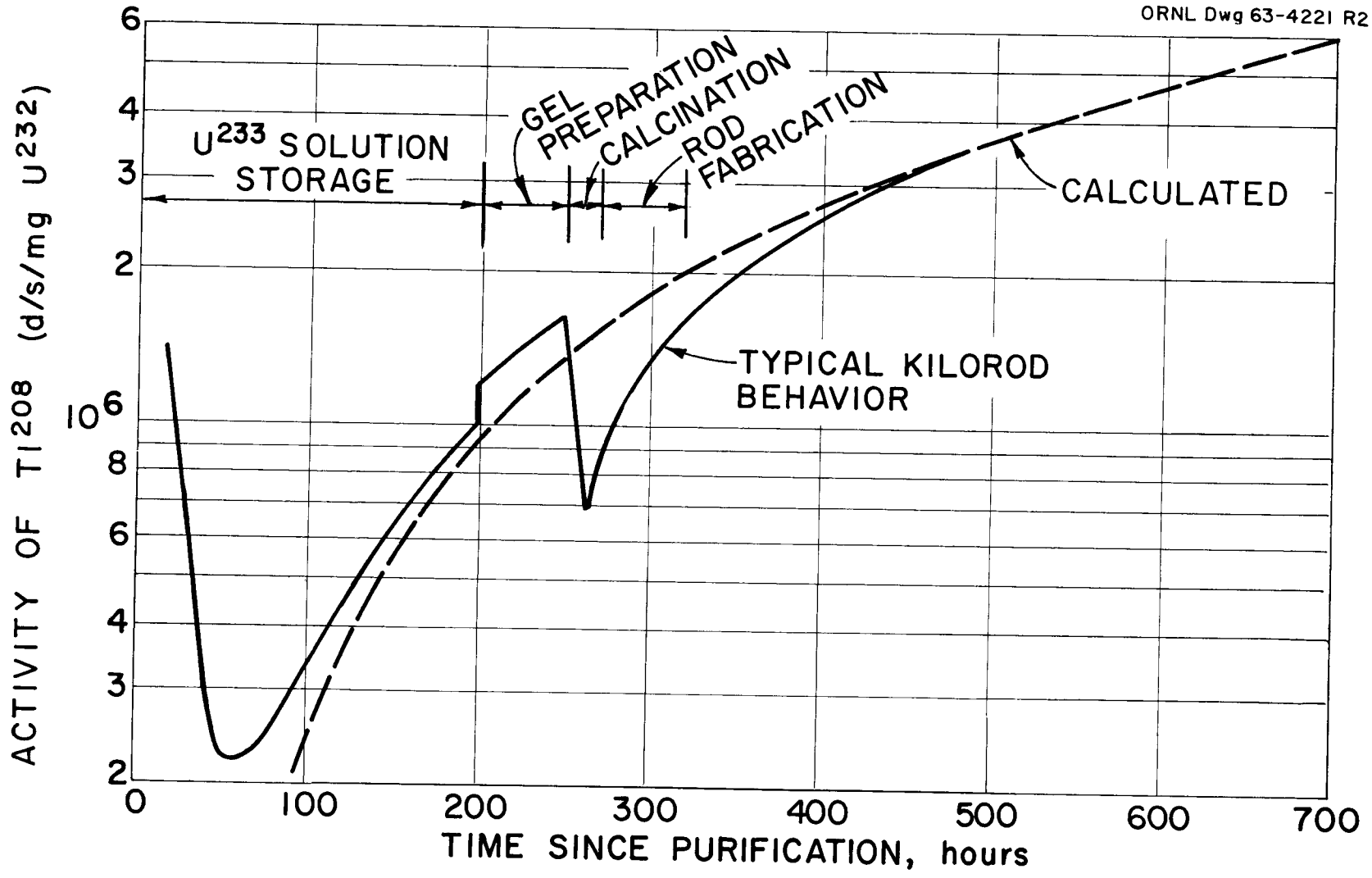

Fig. 10. ^{208}Tl Radioactivity as a Function of Time Since Purification.

1.4 Rod Fabrication (Kilorod)

During the past year, the rod-fabrication part of the Kilorod Facility was completed and operated extensively. At the last reporting,[1] the structural portion of the Kilorod Facility had been completed, but the fabrication equipment had not been installed. The primary purpose of the facility has been to demonstrate remote fabrication technology; thus far, the demonstration has been concerned with Brookhaven National Laboratory's (BNL) fuel rod (Fig. 11). These fuel rods have been made by a combination of procedures,including oxide-powder comminution, vibratory compaction, end-cap welding, decontamination, and inspection. The complete process, as presently operated, is shown in the flowsheet in Fig. 12. In addition to placing the facility and equipment into operation, 720 BNL fuel rods were fabricated.

The salient areas of development and the status of the rod-fabrication program in the Kilorod Facility are given in the discussion which follows. More detailed information may be obtained in several publications.[2,3,4]

1.4.1 Installation of Equipment and Preliminary Evaluation

After installation of the rod-fabrication equipment, cell-containment checks were made before introducing the stand-in oxides (Th—3 wt % $^{238}U)O_2$ into the system. The containment was evaluated with all glove, bagout ports, and service entries in the operating condition. After some minor alterations, an air-inleakage rate of 0.004 cell volumes per min at 1 in. of water pressure difference was measured.

Attention was also given to the noise level associated with the pneumatic vibrator that packs the fuel. Since the noise level in the operating area near the vibrator was slightly above the permissible value (maximum of 90 db, compared with a permissible 86), ear protectors were obtained for the operators.

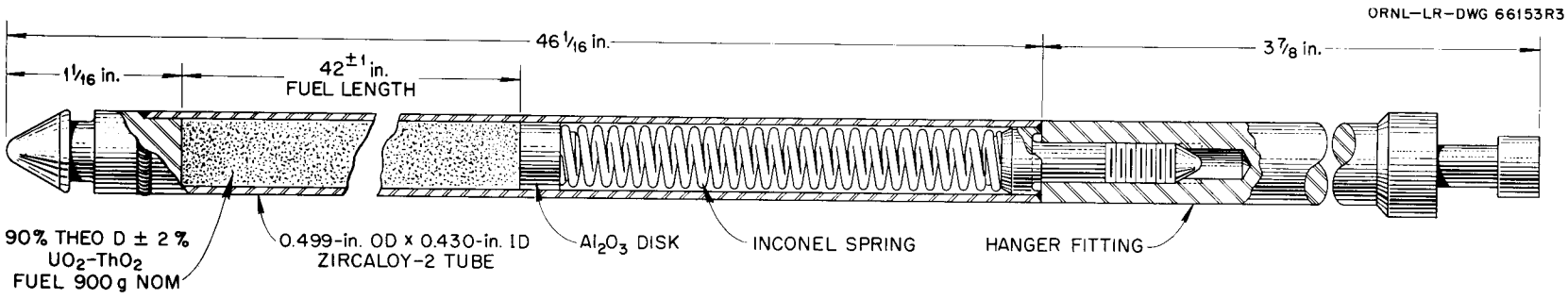

Fig. 11. Design Features of the BNL Fuel Rod.

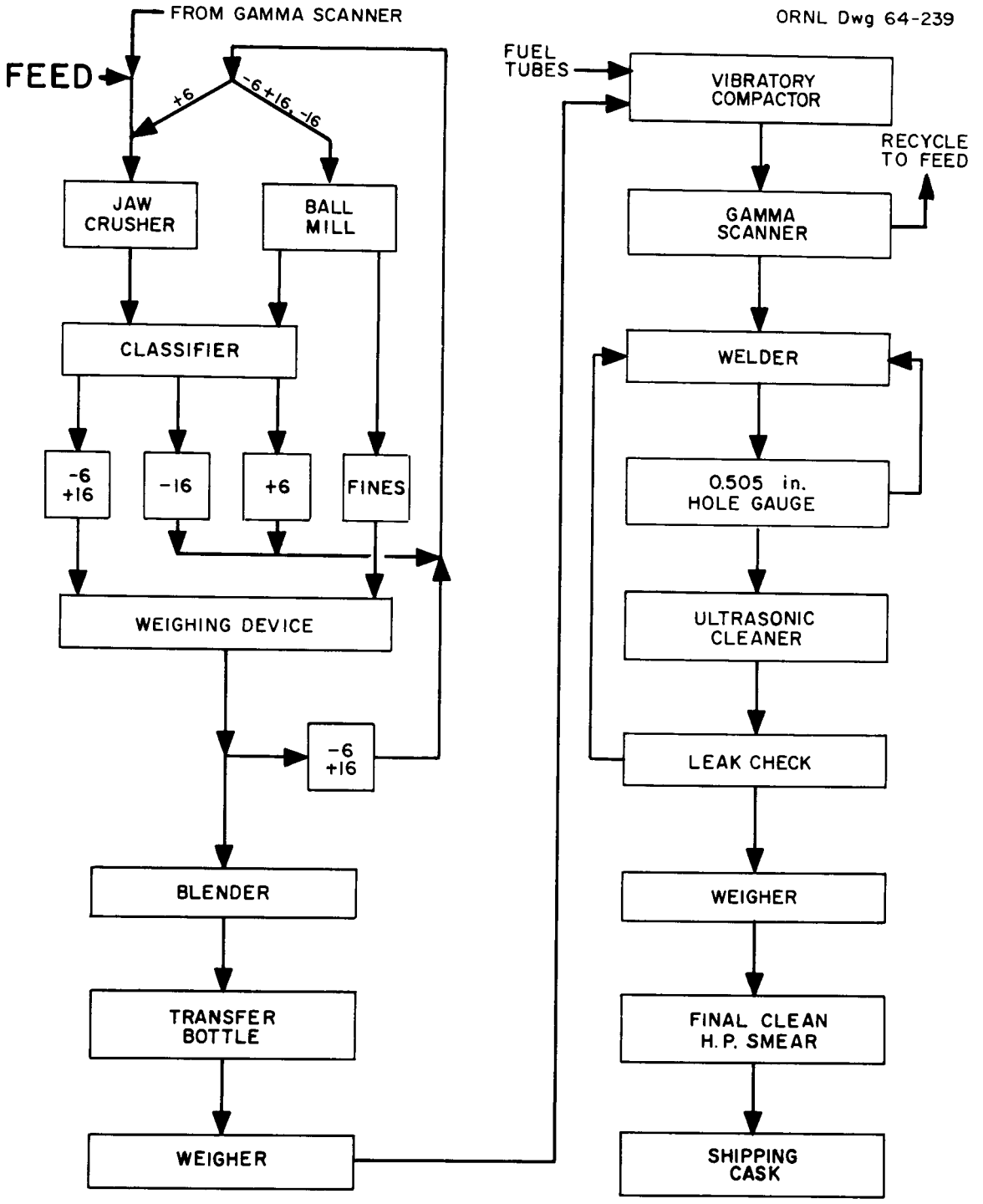

Fig. 12. Rod-Fabrication Flowsheet.

Instrument and functional checks were made on each piece of equipment before operation. These checks corrected a number of alignment and minor operational problems. Operators were trained during the preliminary checkout period.

1.4.2 Operating Experience with Stand-in Oxide

To further evaluate and test the facility and equipment before ^{233}U-bearing oxide was used, operations were carried out with depleted uranium-thorium oxide. During this period, the final procedures were selected, and final modifications of the process were made.

In the tests, it soon became evident that the powder-conditioning equipment was the area of major concern. Despite extensive efforts to contain dust within the system, oxide dust accumulated on the equipment. The abrasiveness of the oxide powder caused extensive trouble with the ball mill, particularly with bearings and other wear surfaces. Eventually the special ball mill, designed for remote operation, was made to operate, although not in a way that completely satisfied the program requirements. Other powder-conditioning equipment, after minor adjustments, performed well. During the cold runs, there was no evidence of "blinding" of classifier screens. Material balances made during the cold runs showed an average holdup of only 2 kg of oxide in the complete system.

During the operation of the vibrator system, several modifications were made. The need to observe the feeding of the classified oxide fuel into the rod required the elimination of the dust boot over the end of the feeder trough. Although removing the boot increased the dusting, it was felt that adequate feeder control could not be obtained without observing the feeding. The chuck system for holding the rod was changed to utilize a slightly modified Swagelok tube coupling. This coupling uses a standard 1/2-in.-pipe-to-1/2-in.-tube male connector, with a specially machined split ferrule. The original chuck was replaced because of the expense and difficulty of replacing it in the event of a failure. During the cold operations, failure of the Swagelok chuck was usually observed after packing 10 to 12 rods;

therefore, it was planned to change the Swagelok tube coupling after packing six rods. Experience in the cold runs indicated also that a number of failures in the other components of the vibrator chuck assembly should be anticipated because of the extremely high levels of acceleration associated with the Branford vibrator (reportedly as high as 20,000 to 100,000 times as large as the acceleration due to gravity).

In the operation of the vibrator, it was found that the freedom of movement of the anvil, to which the fuel tube to be filled is attached and upon which the pneumatic hammer impinges, is a very important factor. The anvil must be allowed to move about 1/16 in. to obtain the desired compaction. If the anvil is not allowed to reciprocate, a reduction in packed density of 8 to 10% is observed. Some difficulties were experienced with the Branford vibrators; however, most of these were operational and were corrected.

After demonstrating the ability of the powder-preparation equipment to produce powders of three size fractions for loading into the fuel tubes, it was decided to modify the system to produce powders of two sizes. The decision to operate the system with two size fractions was based on two factors: (1) The two-particle-size system is equal to the three in attainable compaction density, and (2) it is much easier to operate, especially with a remotely controlled system. During the cold runs, the binary mixture was optimized to consist of a charge of 55% of a classified -6 +16 mesh fraction, and 45% of an unclassified ball-mill fraction, which is almost 50% -50 +140 mesh and 50% -140 mesh. The ball-mill fraction is produced by controlling the charging rate of the mill and the amount of milling time. With this distribution, 20 cold samples were packed, and they had an average bulk density of 90% of the theoretical, with a deviation from rod to rod of less than 1%. The density profile, measured with the gamma scanner, was well within the specified ±2%, with the majority of the rods showing a deviation of less than 1.5%. The results were most gratifying, because they had not been predicted from laboratory experience.

1.4.3 Operation with ^{233}U

After advancing the flowsheet and equipment in cold operation to a stage where the production of fuel rods meeting specifications had been demonstrated, ^{233}U was introduced to the system. Although the facility and equipment had been exhaustively tested and improved, initial operations were not smooth, and numerous difficulties were again encountered. However, all these problems were met satisfactorily, and the facility has now demonstrated sustained production at the design capacity of 15 rods per day.

A complete analysis of the system has not yet been made, but the experience accumulated in operating the system clearly validates the design and principles on which it is based and shows that remote fabrication of $(Th\text{-}^{233}U)O_2$-bearing fuel rods on a routine basis is technically feasible.

The specifications to which the fuel rods have been made include, in addition to the dimensional tolerances, a requirement that the fuel rods have a nominal density of 90% of the theoretical density of the mixed oxides, with the deviation in average density from rod to rod not to exceed 2% of the theoretical density. Further, within an individual fuel rod, the density, as determined through a 1/8-in. x 3/8-in. collimator in the gamma scanner, should not vary more than ±2% of theoretical density from the average for that rod. Density profiles for fuel rods, one meeting density specifications and one not meeting specifications, are shown in Fig. 13.

Since starting "hot" operation on June 16, 1963, 720 fuel rods containing 650 kg of powder have been produced and shipped to BNL. The facility was operated in campaigns of 120 rods. After each campaign, production was interrupted while a "criticality cleanup" was made. During the period between campaigns, the operations in the facility were assessed to determine areas where improvements could be made, and routine maintenance was performed.

Y-55931

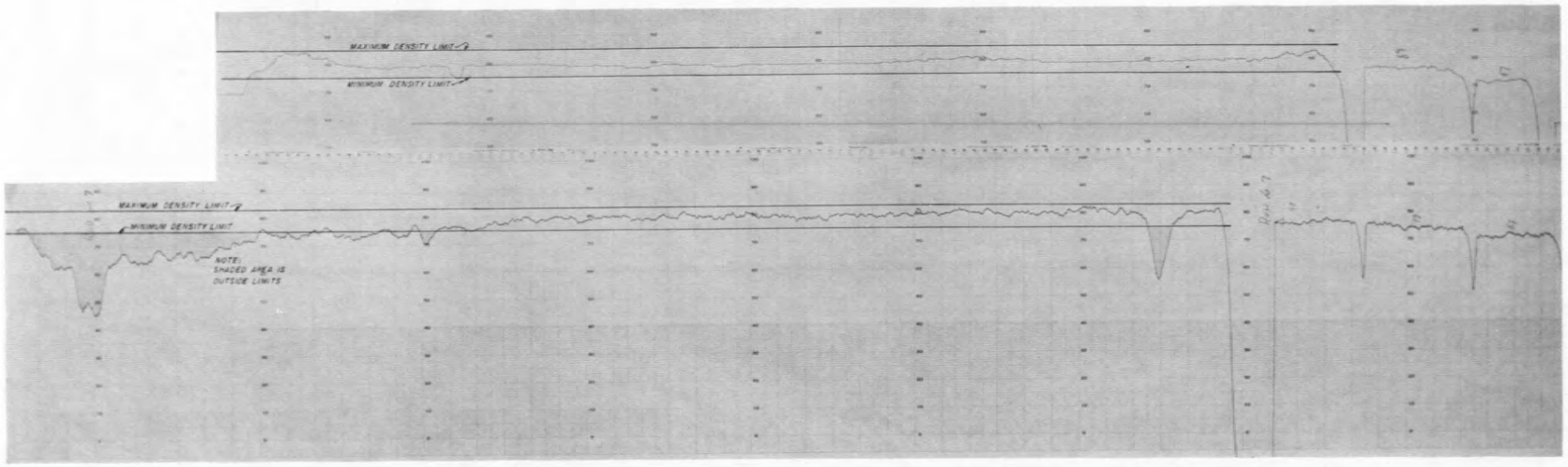

Fig. 13. Density Profiles of Brookhaven National Laboratory Fuel Rods.

The flowsheet and method of operation now used in the rod-fabrication facility make possible a very high utilization of the powder processed. About 90% of the powder is utilized, with about 5% removed for analytical samples and about 5% lost from the system due to spillage. The spilled material cannot be used in rods because of contamination, and so it is removed and accounted for in the intercampaign criticality cleanup. The closed material balance, which includes process losses, analytical samples, and an estimate of the system holdup shows a net loss of 0.3% of the material processed.

No loss of feed or rods occurs when the density specifications are not met. This economy was effected by gamma-ray scanning the fuel rod before making the end closure weld. The reject rate as determined by the gamma scanner has ranged from a high of about 30% to a low of 3%, the present value. The feed material is removed from the rods that fail to pass the density specification and is returned to the powder-conditioning system to be used in subsequent rods. The returned fuel tubes are simply reloaded. The sole reason for rejecting rods has been the variations in the point-to-point density along the length of the rod in excess of the ±2% specification.

Changing the particle-size distribution and manner of operating the ball mill aggravated problems found during the cold runs. Malfunctioning of the indexing mechanisms in this equipment was a major source of delay during the early months of hot operation, and the mill was replaced with a simpler ball mill that would have to be loaded and unloaded with gloved hands. This new mill does not solve the general problem of remote milling, but a solution to the problem has been found in the use of a larger continuous ball mill, developed subsequently. The remainder of the equipment performed satisfactorily; infrequent breakdown and maintenance has occurred.

The daily production averaged over a period of seven months is only six rods per day. The reason this figure is far below the design capacity of 15 rods a day is that during the first few months, training and equipment difficulties kept the

production rate low. Initially, about 240 min were required for the production of a fuel rod; during the last four months, rods have been routinely processed at a rate of one rod in 40 min. During the first campaign, equipment on-stream time averaged about 30%, and the facility operated at only 16% of the 15.5-rod-per-day ultimate capability. During the last five campaigns, equipment on-stream time averaged 74%, and the efficiency ranged from 51 to 62%. Thus, it is concluded that when staffed with a sufficient number of proficient operators, the facility in its present state can be operated for an extended period at the design capacity of 15 rods a day with an on-stream time of 70% (average of 10.5 rods a day).

2. THORIUM-URANIUM FUEL CYCLE DEVELOPMENT FACILITY

Development of the thorium fuel cycle must eventually include an economic analysis of the various fuel-element reprocessing and fabrication techniques at pilot production levels. Since there appears to be an economic advantage in reducing the amount of decontamination in reprocessing and because of the buildup of radioactivity in fuels by the decay of ^{232}U, it is desirable to have a heavily shielded facility in which to develop and to study the economics of a variety of integrated fuel reprocessing schemes. The TUFCDF is being constructed to fulfill this need.

The facility has been sized to accommodate integrated recycle processes with equipment reduced in size from the anticipated production units so that a realistic and reliable basis for technical and economic analyses will exist. A conceptual design, based on the size, shielding, containment, and developmental flexibility outlined in the criteria[5] was completed in July 1962. A report[6] on this design was presented in December 1962. Title I design was started in January 1963 and completed in December 1963, with very little change in the concept. Title II design is expected to start early in 1964.

2.1 Building Design

The facility will be constructed in the Melton Valley Area near the Transuranium Processing Plant and High Flux Isotope Reactor (Fig. 14). It will be an

PHOTO 64020

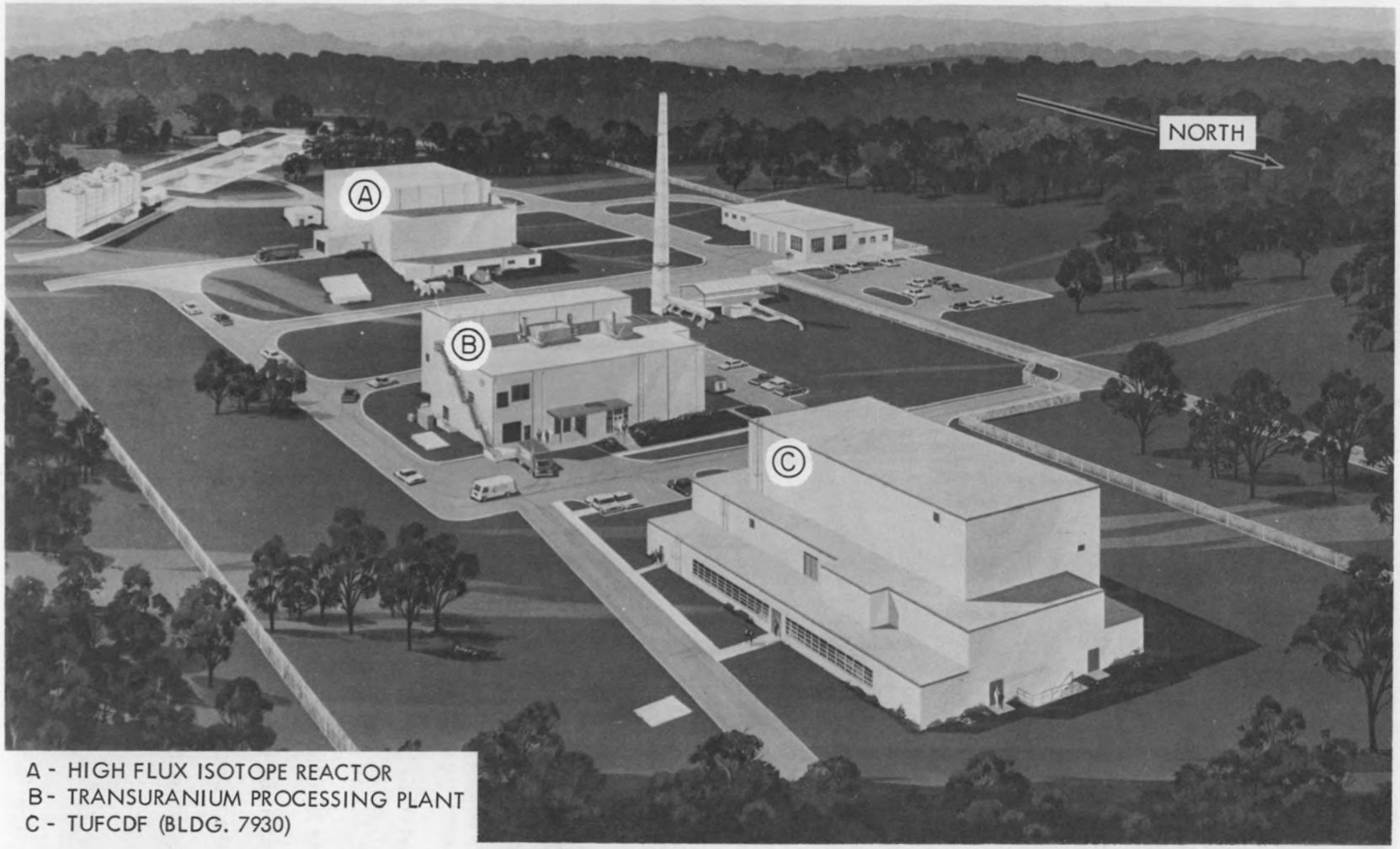

A - HIGH FLUX ISOTOPE REACTOR
B - TRANSURANIUM PROCESSING PLANT
C - TUFCDF (BLDG. 7930)

Fig. 14. Area Map Location of TUFCDF.

irregularly shaped three-story building, approximately 162 ft long and 124 ft wide, with a partial basement. The first floor (Fig. 15) provides space for offices, change rooms, operating areas around the cell enclosures, a fuel-storage basin, and a receiving area. The second floor provides space for chemical makeup, sampling of in-cell processes, cask decontamination, a "warm" shop, a development laboratory, and the mechanical and electrical equipment for the building. The third floor is a high-bay area, which includes the cell-roof area and provides facilities for entry of cell services and cell access. This bay is provided with a 50-ton crane to handle casks large enough to accommodate fuel elements up to 12 ft long. The basement will provide space for access to the equipment storage cell and for the vulnerable equipment associated with the chemical cell. The building acts as a second line of containment around the cell complex.

The primary zone of containment for the facility is made up of six shielded cells and an associated glove maintenance room and air lock. Four of the cells provide the operating space for the process equipment, while two provide for supporting functions. The operating cells are arranged in a line with one of the service cells, which will be used for decontamination and as a radiation lock, "teeing" off from the line at the point where the two large central cells join. This arrangement provides for a high degree of mobility for movement of equipment within, into, and from the shielded area.

The two large cells are remote-maintenance cells. The mechanical-processing cell provides space for operations incidental to irradiated fuel recovery and reconstitution of fissile and fertile materials into forms suitable for use in fuel element manufacture. The contaminated-fabrication cell provides space for fabrication operations through the point at which all fissile and fertile material is contained and sealed in fuel cladding. The chemical cell can be either a remote-maintenance or a contact-maintenance cell, while the clean-fabrication cell used for final inspection of fuel rods and assembly and inspection of fuel elements is a contact-maintenance cell.

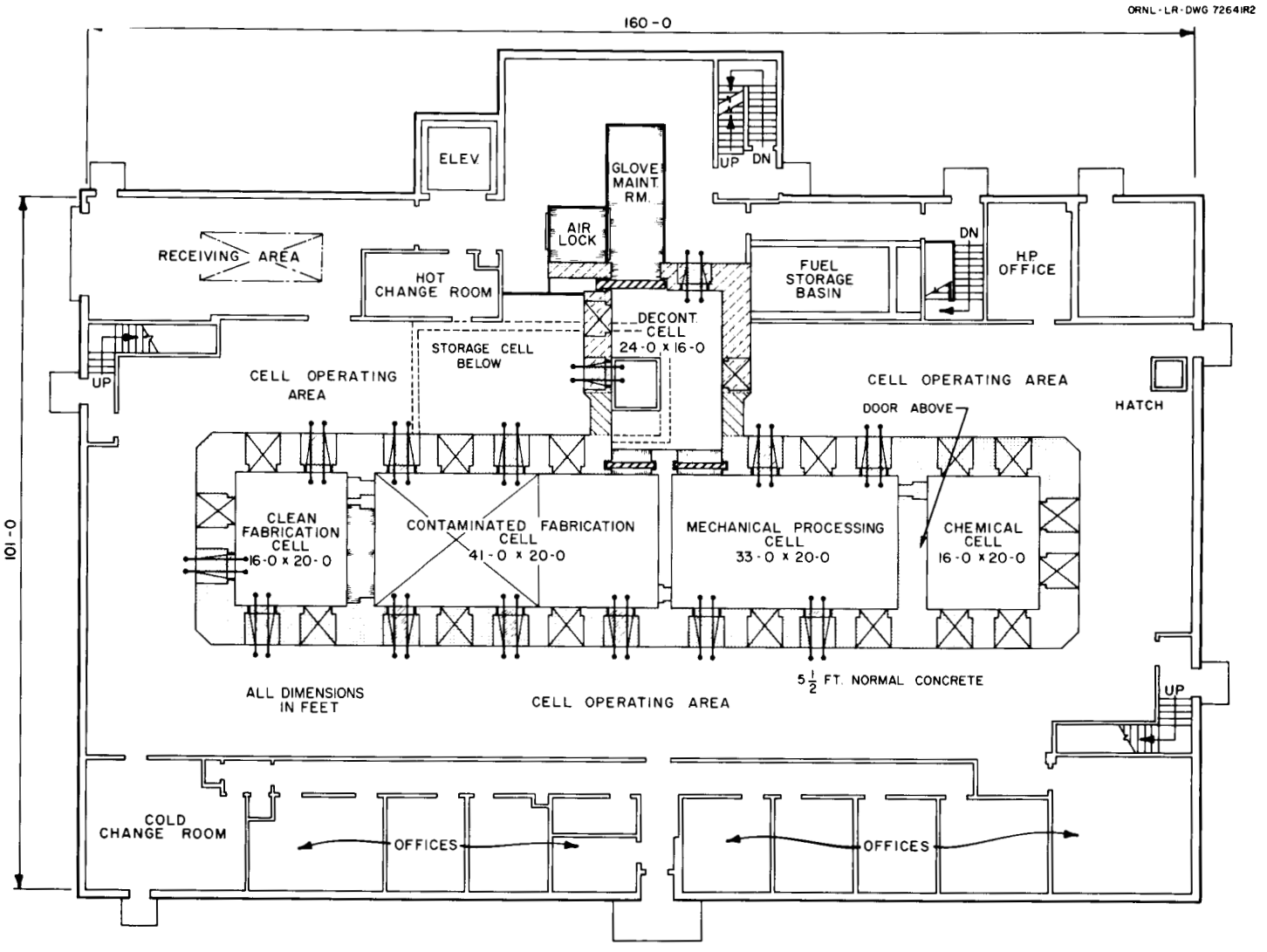

Fig. 15. First Floor Plan—Thorium Fuel Cycle Development Facility.

All the remote-maintenance cells and the decontamination cell are lined with stainless steel. The service penetrations for all cells are provided with seals to confine radioactivity. Provisions have been made for future conversion to an inert atmosphere in the remote-maintenance cells, the decontamination cell, equipment-storage cell, and the glove-maintenance room to permit processing of pyrophoric materials.

The cells are capable of processing and refabricating fuel assemblies as long as 12 ft and containing as much as 35 kg of thorium-uranium fuel irradiated to 25,000 Mwd/metric ton and decayed for 90 days. To do this, all operating cells are provided with the equivalent of 5-1/2 ft of normal concrete up to the electromechanical manipulator bridge level, and 4-1/2 ft of concrete above this level. Figure 16 is a sectional elevation showing the common roof line of all operating cells with the varying floor levels required to provide different in-cell heights to permit processing and refabrication of the power-reactor-size fuel elements. This section also shows the bridge crane and electromechanical manipulator remote-handling equipment along with the modular arrangement of windows and master-slave manipulators.

2.2 Preparation of Thoria-Base Solids

The solids-preparation equipment to be installed in the TUFCDF will, insofar as reasonable, be a scaled-down version of facilities that would be required for a similar function in a production-scale thoria-urania fuel-assembly fabrication plant. All major operations will be accomplished by prototype equipment, from which it is anticipated that useful data relative to reliability, maintenance, and operating cost on a plant scale, will be obtained.

Solids will be prepared by the sol-gel process, which in its various stages of development has been described numerous times.[7,8] In the process description that follows will be given a summary of information presented in earlier reports as well as some information appearing in more detail in other portions of this report. Also a summary description of the process equipment will be given.

ORNL-LR-DWG 75591R

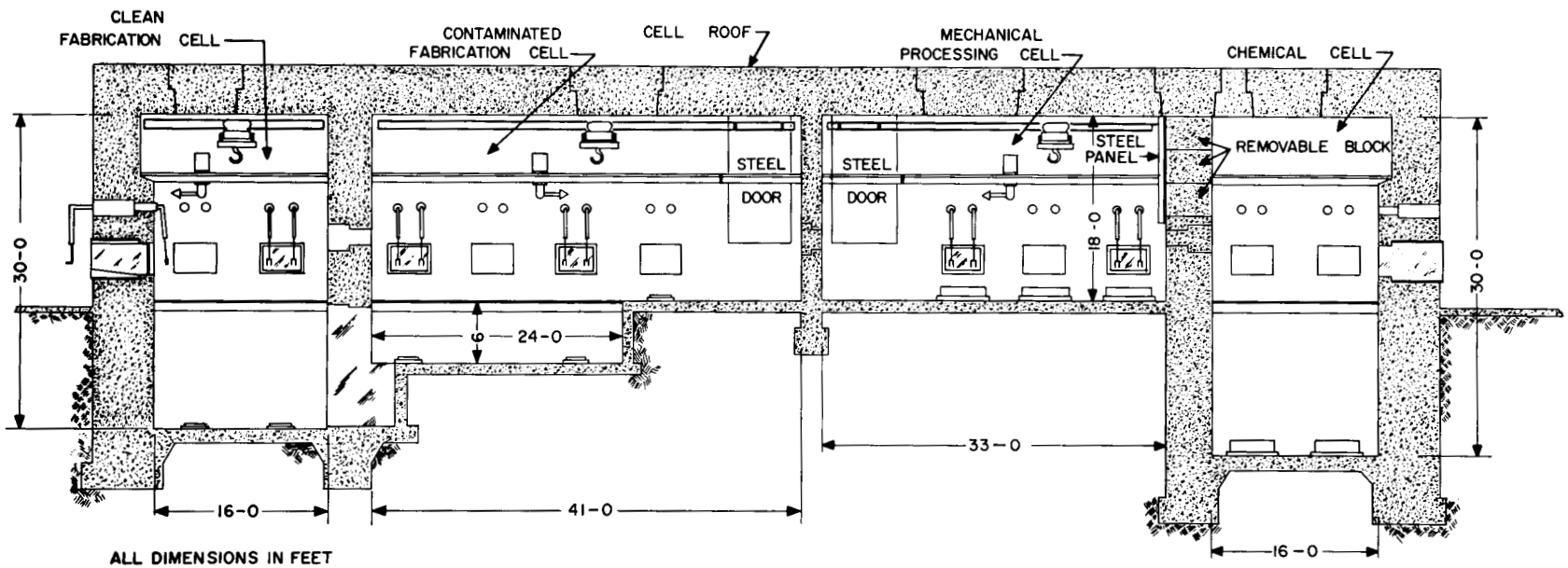

Fig. 16. Sectional Elevation of TUFCDF Process Cells.

2.2.1 Description of Sol-Gel Process

In the sol-gel process, thoria is dispersed into a stable sol having a very large crystallite surface area per unit weight (about 80 m^2/g of ThO_2), uranium is adsorbed on the thoria surface, and the sol is dried in shallow pans to form a gel which is calcined to form very dense (more than 99.5% of theoretical) homogeneous particles suitable for vibratory compaction. A simplified process flowsheet was shown on page 9. The individual steps are discussed below.

Steam-denitrated ThO_2 is dispersed (peptized) by the nitrate ion from uranyl nitrate. The following procedure must be used in order to produce a sol with the desired rheological properties. A ThO_2 slurry (10 to 12 M in ThO_2) is added to an agitated solution of uranyl nitrate that contains the proper amount of nitrate for dispersion. The uranyl nitrate concentration should be such that enough water is added to yield a ThO_2 concentration of approximately 4 M.

After thorough mixing, the slurry is agitated for about 1/2 hr at 80 to 90°C to achieve complete dispersion. The amount of nitrate required to achieve complete dispersion is 0.077 mole of nitrate per mole of ThO_2. However, this amount of nitrate prevents complete uranium sorption on the ThO_2 surface, due to the low pH. Therefore, the pH of the sol is raised by adding NH_4OH in an amount equal to 0.017 mole per mole of ThO_2, which allows complete uranium sorption. Agitation for 1/2 hr is required after pH adjustment.

The NO_3^--to-Th mole ratio of 0.077 required for dispersion fixes an upper limit on the amount of uranium that may be added as uranyl nitrate. If stoichiometric uranyl nitrate is obtained from solvent extraction, the maximum permissible uranium-to-thoria mole ratio is 0.0385; this ratio is reduced to 0.03 if the nitrate-to-uranium ratio is increased to 2.56. The uranium content may be increased to about 10 mole % by adding more uranium as ammonium diuranate.

After uranium sorption is complete, the sol is dried in shallow pans at the appropriate depth (usually 1/2 to 1 in.) to fix at least one of the particle dimensions. The drying takes 24 hr at a liquid temperature of 80 to 90°C, with the final solids

temperature greater than 100°C but less than 135. This dried gel product will lose less than an additional 7% in weight when calcined to 1150°C.

The final step in the sol-gel process is calcination, which produces densification of the gel and reduction of the uranium to the tetravalent state. Densification is accomplished by heating the dried gel to 1150°C. The uranium reduction is accomplished by soaking for at least 4 hr at 1150°C in an Ar—4% H_2 atmosphere (a nonexplosive mixture), followed by cooling to room temperature under argon. Both steps are accomplished in one furnace.

The properties of the uranyl nitrate solution and the thoria powder required for successful operation of the sol-gel process are as follows:

Uranyl Nitrate Solution

1. NO_3^-/U mole ratio ≤ 2.4
2. Al^{3+} <100 ppm
3. $^{233}U \approx 150$ g/liter

Thoria Powder

1. Specific surface area, >40 m^2/g
2. N/Th <0.05
3. Those properties obtained by contacting preheated $Th(NO_3)_4$ crystals at 200°C, then steam contacting for 6 hr, during which time the temperature is raised from 200 to 475°C, with 3 hr of heating at $\geq$425°C

Those items of sol-gel process equipment that will contain radioactive material will be installed in the mechanical processing cell. They consist of a thoria-charging hood, a ^{233}U storage tank, and a metering system for the uranyl nitrate solution.

The thoria-charging hood will be a stainless steel box designed for alpha containment and provided with the following facilities: storage space for the ThO_2 transfer containers, a set of balances, a decontamination system, and a ThO_2 slurry tank. The ThO_2 slurry tank will be a 12-in.-diam tank 8 in. high, with a 60° included-angle conical bottom, a 90° included-angle conical top, fitted with a 4-in. flanged opening and a water-spray system for wetting the ThO_2 powder.

The ^{233}U storage tank will be a 2-in.-thick slab tank, 7 ft wide and 7 ft high, having a tapered bottom with 120° included angle, to provide sufficient uranyl nitrate for 7 to 21 operating days. It will be located adjacent to the north cell wall and have a 10-mil cadmium sheet attached to the tank surface adjacent to the cell wall. This tank will hold 50 gal of uranyl nitrate solution and be critically safe for concentrations of ^{233}U up to 400 g/liter.

The uranyl nitrate solution metering system will consist of two stainless steel tanks 3-1/2 in. diameter and 5 ft long, plus instrumentation for measuring liquid level, and equipment for transfer of uranyl nitrate to either of two destinations. The metering will be done by filling a tank slightly above the overflow point and allowing the surplus to drain back to the storage tank. Liquid will be discharged by pressurizing the metering tank, causing liquid to flow to a small head pot. The quantity of solution transferred will be measured by means of bubbler-type liquid-level sensing devices. From the head pot, it will flow by gravity to the blend tank or to an ammonium diuranate precipitation tank to be installed in the future if required.

This metering system will be capable of delivering to within ± 3% of a predetermined volume. After delivery is complete, it will measure the transferred quantity to within ± 1%.

2.2.2 Sol-Gel Process Equipment

The sol-gel process equipment is to be installed in the mechanical-processing cell and is to use uranyl nitrate and virgin, steam-denitrated thorium nitrate as feed. All equipment will be sized for a daily product rate of 35 kg of calcined ThO_2-UO_2. The major equipment items are a ^{233}U transfer hood, a blend-tank system, a sol-metering system, a horizontal tray dryer, and a 3-in. vertical tube furnace.

The ^{233}U transfer hood will be a stainless steel box designed to provide alpha containment during transfer of the ^{233}U solution. It will have a decontamination system, instrument connections for liquid level and density probes, a steam jet for

discharging the carrier contents into the ^{233}U storage tank located in the mechanical-processing cell, control valves, and be constructed in such a manner that lead bricks may be stacked around it for shielding if required.

The blend tank will be 1.75 in. thick, 5.5 ft wide, and 6 ft high, with a 60° included-angle conical bottom and will be connected to a 15-gpm pump and a heat exchanger. Other items that will be provided are: liquid-level instruments, a sol-sample station, vapor condenser, valves, and a spray header to rinse all inside surfaces. The valves and pump will be mounted with disconnects in a manner suitable for remote removal and replacement.

The sol metering system will provide a metered volume of sol about every 1.5 hr to the semicontinuous tray dryer. It will consist of a constant-volume overflow type metering tank plus facilities for an "acid egg" type transfer to the dryer. The terminus of the discharge line will be cooled to cause condensate to form on the cool surface inside the pipe and flush any solids away, and also to serve as a vapor-liquid separator in order to prevent splashing.

The horizontal tray dryer will be equipped with shallow pans pinned to a horizontal conveyor chain that will move the filled trays over heated surfaces on two levels, invert the trays directly over a 3-in. vertical tube furnace, jar the trays to remove all solids, and elevate and reposition the trays for the next cycle. The dryer will contain 22 trays, each 2 ft by 1 ft. Each tray will be 1-1/2 in. deep, with a weir 1/2 in. high dividing the trays into two 1-ft by 1-ft sections. The dryer will be of all stainless steel construction.

The 3-in.-diam vertical tube furnace to be used for calcining is to be located directly below the dryer return end and over a rotating disk that acts as a flow-regulating valve for the calcined solids. The furnace will consist of three zones: The top zone, about 18 in. long, is the "solids-preheat" zone, in which the dried gel moves downward and is heated by the hot gases moving countercurrently. The middle zone, about 24 in. long, is the calcining zone, where the solids are held at 1150°C for at least 4 hr. The bottom zone, about 6 in. long, is the "solids-cooling"

zone, where the hot calcined solids moving downward are contacted and cooled by upward moving argon.

The vertical tube will be made of alumina, with 1/4-in.-thick walls. Heat will be supplied by twelve 400-w-capacity, silicon carbide resistance heaters arranged perpendicular to the axis of the furnace. Flow out of the furnace will be controlled by a rotating disk located below the vertical tube. The drive motor for this flow-regulating disk will be controlled to maintain a full charge in the furnace.

2.3 *Oxide-Fabrication Equipment*

The overall objective of the TUFCDF oxide-fabrication equipment is to demonstrate the technical and economic feasibility of the remote fabrication and assembly of rod-type fuel elements containing $(Th\text{-}^{233}U)O_2$ by the bulk-oxide, vibratory-compaction, mechanical-assembly route; pilot-plant-scale equipment will be used. The equipment will be of production type in order that the information gained will be applicable, both technically and economically, to a full-scale production facility.

The equipment for making and inspecting fuel rods will be versatile and capable of accommodating pins 2 to 10 ft long and 1/4 to 3/4 in. in diameter and will have a capacity of about 35 kg/day. The assembly and final inspection equipment will be greatly influenced by the configuration of a particular fuel element design; therefore, the design of this equipment will be based on a selected fuel element. A slightly modified Elk River Reactor fuel element (Fig. 17) was recently chosen as the design reference for the assembly equipment. Other assemblies can be accommodated by retooling the equipment.

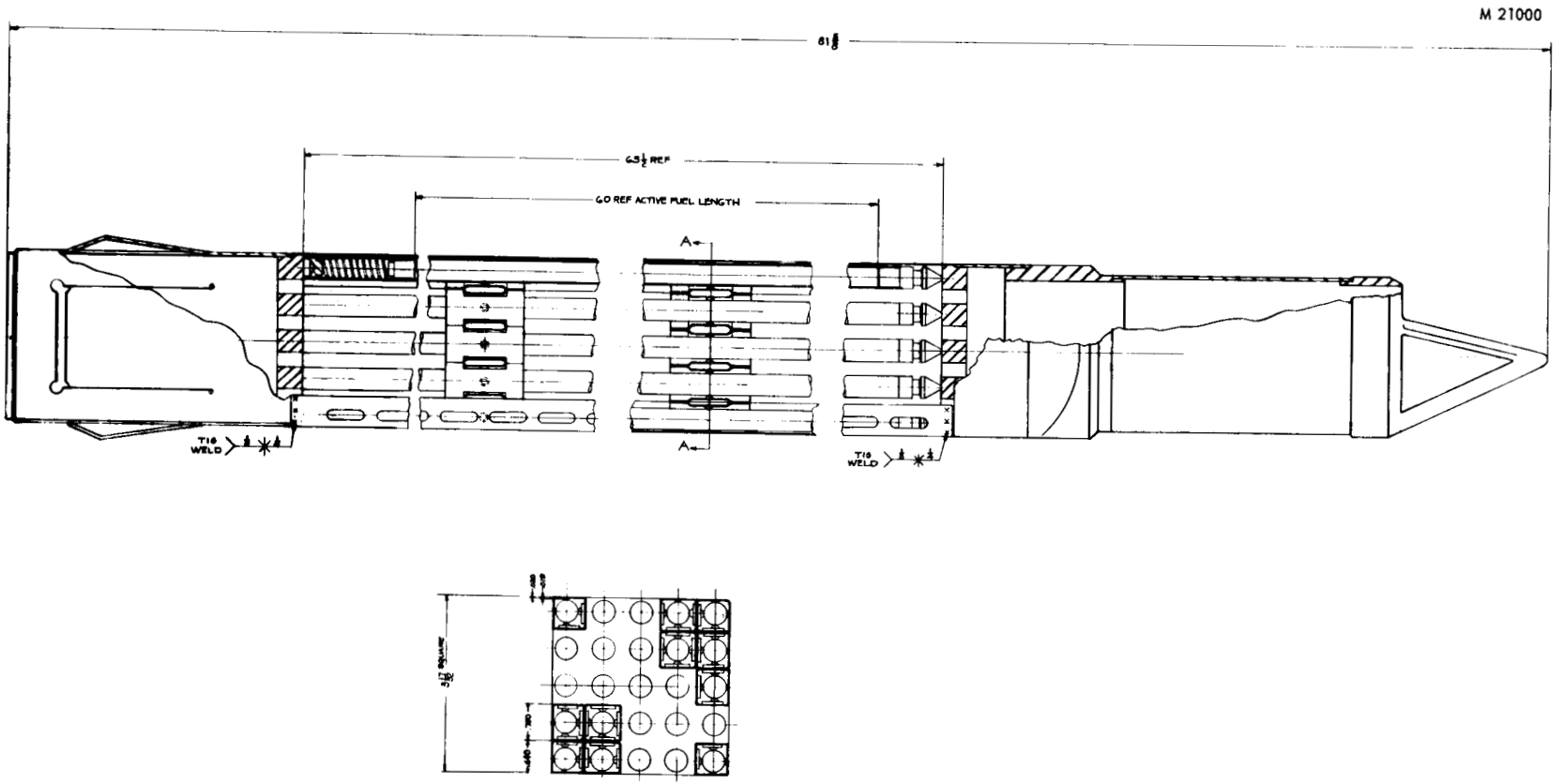

Fig. 17. Elk River Reactor Fuel Element.

At this time, all the fabrication equipment has been conceptually designed, and design and development of the process equipment is starting. The fabrication, equipment, and current status of the program will be discussed in the sections that follow.

2.3.1 The Process

The procedure for making the rod-type fuel elements consists in (1) sizing of the sol-gel oxide for vibratory compaction, (2) vibratory compaction of fuel rods, (3) fuel-pin end-cap welding and inspection, (4) fuel rod decontamination, (5) assembly of fuel pins into fuel elements, and (6) final inspection. A detailed flow diagram is shown in Fig. 18.

In the process, bulk oxide produced by the sol-gel process in an adjacent cell first will be sized and separated into size fractions by a system of crushing, grinding, and classification as required for vibratory packing. For equipment-design purposes, it has been assumed that a combination of three particle sizes will be used for vibratory packing of the bulk oxide. Following comminution and classification, fuel for one full pin loading will be dispensed and transferred to a blend-transfer device for conveying the fuel to the vibratory-compaction apparatus. The blend-transfer device will blend and transfer simultaneously two rod loadings at a time. In the vibratory-compaction apparatus the blended fuel is packed into fuel tubes.

Following compaction, each fuel pin is weighed, and the axial density variation of the column of compacted fuel is measured with a gamma-ray-absorption scanner. Next, the fuel rod is capped, the cap is welded to the fuel tube by a fusion welding process, and the fuel rod is moved to decontamination apparatus. This apparatus also serves as a transfer device for moving the rod from the powder-preparation and rod-fabrication area (clean-fabrication cell) to the inspection and fuel element assembly area (clean-fabrication cell).

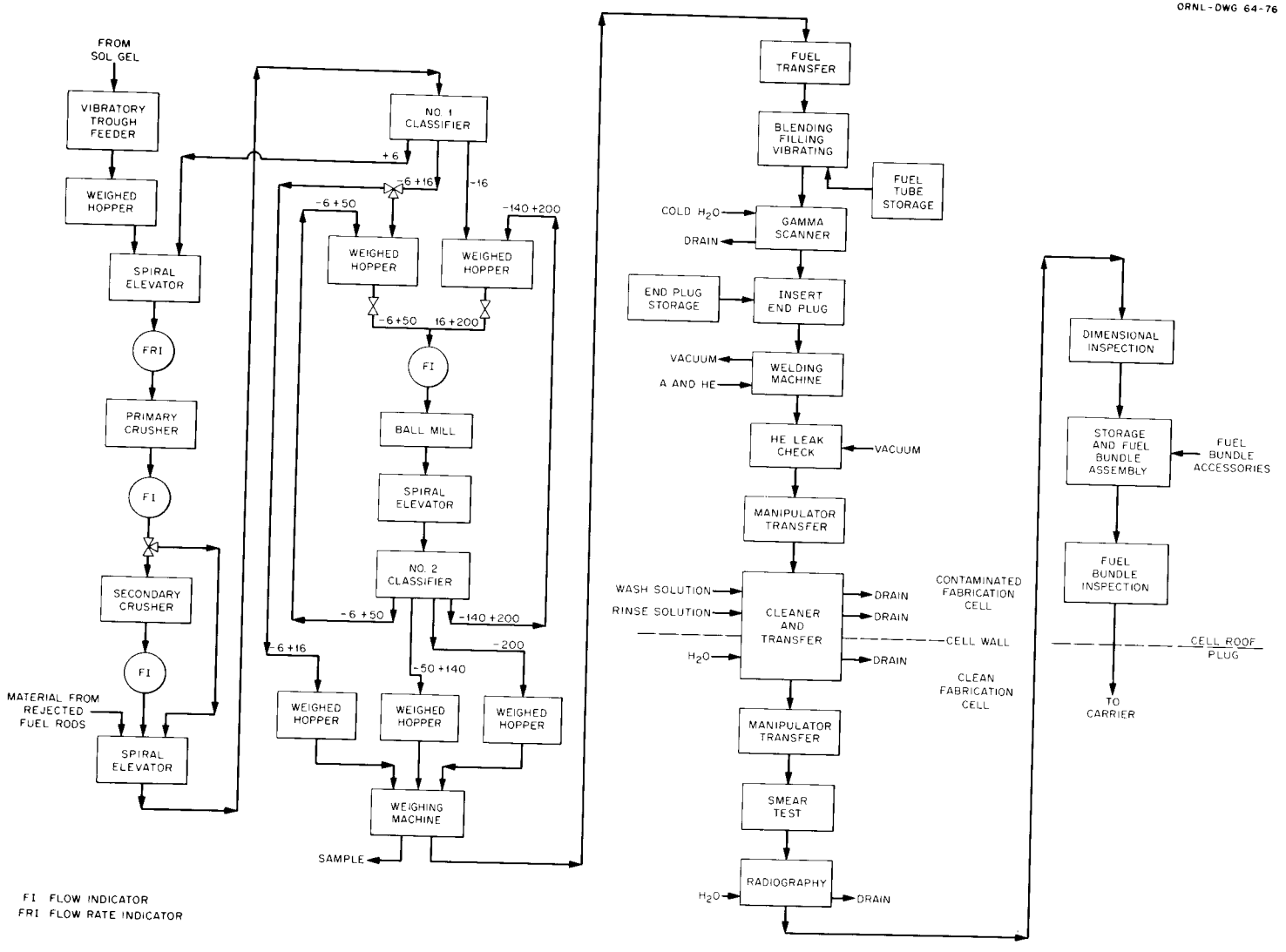

Fig. 18. Fabrication Flowsheet for Oxide Fuel Element.

In the clean-fabrication cell, the rods will be checked immediately for contamination. Then, the end-cap welds will be inspected, and the rods will be tested for dimensional conformity. The final steps will be the assembly of the fuel rods into preconstructed fuel-element mechanical assemblies, and inspection.

2.3.2 Equipment

The layout of the fabrication equipment is divided into two areas, according to the degree of contamination that is expected from the operations. Fabrication operations that involve direct contact with the fuel material or rods in the unsealed condition (powder preparation, vibratory compaction, gamma scanning, and welding) will be done in the contaminated-fabrication cell. Operations after the fuel material is contained in a sealed fuel rod (inspection and element assembly) will be accomplished in the clean-fabrication cell. A general layout of the equipment is shown in Fig. 19.

Each item of equipment located in the contaminated-fabrication cell will be capable of being remotely installed, maintained, and removed by the cell remote-handling equipment. Motors, switches, and complex mechanical components susceptible to wear, damage, or failure will be replaceable with a minimum of effort and without removing the complete equipment item. Contact maintenance can be employed in the clean-fabrication cell; therefore, provisions for maintenance by manipulators in this cell will not be extensive.

In the design of the equipment, aluminum or mild steel will be used extensively, with stainless steel being used only for parts in direct contact with the fuel or where corrosive liquids or atmospheres dictate its use. Elastomers or other organic materials will be used only when absolutely necessary, and, when used, provisions will be made for their easy replacement.

The fabrication and inspection equipment will be built in the form of multistation systems. Transfer of the rods in the multistation system will be done with a special rod-handling machine. Adaptability to the wide dimensional variation of

ORNL-DWG 64-78R

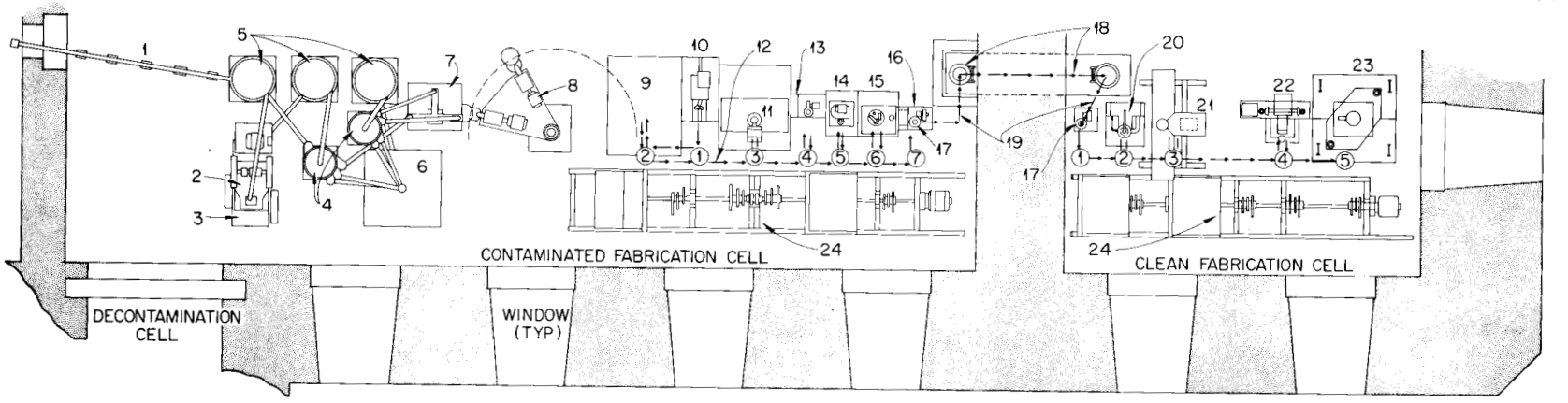

PLAN VIEW

(1) TRANSFER STOP POSITIONS
1. VIBRATORY TROUGH FEEDER
2. JAW CRUSHER
3. ROLL CRUSHER
4. CLASSIFIERS
5. VIBRATORY SPIRAL ELEVATORS
6. BALL MILL
7. WEIGHING MACHINE
8. FUEL TRANSFER MACHINE
9. VIBRATORY COMPACTOR
10. FUEL ROD MAGAZINE
11. GAMMA SCANNER
12. FUEL ROD FLOW
13. REJECT RACK
14. CAPPING MACHINE
15. WELDING MACHINE
16. INDEXING MACHINE
17. FUEL ROD BASKET
18. CLEANER TRANSFER MACHINE
19. TRANSFER IN FUEL ROD BASKET
20. LEAK CHECK MACHINE
21. WELD RADIOGRAPHY MACHINE
22. FUEL ROD DIMENSIONAL CHECK
23. FUEL ELEMENT ASSEMBLY AND INSPECTION MACHINE
24. FUEL ROD TRANSFER MACHINE

Fig. 19. Equipment Layout for Oxide Fabrication.

rods will be achieved when possible by minor adjustment of components; however, the cost of constructing versatile units may dictate partial retooling or complete interchange of certain equipment items.

Operations in the Contaminated-Fabrication Cell. — There are eight important operations in this cell. These are: (1) powder preparation, (2) vibratory compaction, (3) gamma scanning, (4) cap insertion and welding, (5) indexing using the fuel rod basket, (6) leak checking, (7) storing and dispensing empty fuel tubes, and (8) cleaning and transferring rods.

1. Powder Preparation. — In this step, the bulk oxide is prepared for vibratory compaction. Since the oxide is dry, a severe contamination problem presents itself. Therefore, powder-preparation equipment will be designed insofar as practicable to contain the dust; however, absolute dust containment, as experience has shown in the Kilorod Program, is extremely difficult.

The powdering of the bulk oxide begins with the primary crushing step. This crushing will be done with a small-production jaw crusher capable of handling about 200 kg of sol-gel material an hour. Depending on the size distribution required for vibratory compaction, a second crushing step may be necessary. A 6-in. roll crusher capable of processing about 200 kg of oxide an hour will be used for this application. After being crushed, the material will be classified, with the oversize material returning to the crushing equipment.

A ball mill will be used to produce the intermediate and fine fractions for vibratory packing. The current type of ball mill being considered is a continuously operated mill capable of handling about 50 kg an hour. Following the milling operation, the material will be classified, with the undesirable fractions being returned to the mill.

For classification, two 18-in. vibratory-type classifiers will be used. Conveying of the powder in the process will be accomplished by gravity, by vibratory-type powder elevation mechanisms, and by vibratory trough feeders, as appropriate. Control of the process will be accomplished with flow-measuring devices to determine

the flow of oxide to the primary and secondary crusher and to the ball mill. Weighed hoppers will be used to indicate the crushing behavior of the material. Flow-indicating devices will be used to monitor the powder flow at various places in the process. The comminution and classifying equipment will be operated on a schedule of one batch a day.

The quantity from each of the size fractions required for one pin loading will be weighed out with an automatic batch-weigher. This device will use a 1:1-ratio balance with an electronic readout. After the batch composition for one pin loading is weighed out, the fuel will be emptied into a blending container, on the blend transfer device. The blend-transfer device will allow the simultaneous blending and transfer of two separate rod loadings to the vibratory-compaction apparatus. An oblique blending action will be used for blending the powder.

2. Vibratory Compaction. — Vibratory-compaction will be carried out by use of a bottom-actuated pneumatic vibrator system. The pneumatic vibrator being considered as the energy source is a modified reciprocating-piston type. It is inexpensive ($200 to $300) and is expected to be reliable. In order to demonstrate production capabilities, two pins will be packed simultaneously. The other component of the vibratory-compaction apparatus consists of a chuck for holding the rod and vibratory feeders for adding the fuel into the pin.

3. Gamma Scanning. — After being packed, the loaded fuel pin will be moved to a gamma-absorption scanning device where the axial density variation of the filled rod will be determined. The gamma scanner will be capable of detecting a 2% density variation over a 3/8-in. interval of rod length. The gamma scanner will consist of a collimated gamma beam, an NaI detection crystal, and a means of moving the beam along the length of the rod. Present data indicates that the gamma source should be ^{60}Co when scanning 1/2- to 3/4-in.-diam fuel rods, and ^{137}Cs when scanning 1/4- to 1/2-in. fuel rods. A scanning speed of at least 12 in. a minute will be necessary to demonstrate production feasibility.

4. Cap Insertion and Welding. — Following gamma scanning, the filled rod will be moved to a cap-inserting station. This station will consist of a wire-brushing device for cleaning the weld area, another device for inserting the end caps and accessories into the fuel tube, and a vacuum chamber for evacuating and backfilling the tube with helium. The vacuum chamber will also contain a press mechanism for seating the end cap in the fuel tube subsequent to the backfilling with helium. The equipment at this station will be capable of a minimum cyclic rate of six an hour.

After inserting the end cap, the rod will be moved to the welding station where the end caps will be fusion welded by the tungsten inert-gas process. The welding device will consist primarily of a "chill block" rotating mechanism, a torch-positioning mechanism, and an integral means of inserting the rod in the chill-block rotating mechanism. This mechanism will use a collet chucking principle. Positioning of the welding torch will be accomplished in two planes by means of either servo-mechanisms or mechanical alignment cams. The changing of welding electrodes will be done by means of a quick-change welding torch.

The welding unit will be capable of welding at speeds up to 20 in. a minute and will have a cyclic capacity of at least six pins an hour.

5. Indexing by Means of the Fuel-Rod Basket. — The fuel-rod basket will serve a twofold purpose: It will remotely index to a position where rods can be loaded and unloaded, and it will provide a means for holding the rods while transferring them from cell to cell, and for storing rejected rods.

6. Leak-Checking. — The ends of fuel rods will be tested for leaks. The equipment for this inspection will consist of either a variation of a helium mass-spectrometer or of a pressure-sensing instrument. Work is in progress to determine which is better.

7. Storing and Dispensing Empty Fuel Tubes. — A tube magazine will be provided for orderly storage and dispensing of empty fuel tubes. This magazine, which will be loaded with empty tubes in the gloved maintenance area, will store from 40 to 120 tubes, depending upon their diameter.

8. Cleaning and Transferring Rods. — After welding, the rods will be put in a fuel-rod basket that holds ten rods. Filled baskets will be hoisted by the cell crane and lowered into the cleaner-transfer device. This device will incorporate mechanisms suitable for removing surface contamination and for transferring the cleaned rods into the clean-fabrication cell. The cleaning will employ ultrasonic cleaning methods and detergent solutions. A final hot-water rinse will be used to facilitate drying.

Operations in the Clean-Fabrication Cell. — There are five important operations in this cell. These are 1) alpha monitoring, 2) radiographing welds, 3) dimensional inspection, 4) fuel element assembly and inspection, and 5) rod transferring.

1. Alpha-Monitoring. — The fuel rods, immediately upon entry to the clean-fabrication cell, will be tested for transferable contamination by means of a surface-smearing device. The rods will be held by an indexing mechanism and be fed to a device that swabs the rod. The swab will then be removed from the cell and placed in a counting device where the contamination level will be evaluated. Rejected rods will be recleaned until acceptable.

2. Radiographing Welds. — The quality of the end-cap weld will be evaluated by radiographic inspection; an x-ray source coupled with an x-ray-sensitive television camera will be used. A fuel tube in correct position will be rotated 360° while being scanned. The unit will inspect for weld porosity, voids, and inclusions.

3. Dimensional Inspection. — In this operation the fuel-rod bow, diameter, and length will be measured. The measuring device, which will consist of a rack which accepts the fuel rod, will be equipped with a series of probes that sense the specified dimensions.

4. Fuel-Element Assembly and Inspection. — This pair of operations is combined because they are performed by a single device, which provides jigs for the assembly of a complete fuel element, and also is equipped to carry out a dimensional inspection of the finished element. The insertion of fuel rods into a preassembled lattice will be done by the electromechanical manipulator. When the bundle has

received its full complement of fuel rods, the top end fitting will be positioned by the electromechanical manipulator and mechanically attached to the bundle.

The assembled fuel element will then be inspected to ensure that bow and rod-to-rod spacing dimensions are within specified tolerances. This will be done by an inspection jig equipped with feeler probes on coordinate slides. A carriage with indicator heads will measure fuel-element bow.

The completed fuel element will then be withdrawn from the clean-fabrication cell through the port into a shielded shipping cask.

5. Rod Transferring. — Means of rod transfer from station to station during the fabrication process will be required. A special fitting on the in-cell electromechanical manipulator can accomplish this.

3. PROCESS DEVELOPMENT AND EVALUATION

The scope of the Thorium-Utilization Program includes improvement and extension of sol-gel process flowsheets for thorium and thorium-uranium oxide and carbide production. It also includes development of remote Th-^{233}U fuel fabrication techniques and the preparation, irradiation testing, and evaluation of mixed thorium and uranium oxides and carbides, and of thorium alloys. In this section the results of the work in the above areas will be presented.

3.1 Extensions of the Sol-Gel Process

Thorium oxide and 3% uranium oxide-thorium particles prepared by the sol-gel process were sized while in the gel state to a distribution which, after calcining, was suitable for vibratory packing. The control of larger particle sizes was done in the drying step, and temperature and gel-bed depth were the significant variables. A short period of ball-milling of hot gel immediately after drying was necessary to obtain sufficient fine particles. The diameter and speed of the mill, the size distribution of balls, and time were the significant variables for obtaining an optimum fraction of -200 U.S. mesh particles.

Studies of forming and gelling of microspheres (50 to 1000 μ in diameter) of thorium and uranium-thorium oxide sol droplets showed that microsphere formation is feasible by several techniques and can be scaled up readily when done by using a tapered column. The preferred method of forming the spherical sol droplets employs a two-fluid nozzle that discharges sol droplets downward under the surface of an organic solvent that removes water from the sol to form gel droplets in a tapered column. An upflow of 2-ethyl-1-hexanol (2 EH) containing a surfactant is the preferred fluidizing-gelling agent.

A sol-gel process is being developed for the preparation of thorium and uranium-thorium carbides. The oxide sol is prepared as described in Section 1. High-surface-area channel-black carbon is blended with the oxide sol, and the sol is formed into microspheres. The microspheres are calcined to carbide in vacuum or flowing argon at about 1800°C. Densities of dicarbide microspheres as high as 90% of theoretical were obtained.

3.1.1 Particle Sizing

In the present method for preparing 3% uranium-thorium oxide for fuel-rod loading by vibratory packing, the optimum particle-size distribution for efficient packing is obtained by crushing, milling, screening, and blending after the calcination step. Sizing the oxide in the gel stage has been developed and is expected to give the following advantages: Gel is much more friable than calcined oxide, therefore time, energy, and equipment maintenance should be saved; the final product should contain less gas when ground before calcination. The flowsheet for the modified sol-gel process with sizing in the gel step is shown in Fig. 20.

Sizing the gel requires control of the solids depth, temperature and time during sol-drying to give the coarse and medium size fractions. Light ball-milling the dried product is required to give the necessary fines. The procedure has been demonstrated on a 1-kg batch scale.

1. Laboratory Studies of Gel Sizing. — Gel that is formed by drying sol in a tray fractures to a range of particle sizes whose distribution depends on the rate of

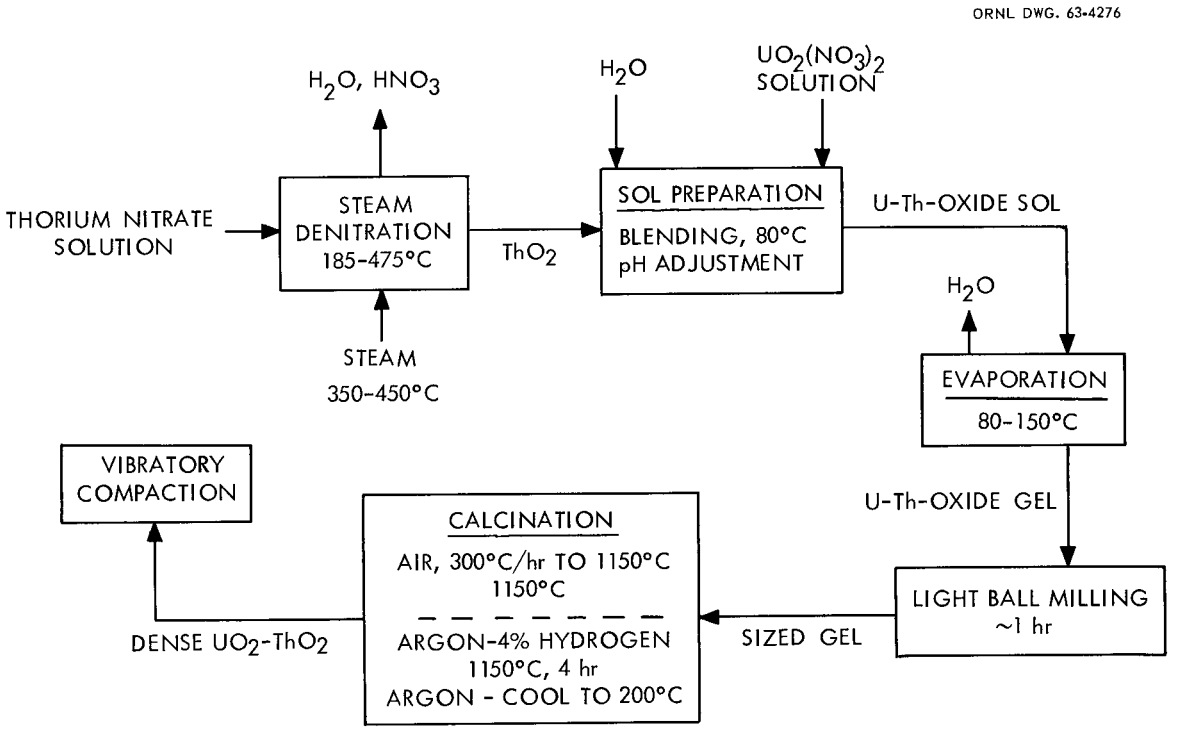

Fig. 20. The Sol-Gel Process with Sizing of the Gel Stage.

drying the gel, once it is formed. The rate, in turn, depends on bed thickness, the maximum temperature of the gel, and the time held at the maximum temperature. The procedure was developed for the thorium oxide gel prepared in the Kilorod Program; consequently, certain factors were held constant, for example, solids concentration (2 M), uranium percentage, depth of sol and thickness of gel. The maximum final gel temperature chosen was 150°C, and the gel was held at that temperature for 1 hr. This time interval and temperature were chosen because they gave a product containing less than 10% of oversize particles (+6 mesh). Lower final temperatures gave from 15 to 20 wt % oversize. In drying sols, although the air temperature is maintained at 150°C, the sol temperature is less than 100°C until all of the free water is evaporated. The temperature of the solids remains below, but approaches, 150°C during the last hour of drying.

The relationship of initial depth of the sol in the drying tray to particle-size distribution is shown in Fig. 21. Two-molar sol at a depth of 2.5 to 3 cm was dried to a gel which, when ball milled for 1 hr, gave a desired particle-size range before calcination. The dry, hot gel was transferred to a porcelain ball mill containing porcelain balls. Batches that were allowed to cool in air absorbed water, causing small particles to stick to the walls and balls of the mill, and to each other. A typical kilogram-size batch of uranium-thorium oxide gel, dried to a final temperature of 150°C, had the particle-size distribution shown in Table 7. The amount of shrinkage of gel particles during calcination at 1150°C was 45 to 55% by volume and about 23% in diameter. When large particles of gel were immersed in water or sol, or sprayed with water or sol, they dispersed into smaller fragments. This provided a method for treatment of the oversize material.

2. Engineering Studies of Gel Sizing. — The effects of ball-milling conditions and of the sol composition and drying conditions were studied with three batches of thoria sol and three of thoria-urania sol. The range of variables was limited, since the thoria product was prepared for a specific purpose, and the thoria-urania product was to be used for a vibratory-compaction test of material sized while in the gel state.

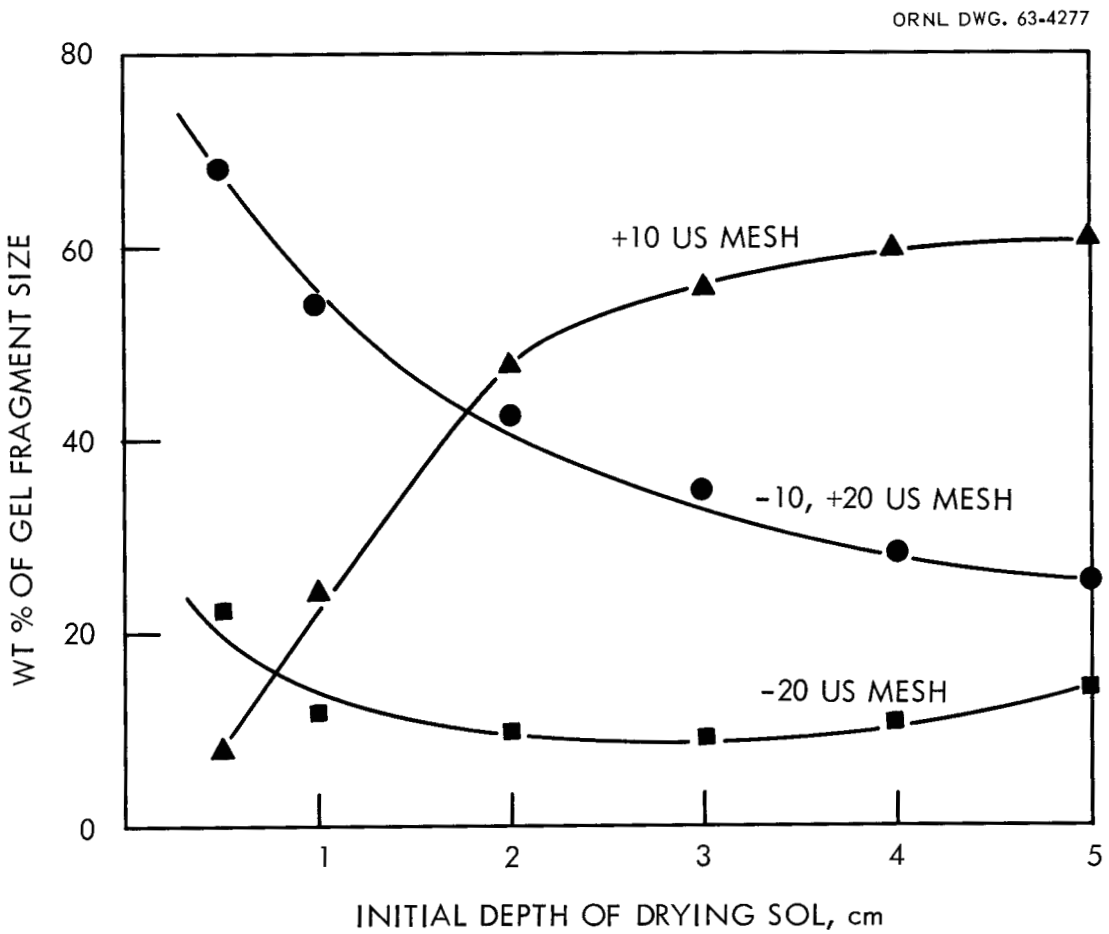

Fig. 21. Effect of Depth of Sol on Dried Gel Fragment Size.

Table 7. Size Distribution of Gel-Sized Uranium-Thorium Oxide After 1 hr of Ball Milling

Drying conditions: Initial sol depth, 2.5 cm; final drying temperature, 150°C; discharged from oven to ball mill hot, milled 1 hr; firing temperature, 1150°C; time, 4 hr; argon - 4% H_2

Size (U. S. std. mesh)	Wt % in Size Range	
	Before Firing	After Firing
+6[a]	9.3	3.4
-6, +10	38.7	32.5
-10, +20	16.8	24.0
-20, +100	9.7	12.2
-100, +200	5.3	3.7
-200	21.0	24.0

[a]Oversize for Kilorod application.

The results show that the amounts of +16 and -16 mesh material may be varied over wide ranges by variations in the ball-milling conditions (Table 8). The weight percentage in each size range was reproducible to about ± 10%. Most of the comminution of +16 material to -16 occurred in the first 20 min of ball milling. Continued milling after 20 min was more effective for reducing the 16-to-100 mesh material to -100 than it was for reducing +16 to -16 mesh. The ball-milling conditions that gave about 40 wt % of -16 mesh material left 8 to 32 wt % of +6 mesh material, which would be too large for most vibratory-compaction uses.

The weight of gel charge, the weight of balls, and the size of balls all significantly affected the size distribution of the product. While the conditions to be used in a larger mill would have to be determined experimentally, the results would guide the selection of conditions. Larger balls break up the larger particles more effectively, while small balls favor the formation of -200 mesh material. The rate of formation of fines increased somewhat, but not in proportion, when either the weight of gel or of balls was increased.

Table 8. Effects of Ball-Milling Conditions on Gel Sizing

Ball mill: 2200-cc porcelain jar, about 5 in. in inner diameter; rotation rate, 78 rpm
Screens: U. S. Standard

	Ball-Milling Conditions				Gel Size Distributions (wt %)			Calcined Oxide Size Distributions (1150°C, air atmosphere) (wt %)					
Material	Weight of Gel (g)	Weight Ratio Balls/Gel	Ball Diameter (in.)	Time (min)	+6	+16	-16	+6	6/16	16/20	20/100	100/200	-200
Thoria	927	0.22	1[a]	10	26.1	56.4	43.6						
	1597	0.13		10	43.3	74.5	25.5	16.4[b]	43.9	6.8	16.3	4.5	12.2
	1394	0.15		20	20.8	56.5	43.5						
Thoria	924	0.22	1	5	43.7	71.9	28.1						
	912	0.22		10	33.4	65.4	34.6						
	1105	0.19		15	26.3	57.5	42.5	12.7	39.9	7.7	18.6	5.9	15.2
	981	0.21		20	31.9	56.6	43.4						
	1603	0.13		30	19.0	53.7	46.3						
Thoria-urania	705	0.57	0.5[c]	120	-	37.0	63.0	25.7	11.0	0.3	0.9	3.7	58.4
	1193	0.36	0.5	120	-	49.6	50.4	34.3	14.5	0.7	0.8	0.8	49.0
	612	0.33	0.5	120	-	40.4	59.6	25.2	14.2	0.8	1.5	1.4	56.9
	999	0.21	0.5	120	-	55.1	44.9	34.2	19.0	1.5	2.0	1.0	42.3
	1003	0.21	1[a]	10	41.6	65.1	34.9	26.3	34.0	5.7	14.9	5.1	14.1
	967	0.21	1	10	41.6	65.3	34.7	22.9	37.7	5.6	14.3	4.9	14.7
	1001	0.21	1	120	-	37.5	62.5	25.4	11.9	0.4	1.8	8.2	52.4
	506	0.41	1	120		24.7	75.3	17.5	6.8	0.4	1.0	9.0	65.3

[a] One-inch balls (approximately spherical Al_2O_3)

[b] This was 6.1 wt % of +4 mesh material.

[c] Half-inch "balls" (ellipsoidial river gravel, about 3/8 x 1/2 x 3/4 in.)

The drying temperature and the NO_3^-/Th or NH_3/Th mole ratios in the sol significantly affected the size distributions in the product, while the other sol composition and drying variables had little effect (Table 9). The size distributions did not vary significantly over the range 1.9 to 3.2 cm of sol depth in the drying trays. Also, increasing drying time from 22 hr to 70 hr had little effect. Thoria-urania sols dispersed under optimum conditions gave about the same size distribution as thoria sol when dried under comparable conditions. The amount of +6 mesh product decreased from 20 to 30 wt % at a 90°C drying temperature to 9 to 16 wt % at 135°C and 2% at 155°C. An increase in the NO_3^-/Th and NH_3/Th ratios using the 135°C drying temperature also reduced the fraction of +6 mesh to 2 wt %. The fractions of -16 and -200 mesh material were nearly the same for all drying temperatures (35 to 40 wt % and 11 to 15 wt %, respectively, for 10 min of ball milling). Thus, the principal effect of the drying temperature was to determine whether the large particles were +6 or 6 to 16 mesh.

The rates of evaporation in the drying ovens were limited by the heat transfer; visible bubbling did not occur. In the atmospheric drying oven, the air temperature and sol temperature remained below the temperature set on the thermostat for most of the drying, and approached 135 or 150°C only as the gel approached dryness. The gel was charged into ball mill jars preheated to about 100°C. No caking was observed, and all the product discharged as free-flowing material. The densities of the thoria-urania products were 8.7 g/cc when vibratorily packed in 1/2-in.-diam, 6-ft-long tubes.[9]

Several possible improvements should be tested if gel sizing is to be used in a future installation. A continuous ball or rod mill designed to discharge only -6 or -10 mesh material could be used to eliminate the oversize and the messy charge and discharge operations. A large mill diameter and large balls or rods would probably crack the large gel particles without producing an excess of fines. Routine preparation of material which will pack to 8.9 or 9.0 g/cc should be demonstrated with the best procedures indicated by the previous results.

Table 9. Effects of Sol Composition and Drying Conditions on Gel Sizing

Sol: 2 M ThO_2 charged to drying oven; pH adjustment of thoria-urania sols by addition of ammonia in a 0.017 = NH_4OH/Th mole ratio

"Vacuum" drying oven: Slight vacuum with small air purge; about 90°C

Atmospheric-pressure drying oven: 750-w on-off control set for final temperature of 135 to 150°C; small air purge

Ball-mill conditions: 2200-cc porcelain jar, about 5 in. in inner diameter; about 1000 g gel and 210 g of 1-in. Al_2O_3 balls rotated at 78 rpm for 10 min, unless otherwise noted.

Material	NO_3^-/Th Ratio in Sol		Dry Conditions			Gel Size Distributions (wt %)			Calcined Oxide Size Distributions (wt %) (1150°C, air atmosphere for calcination)					
	Added	Total	Sol Depth (in.)	Final Temperature (°C)	Time (hr)	+6	+16	-16	+6	6/16	16/20	20/100	100/200	-200
Thoria-urania	0.077	0.109	3/4	135	~22	33.3	62.7	37.3	-	-	-	-	-	-
	0.077	0.109		155	~22	19.5	59.0	41.0	2.0	46.9	10.3	24.0	4.7	12.1
	0.077	0.109[a]		135	~22	24.0[a]	60.1	39.9	8.9[a]	45.5	7.6	20.4	4.8	12.8
	0.077	high		135	~22	9.7	53.6	46.4	1.9	40.6	12.6	28.2	5.5	11.2
	0.077	0.138	1-1/4	90	>500	41.6	65.1	34.9	26.3	34.0	5.7	14.9	5.1	14.1
	0.077	0.138	1-1/4	90[b]	>500	35.0[b]	63.4	36.6	-	-	-	-	-	-
	0.077	0.109	3/4	135	~22	18.4[f]	32.4	67.6	9.8[f]	20.7	2.1	9.8	13.5	44.1
	0.077	0.138	1-1/4	90	>70	-	37.5[f]	62.5	25.4[f]	11.9	0.4	1.8	8.2	52.4
Thoria	0.077	0.109		135	~22	33.4	65.4	34.6	-	-	-	-	-	-
	0.077	0.125		135	~22	31.1	68.6	31.4	-	-	-	-	-	-
	0.070	0.125		135	~22	26.1	56.4	43.6	-	-	-	-	-	-
	0.077	0.125		148	70	13.4	57.0	43.0	-	-	-	-	-	-
Thoria	0.070	0.125	3/4	135	~22	43.3[c]	74.5	25.5	-	-	-	-	-	-
	0.070	0.125	1-1/4	135	~22	47.4[c]	75.7	24.3	-	-	-	-	-	-
	0.077	0.125	1-1/4	135	66	35.5[c]	20.2	19.8	-	-	-	-	-	-
Thoria	0.077	0.109	1	135	~22	19.0[d,e]	43.7	46.3	-	-	-	-	-	-
	0.077	0.125	3/4	150	~22	8.7[e]	34.1	65.9	-	-	-	-	-	-

[a] No pH adjustment.

[b] Gel dried at 90°C and then heated to 150°C before ball milling.

[c] About 1600 g of gel and 0.13 ball/gel weight ratio used for ball milling.

[d] About 1600 g of gel and 0.13 ball/gel weight ratio.

[e] Thirty minutes ball-milling time instead of 10 minutes.

[f] Ball-milling time of 120 minutes instead of 10 minutes.

3.1.2 Formation of Gelled Microspheres from Oxide and Oxide-Carbon Sols

Laboratory and engineering studies were conducted for the formation of near-perfect microspheres of thorium oxide, uranium-thorium oxide, and uranium oxide-thorium oxide-carbon gels 30 to 1000 μ in diameter. The preferred method of microsphere formation is jet-dispersion of sol from a two-fluid nozzle into a liquid that has negligible solubility in the sol, moderate capacity for dissolving water, and negligible tendency to extract thorium, uranium, or carbon from the sol. Slow extraction of water from the sol microspheres leads to strong gel microspheres, which can be handled, further dried, and finally fired to dense spheres of oxide or carbide. In the jet of the spray nozzle, the sol is discharged from a capillary tube at the center, and the forming liquid flows concurrently from an annulus around the sol duct. The organic extractant also disperses the very fine stream of sol to droplets. In this system, ThO_2 and uranium-thorium oxide particles 50 to 1000 μ in diameter have been formed and dried. An alternative involves dispersion of the sol by pouring it into solvent stirred in a pot.

In order to prepare sols suitable for forming microspheres, it was necessary to modify the basic sol-gel process. The schematic flowsheets for the modified processes are shown in Fig. 22. Oxide sols 2.5 to 5 M in Th or U + Th have been successfully formed into spheres, using 2-ethylhexanol as the sphere-forming and water-extracting fluid, with Armour Ethomeen S/15 as a surfactant. For oxide-carbon sols having a C/Th mole ratio of 4.5 to 5, the ThO_2 concentration range for well-formed spheres was from 1 to 2 M, depending on the viscosity of the sol and on the size of spheres desired.

Column operation appears to be more promising than a stirred pot for microsphere preparation in a remotely operated plant because, in a column, droplet sizing and sphere suspension can be controlled separately. With a feeder mechanism that can deliver controlled, uniform droplets, semicontinuous operation is possible. Technology for remotely operated pumps, valves, and columns using organic extractants is well developed. Column operation has been shown to give oxide microspheres having a range of desired sizes between 50 and 1000 μ, and also other desired properties such as good integrity, high density, and extremely high strength.

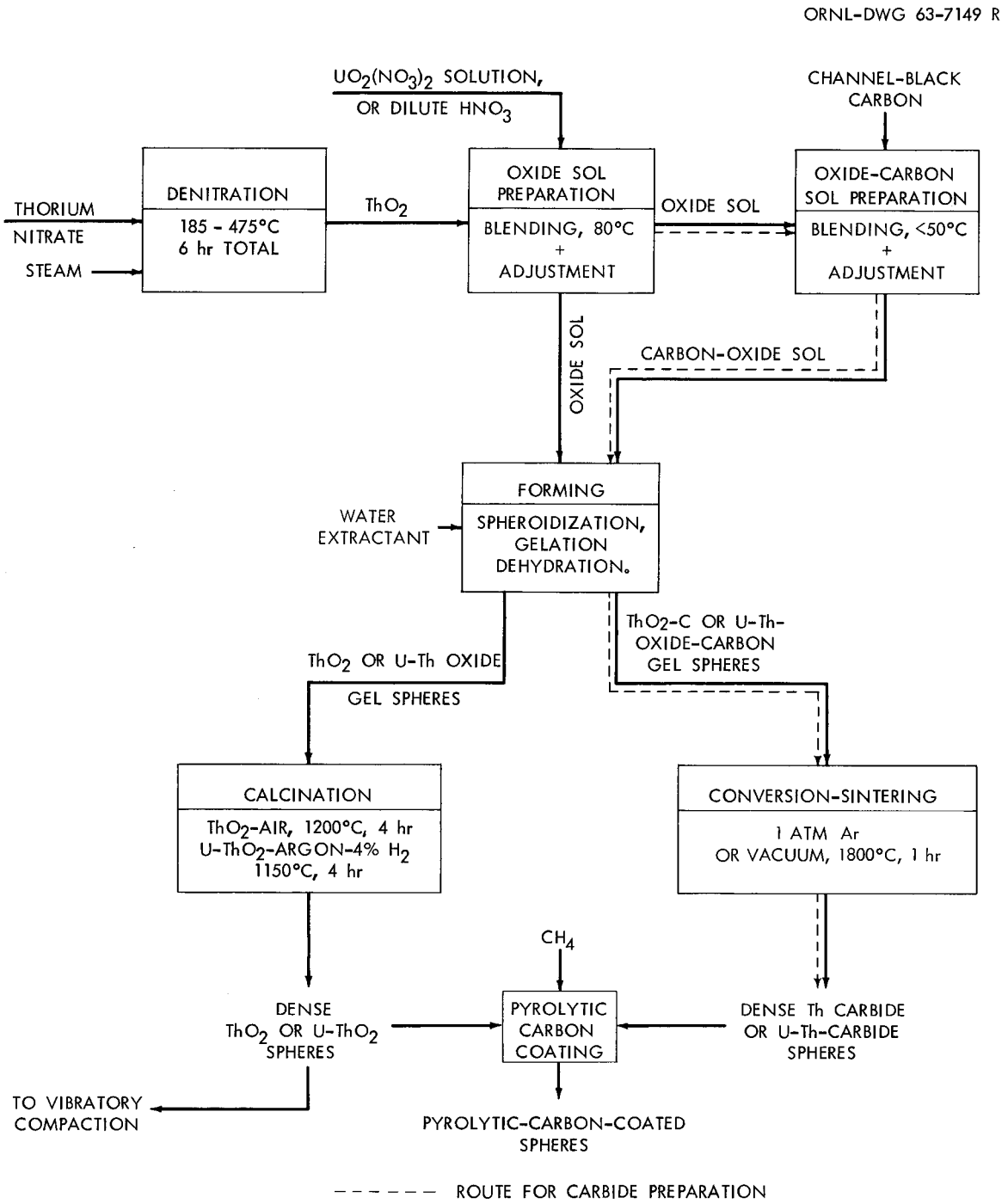

Fig. 22. Sol-Gel Process for Preparation of Dense Spheres of U-Th Oxides or Carbides.

The scope of engineering development included the design and testing of two kinds of spray nozzles for forming sol spheres, three sizes of drying columns and distillation equipment for removing water from the extractant.

Laboratory Studies

1. Preparation of Oxide Sols. — Thorium oxide sols and sols with U/Th ratios of up to 0.05 were prepared by the same procedures optimized for previous sol-gel flowsheets.[10] Uranyl nitrate solutions with NO_3^-/UO_2^{2+} ratios as low as 1.5 were stable and were used to obtain higher U/Th ratios without exceeding the preferred NO_3^-/Th ratio. For special, accelerated irradiation tests, a uranium-thorium oxide sol containing about 8% uranium is needed. The standard sol preparation, with uranyl nitrate as the source of uranium, can be used up to about 5% uranium without exceeding the maximum allowable NO_3^-/ThO_2 mole ratio. For the 8% uranium-thorium oxide sol at a concentration of 3 M ThO_2 (optimum for forming 200- to 600-μ-diam spheres in 2EH), an NO_3^-/ThO_2 mole ratio of 0.06 rather than 0.077 was required to control viscosity to a value low enough to permit passage through the orifice of the forming nozzle. The preparation was made by dispersing steam-denitrated ThO_2 with 0.06 mole HNO_3 per mole of ThO_2, then mixing $UO_3 \cdot 2H_2O$ with the thoria sol. Forming and drying 200- to 400-μ spheres in the intermediate column with the two-fluid nozzle and drying with 2EH-Ethomeen S/15 gave no unusual problems.

2. Preparation of Oxide-Carbon Sols. — The procedure used to add the carbon necessary for carbide formation to the sols is discussed in Section 3.1.3.

Of the 14 water-immiscible solvents screened (including alcohols, esters, hydrocarbons, and ethers) for oxide-carbon microsphere formation, 2-ethyl-1-hexanol (2EH) was the most successful. The criteria for selection were: (1) formation of a high percentage of spheres, and (2) a minimum of surface defects and internal voids after drying and firing. In addition to having a favorable combination of physical and chemical properties for forming, the 2EH flash point is 185°F. The water-2EH azeotrope boils at 98°C, providing a simple method for regenerating the solvent.

In early work on microsphere formation, CCl_4 was used with varying amounts of isopropyl alcohol to give controlled capacities for water. Carbon tetrachloride—20% isopropyl alcohol worked well in a stirred-pot method for forming and drying, but very poorly in a column. In screening other solvents for column operation, halogenated solvents and other toxic solvents were avoided because of likely health hazards and halogen contamination of the product. Solvents having a low flash point were also eliminated because of the fire hazard.

3. Selection of Surfactants. — To form spheres of thorium oxide or uranium-thorium oxide, a surfactant was added to the organic phase in order to prevent the sol droplets from coalescing, adhering to the walls of the column, distorting, or clustering. Of about 20 surfactants screened, only the water-in-oil types exerted any beneficial modification of the drying solvent (2EH). The anionic surfactants, for example, Geigy's Sarkosyl-O (oleyl amide of N-methylglycine) extracted some of the thoria into the organic phase. Cationic surfactants were satisfactory for ThO_2 sols, and, of these, Geigy's Alrosperse-100 and Amine-O and Armour Ethomeens, T/15, S/15, 18/15 were best. Non-ionic surfactants were required for preparations that contained uranium.

For sols containing carbon, the lyophilic carbon itself behaved as a surfactant in 2EH, but, without the use of additional surfactant, carbon tends to transfer to the organic phase. The non-ionic fatty acid derivatives of Carbowax appear to give spheres having surfaces with the fewest defects and to prevent extraction of carbon. Of these, Hodag 40 R (mixed mono-oleate and mono-ricinoleate of Carbowax 400), Paraplex-62, and 2-octanol were the most effective.

Engineering Studies

1. Dispersion and Drying by Agitation in a Pot. — The first microsphere-formation studies were done with thoria. A 2 M thoria sol was converted to spheroids by adding it in a fine stream at room temperature to carbon tetrachloride, containing 10 to 30% by volume of isopropyl alcohol, which was agitated by a flat-blade rotary agitator (100 to 500 rpm). At the end of 10 to 20 min of agitation, the sol drops had

set to gel beads, which were separated from the forming bath, washed free from CCl_4 with isopropyl alcohol, oven dried at 100°C, and then fired for 4 hr at 1200°C. Similar procedures were also used to form microspheres from thorium oxide-carbon and 3 wt % uranium-thorium oxide-carbon. Variations in conditions were required for each type, as illustrated by Table 10.

The thoria microspheres formed at 370 rpm had (after firing) the following physical properties: density by helium pycnometry, 9.94 g/cc; BET (N_2) surface area, 0.006 m^2/g; average geometric surface area, 0.003 m^2/g; average crushing strength (10 particles) 976 g (the range was 622 to 1722 g). The thoria-carbon spheres were more porous, had a "matte" rather than reflective surface and were weaker, but sufficiently strong for process handling.

About 700 g of thoria spheres and several 60-g batches of uranium-thorium oxide spheres of 150 to 250 μ diameter and of high density and good strength were prepared by this method for various groups for use in further experimentation.

2. Development of Dispersion Nozzles. — Preparation of microspheres of controlled diameters by the extraction of water into a solvent requires the formation in the solvent of sol droplets of a controlled diameter. Conversion of sols 0.5 to 5.0 M in Th + U oxides to calcined oxide microspheres of near theoretical density requires that the sol drops first formed be 2 to 4 times the final diameter desired. A primary objective in the microsphere-preparation studies was to produce 150- to 250-μ-diam microspheres. However, other sizes will probably be desirable for particular uses, and therefore a technique which could be controlled to give spheres having a diameter anywhere in the range of 5- to 1000-μ-diam was desired.

The breakup into droplets occurs by several mechanisms, the predominant one depending on the sol properties and flow rates, the nozzle dimensions, and the properties and agitation of the drying solvent. The conditions that result in these mechanisms for the breakup of liquid jets have been correlated with the relative velocity of the jet and the solvent used as dispersion medium. These mechanisms and the important variables are as follows:

Table 10. The Effect of Stirring Speed on the Size of Oxide and Oxide-Carbon Microspheres

Sol Composition:

A. ThO_2 sol: 4.6 moles ThO_2/liter; HNO_3^-/ThO_2 mole ratio, 0.077; surfactant, Span-80.

B. ThO_2-carbon sol: ~1 mole ThO_2/liter; C/ThO_2 mole ratio, 5 NO_3^-/ThO_2 mole ratio, 0.077; ethoxylated soybean oil surfactant.

C. (ThO_2-3 mole % UO_2) - carbon sol: ~1 mole ThO_2/liter; C/ThO_2 ratio: 4.3; NO_3^-/ThO_2 ratio: 0.077; ethoxylated soybean oil surfactant.

Apparatus: Flat-blade rotary turbine stirrer in a 4-liter beaker

Forming Fluid: Carbon tetrachloride - 20 volume % isopropyl alcohol

Gelling Time: About 20 min

Temperature: About 26°C

Sol	Stirring Speed (rpm)	Mean Particle Size[a] (μ)	Particle Size Distribution[b] (γ)	Yield of 150- to 250-μ-Diam Particles (%)
A	330	190[c]	1.6	45
	350	182[c]	1.4	50
	370	160[c]	1.4	56
B	230	194	1.5	47
	300	100	1.6	5
	300	104	1.6	5
C	200	255	3.3	35
	240	115	2.3	20
	265	132	1.5	30

[a]Geometric mean

[b]Standard deviation from geometric mean

[c]Calcined at 1200°C for 4 hr

1. At low flow rates of sol and with the nozzle stationary with respect to the dispersant, the drop is formed in agreement with the hanging-drop model. The drop size is controlled by the wetted perimeter of the nozzle, the interfacial tension, and the density difference between the two phases.

2. When a continuous jet of liquid is formed with only a moderate velocity difference between the two phases, the liquid jet breaks up into lengths of about 4.4 diameters, which then form drops with diameters about twice that of the jet. This behavior has been predicted theoretically and observed experimentally,[11] and is termed a "varicose disturbance".

3. At velocities above a critical velocity, the breakup is controlled by viscous and inertial forces that result in disruption of the jet and the formation of droplets of small diameter. This mechanism would probably give less uniform drops than either the falling-drop or the varicose mechanisms.

The falling-drop mechanism was studied by discharging the sol through an orifice (0.006 in. or 0.015 cm was the most common diameter) at a low flow rate with a few inches of sol-fluid head. Theoretically, the drop diameter D should be related to the orifice diameter d, the interfacial tension γ, and the density difference between sol and solvent $\Delta\rho$ by:

$$D = \left(\frac{6d\gamma}{\Delta\rho \underline{g}} f\right)^{1/3} . \qquad (1)$$

The empirical correction factor f is usually about 0.6 for liquid drops. The constant $\underline{g}$ is the gravitational constant. Substituting values for a 3 $\underline{M}$ thoria sol and an interfacial tension of 15 dynes/cm, the values of D and d in cm are related by:

$$D = 0.4d^{1/3} . \qquad (2)$$

Thus, the 0.015-cm-diam orifice would give about 1000-μ-diam drops. Droplet diameters in agreement with the falling-drop model were obtained. However, the very small orifices (less than 0.001 in.) necessary to obtain the smaller drops desired were not practical due to plugging by the thixotropic and pseudoplastic sols.

In one study of the hanging drop model, a 4.9 M thoria sol was fed through a 6-mil-diam orifice immersed in 2EH containing 0.1 vol % Paraplex G-62. The interfacial tension between the sol and organic phases was 15.4 dynes/cm, and the density difference was 1.33 g/cc. From Eq. (1) the predicted droplet diameter would be 870 μ, which would give a diameter of 440 μ after calcination at 1150°C. The diameter of the calcined thoria spheres prepared by the preceding procedure measured 540 μ (Fig. 23). If the empirical factor f in Eq. (1) is 1.0, then the predicted sol drop diameter is 1030 microns which would shrink to 520 microns after calcination. With f equal to 1.0 the experimental agreement with Eq. (1) is within 4%.

The most promising technique for obtaining the desired sizes of droplet is an application of the varicose mechanism with a two-fluid nozzle. This nozzle has the conformation commonly used for a gas-driven liquid-atomizing spray nozzle (Fig. 24). The sol is fed through the center tube, while the drive fluid (2EH or any other drying solvent used) is fed through the concentric outer nozzle. The two-fluid nozzle using a drive fluid has an advantage over a single nozzle without a drive fluid in that the sol channel may be much larger, thus reducing the probability of plugging. When the sol drop is produced by the varicose mechanism, the sol jet stream diameter must be about half the desired drop diameter. If it were necessary for the nozzle diameter to be the same size as the sol jet stream, the nozzle orifice would have to be undesirably small (0.005 to 0.100 cm). However, the drive fluid coming from the annulus can accelerate the sol stream after it leaves the nozzle and thus reduce the diameter of the sol jet. In this manner, a 0.005-cm-diam sol jet stream can be obtained from a much larger nozzle. In addition, the sol jet diameter may be varied by varying either the sol flow rate or the drive-fluid flow rate. For a simple nozzle, the sol droplet diameter is controlled only by the orifice diameter. Still another advantage is that the critical velocity above which disruption by viscous and inertial forces

ORNL-PHOTO 64192

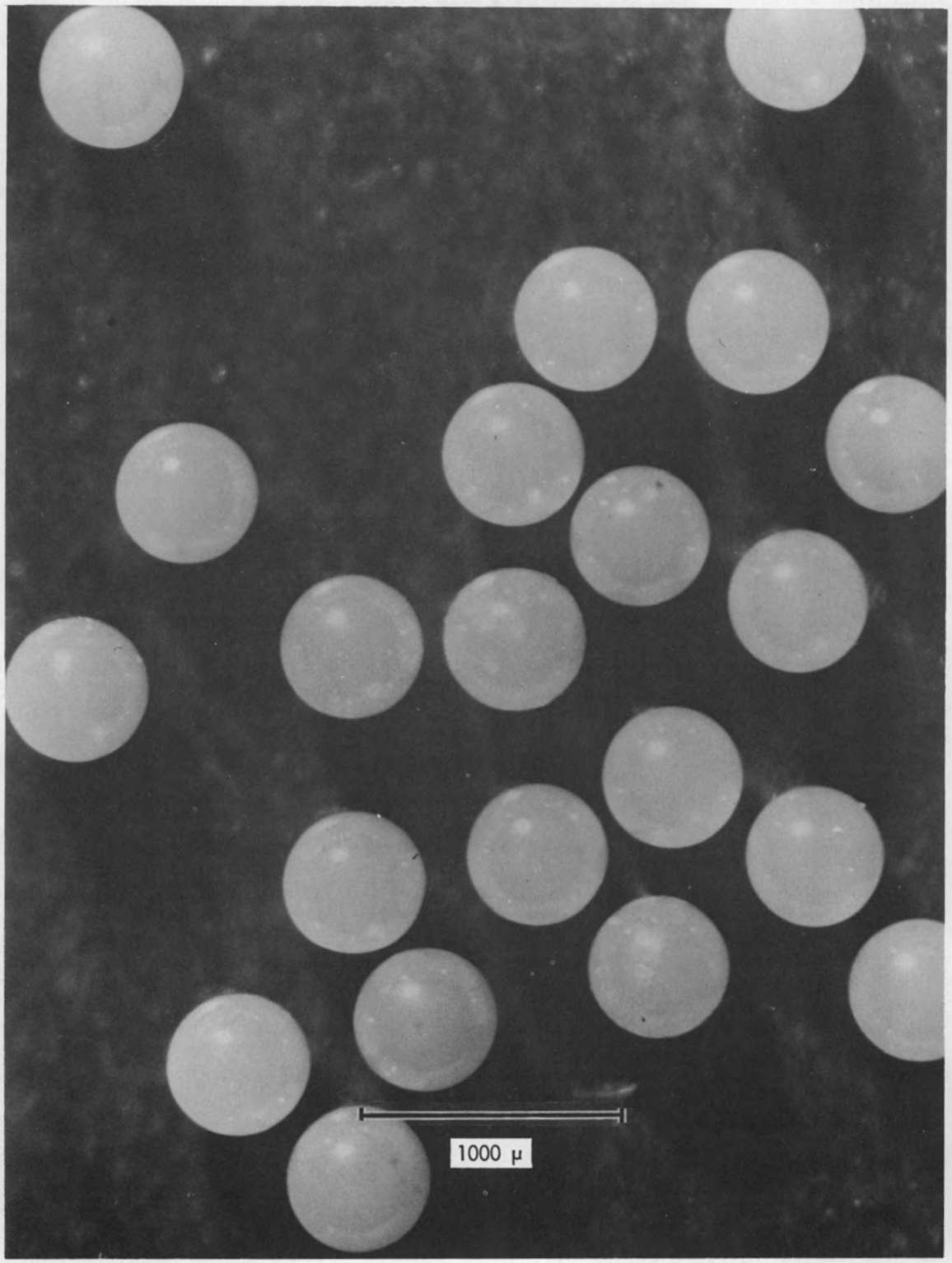

Fig. 23. Thoria Spheres Formed in a Fluidized Column of 2-Ethylhexanol and Paraplex G-62 and Calcined to 1150°C.

ORNL-DWG 64-243

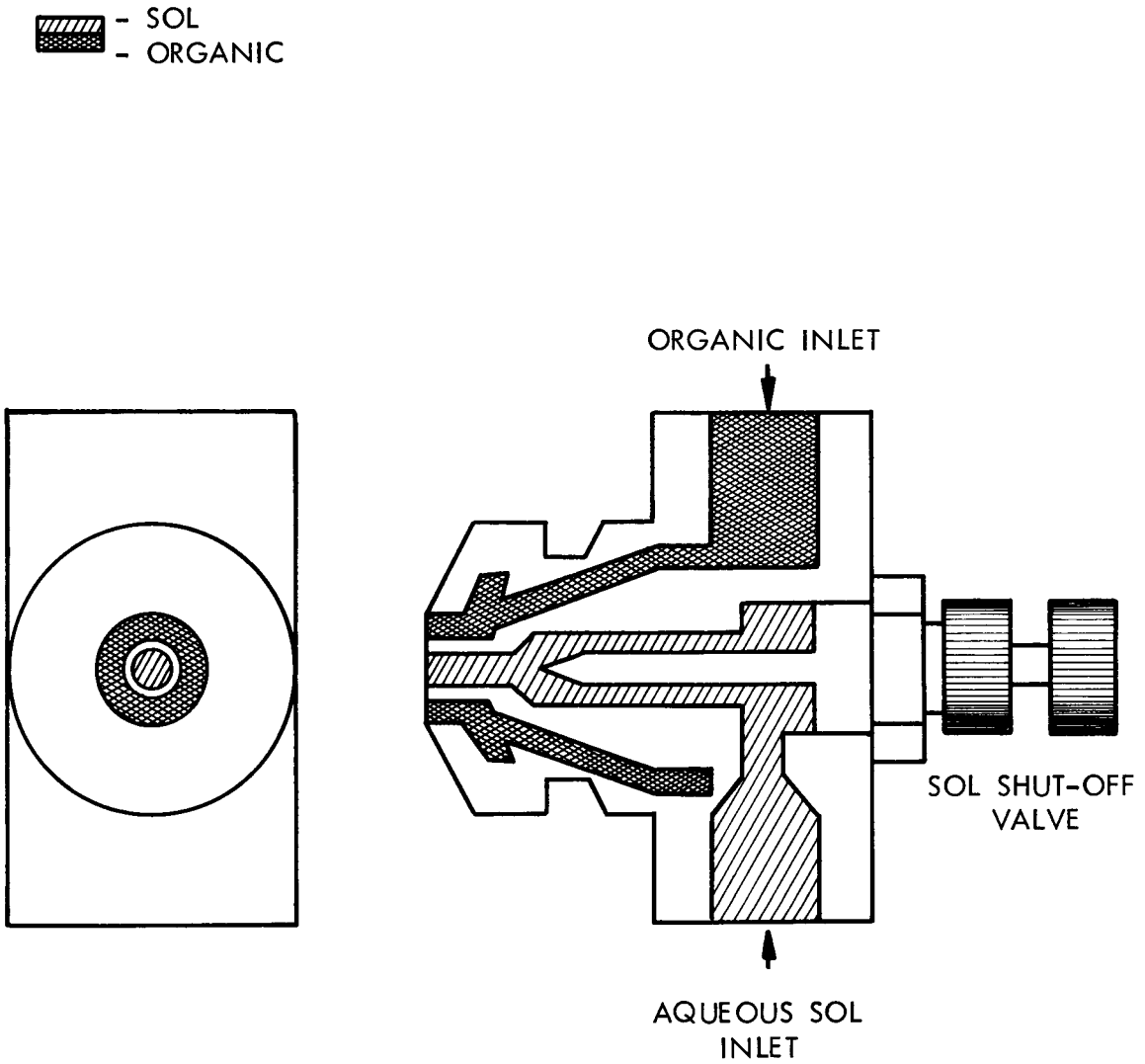

Fig. 24. Front View and Cross-Section of a Two-Fluid Nozzle.

occurs would be low for the small sol jet diameter and the high-viscosity drying solvent. Therefore, the varicose disturbance mechanism of jet breakup would not be practical for a simple single nozzle since the falling drop and disruptive mechanisms might even overlap. By using the two-fluid nozzle, the relative velocity of the sol jet and the adjacent solvent is small, even though the velocity of the jet relative to the nozzle is large.

The droplet diameter to be expected from the two-fluid nozzle in the varicose-disturbance-mechanism regime may be estimated by assuming that the sol jet is accelerated to the drive fluid velocity and then breaks up to give sol drops whose diameter is about twice the jet diameter. A volume balance gives the following relationships:

$$\text{Sol flow rate} = f = \left(\frac{\pi d^2}{4}\right) V \cong \left(\frac{\pi D^2}{16}\right) V,$$

where d = the sol jet diameter,

D = the droplet diameter,

V = the drive fluid velocity.

The drop diameter may be expressed in terms of sol flow rate and solvent (drive fluid) flow rate by using the expression:

$$\text{Drive fluid flow rate} = F = AV,$$

where A is the nozzle area (area of the annulus) for the drive fluid flow.

Solving for the drop diameter:

$$D = 2.3 \sqrt{\frac{f}{F} A}.$$

Actually, the drive fluid will be slowed down by both the sol and the surrounding solvent. Therefore, the value of D calculated from this equation will be a minimum. Experimental values might be appreciably larger, especially for small drive-fluid-nozzle areas.

In one study of the varicose-disturbance mechanism a 4.9 M thoria sol was fed through the fluid side of a pneumatic atomizing nozzle (Fig. 24) into the top of a column containing 2EH with Sarkosyl O as a surfactant. The organic phase was metered through the air side of the nozzle to increase the velocity of the sol stream. The nozzle setup used was fluid nozzle 2850 and air nozzle 120 which has a drive fluid flow area of 6.0×10^{-2} cm^2. At respective sol and organic flow rates of 1.4 and 440 cc/min, about 65 g of thoria spheres were produced with a mean diameter of 250 μ (after calcination to 1150°C). During this initial feasibility run, 80% of the oxide was within the size range 200 to 300 μ. Equation (3) predicts a sol-droplet diameter of 320 μ, which would shrink to 160 after calcination. The 2EH has a high viscosity; consequently, slowing down of the sol jet by the quiescent bulk solvent probably causes the experimental observed diameters to be larger than those calculated according to Eq. (3).

3. Drying Column for Spherical Sol Droplets. — The feasibility of producing thoria, thoria-urania, and thoria-urania-carbon spherical particles with diameters of 100 to 1000 μ was demonstrated in a fluidized column in which 2EH was used as the forming and drying medium. The sol is dispersed into droplets at the top of a tapered glass column and allowed to settle until the droplet reaches its terminal (fluidizing) velocity. Droplet coalescence and glass wetting are prevented by dissolving a suitable surfactant in the organic phase as discussed above. As water is being extracted from the aqueous sol phase into the organic medium, gelling of the sol droplets occurs, thus allowing the spheres to be removed from the bottom of the column after a holdup time of 10 to 30 min. The gelled particles are dried at 100°C to remove the excess organic liquid and to reduce the water content of the gel to about 5 wt %. On firing to 1150°C, the thoria and thoria-urania spheres have densities close to theoretical crystal density, and they have very high crushing strengths.

Three different tapered glass columns were used in the microsphere studies. The smallest column system (15 in. long and tapered from 1/4 in. ID at the bottom to 1 in. ID at the top) contained only 200 ml of organic solution and was used for testing surfactants. The largest column system studied (described in ORNL-TM-642) held 6

liters and was used for testing the feasibility of using a two-fluid nozzle for making sol droplets. This column is glass and has an included angle of 5°, which creates an uncontrollable flow separation at the column wall. Because of the flow separation, the droplets and gelled spheres were in continuous vertical motion in the column, increasing the probability of droplet coalescence and agglomeration. The bottom organic entrance section to this column is a 3-in.-to-1-in. glass reducer. This increases the flow-instability problem. A flow distributor plate (37 holes, 3/32-in. diam) with 32% free area was inserted below the tapered column at the 1-in.-ID section in an attempt to improve the flow pattern, but it was not significantly improved.

The most satisfactory column system contained 2 liters of solvent and was used for studying the formation of droplets from orifices of different sizes and for producing 30- to 40-g samples of carbon-thoria-urania spheroids. The glass column has a converging, tapered entrance section, 12 in. long, decreasing from 1-1/2 in. to 1/2 in. in inner diameter. The fluidizing (diverging) section of the column increases from 1/2 to 1-1/8 in. in inner diameter in a 24-in. length (included angle of taper is 1-1/2°). Even at a Reynold's number of 400 (based on 1/2-in. diam) the first few droplets produced in the column indicated flow separation at the wall; however, as the droplet population increased, a bed of droplets was formed which dampened the flow instabilities. Within 20 minutes at a sol flow rate of 15 to 20 cc/hr, two distinct beds or layers were formed. A bed containing liquid sol droplets was separated by approximately 1 in. and was above a second bed of gelled particles. The Stokes velocity for a gelled particle is 1.3 to 1.4 times greater than that for a newly cormed droplet (5 M thoria sol). This two-layer phenomenon, which might permit the continuous operation of a column, has persisted throughout several runs in which a uniform droplet size was achieved.

A larger column system was made and installed (Fig. 25) to study the effect of scaleup on flow patterns and to study further the feasibility of a two-fluid nozzle for making droplets. In order to make calcined thoria spheres in the size range of 150 to 250 μ from a 4.9 M thoria sol (density is 2.16 g/cc), droplet diameters between 298 and 495 μ would be required. For an idealized system with this size distribution,

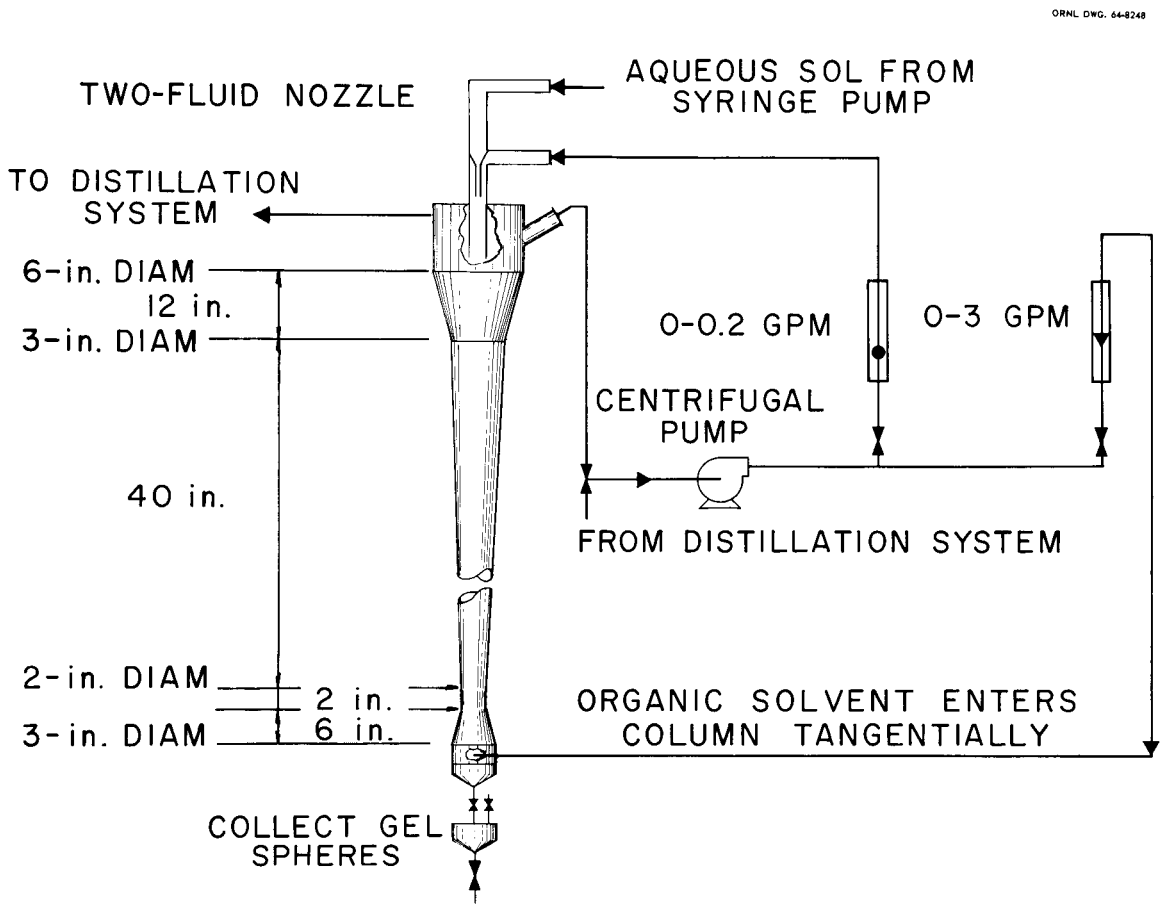

Fig. 25. Schematic Flow Diagram of Equipment for Producing Gel Spheres from Aqueous Sol.

the ratio of Stokes' terminal velocities of the largest gelled particle to the smallest droplet would be 3.81. For a given flow rate this would correspond to a ratio of column diameters of 1.95. With uniformly sized droplets the same ratio of Stokes' terminal velocities reduces to 1.38, corresponding to a required ratio of column diameters of 1.18. Thus, the ultimate sol droplet size distribution that can be achieved will strongly influence the final column design.

About 60 g of calcined thoria spheres (Fig. 26) in the size range of 500 to 600 μ were prepared for studies of their properties. The gel spheres were made by fluidizing "free-fall" sol droplets in 2EH containing 0.1 vol % Paraplex G-62. These spheres were then calcined at 1150 to 1200°C. A cross-sectional view of the calcined spheres is shown in Fig. 27. No indication of internal porosity was detected by either optical or electron microscopy. The following physical properties were determined on the calcined spheres (from runs ICX-16 and ICX-18) density measured by He pycnometry: 9.91 to 9.98 g/cc; BET surface area, 0.003 m^2/g (surface area of perfect spheres of the same diameters: 0.0011 m^2/g; Crushing strength of 20 particles: Fourteen particles did not break at 5710 g (load limit of testing device) and six fractured at an average load of 5425 g.

About 150 g of thoria-urania-carbon gel spheres were prepared for testing various carbon sol preparations. These spheres were made in a fluidized column of 2EH containing Paraplex G-62 surfactant.

4. Method for Drying. — The 2EH fluidizing and gelling solvent extracts water from the sol microspheres, becoming saturated at 2.55 wt % water, but a continuous single-stage distillation can remove the water and regenerate the 2EH. This process would be easy to operate remotely and would require little space inside a "hot" cell.

In the proposed distillation process, a sidestream of 2EH is taken from the sphere-forming system and preheated with the dried 2EH (Fig. 28). The water-saturated 2EH then passes into the still where most of the water goes into the vapor phase. The 2EH, whose vapor pressure is lower, concentrates in the pot. The compositions of the liquid and vapor streams leaving the still are controlled by the temperature (Fig. 29). If the sphere-forming process is operated with 2EH containing

PHOTO 68119

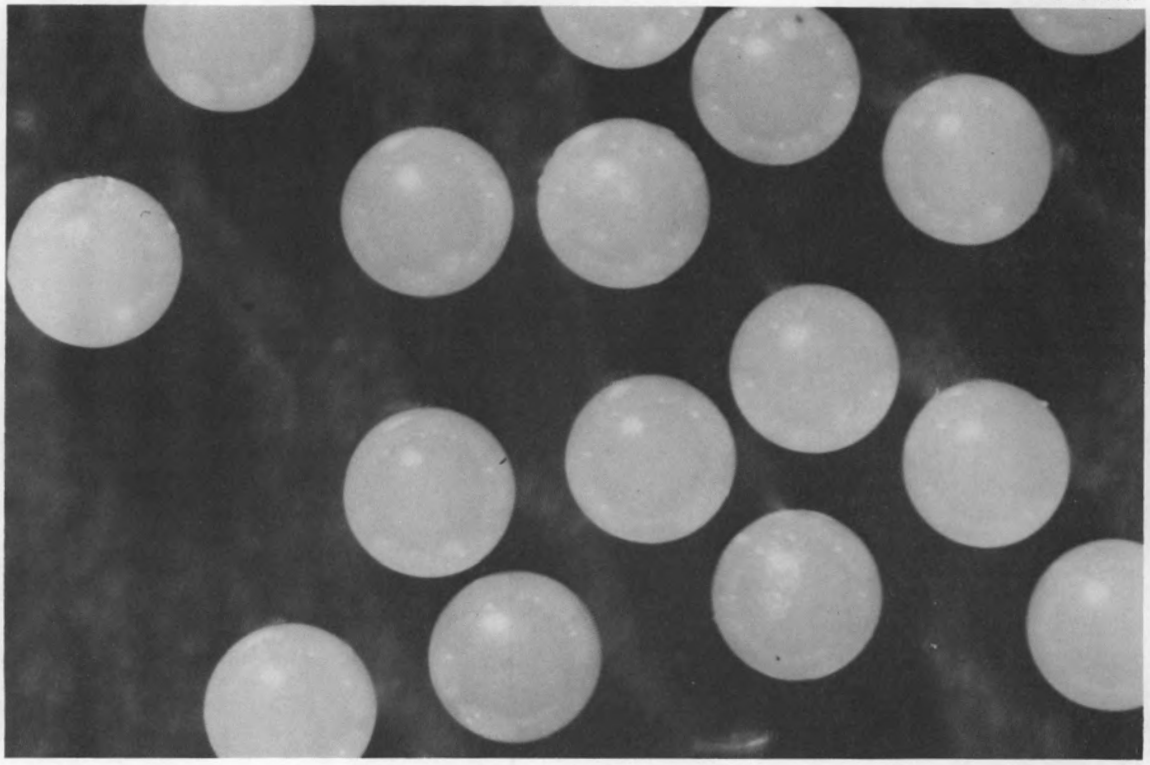

Fig. 26. Sol-Gel Thoria Microspheres Formed by Fluidizing Free Fall ThO_2 Sol Droplets in 2-Ethyl-1-Hexanol. Calcined at 1150°C. (500 to 600 μ diam).

PHOTO 64193

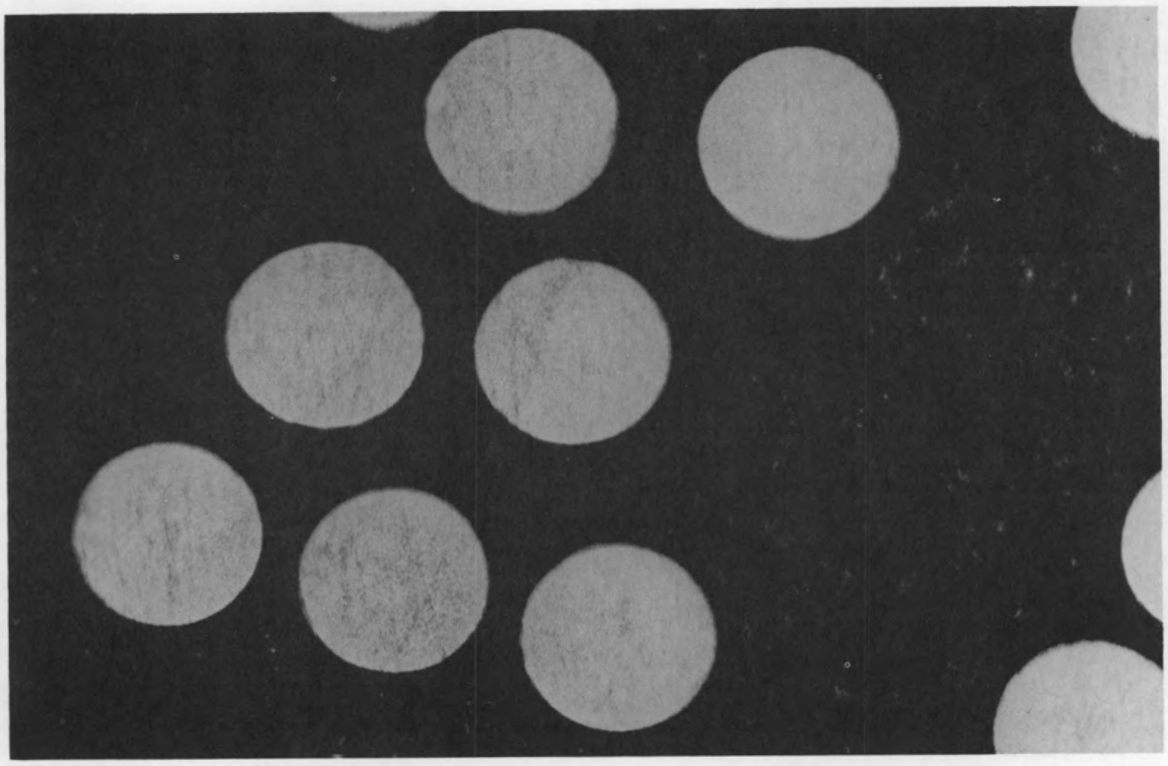

Fig. 27. Cross Section of Thoria Spheres Formed in 2-Ethylhexanol and Paraplex G-62 and Calcined to 1150°C.

ORNL DWG. 65-440

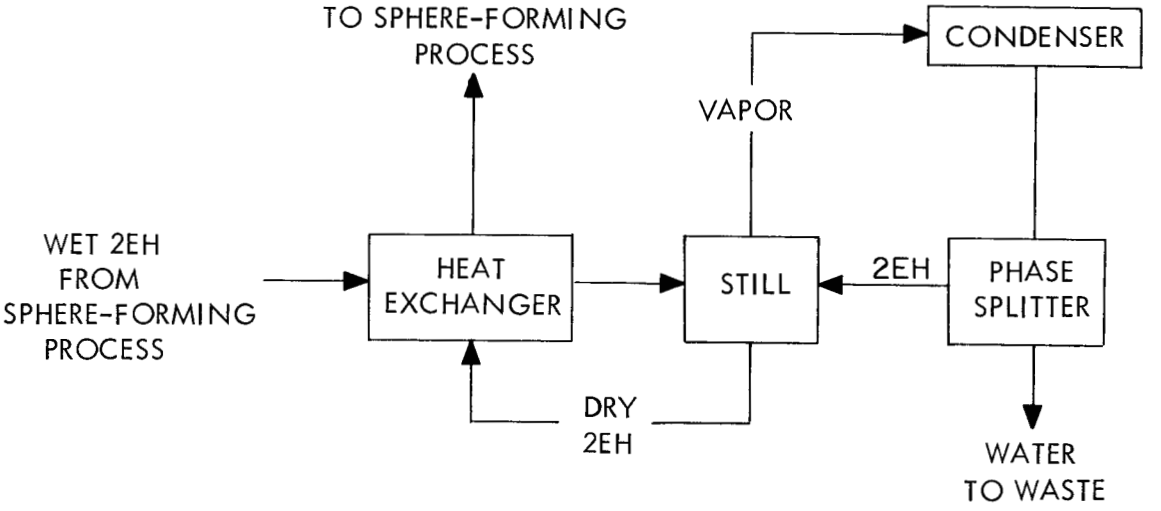

Fig. 28. Flowsheet for Drying Process for 2-Ethylhexanol (2EH).

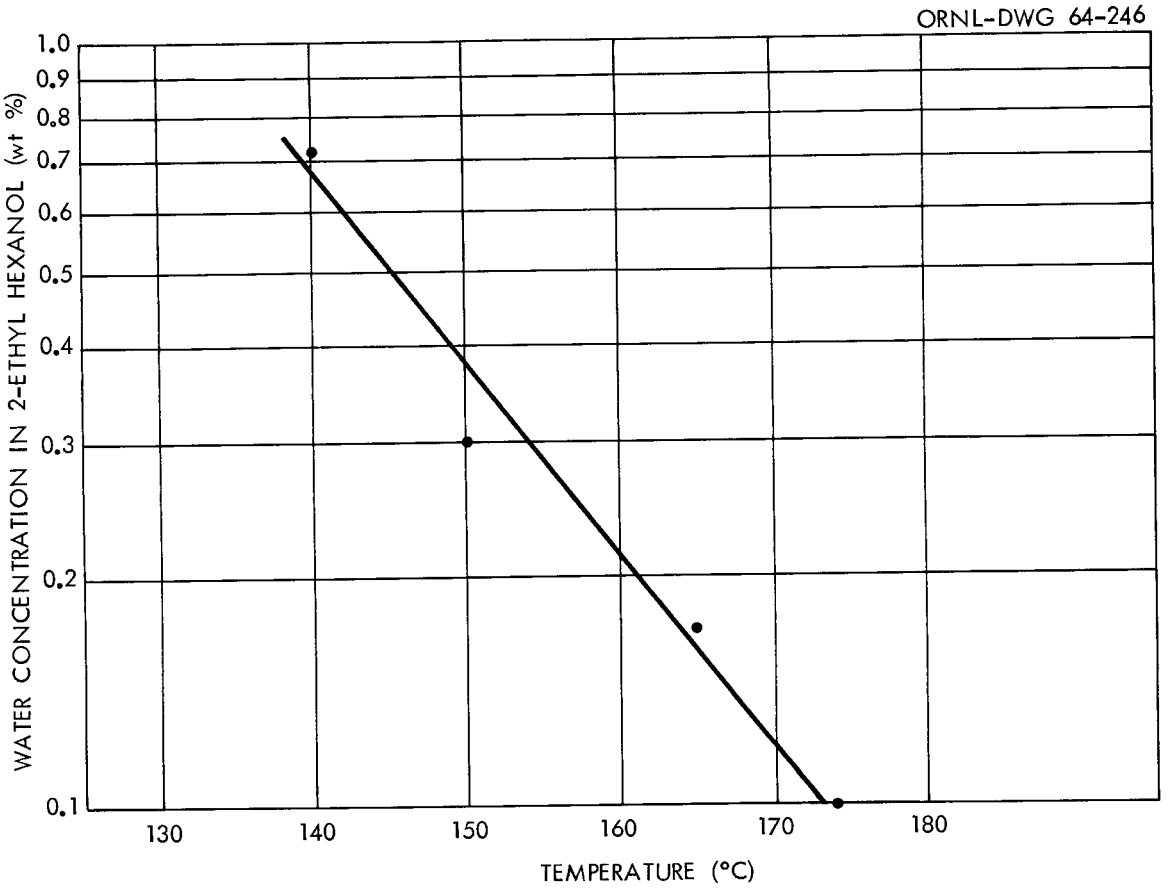

Fig. 29. Temperature Dependence of Water Content of 2-Ethylhexanol (2EH).

1 wt % water and if the still is operated at 145°C, 10% of the feed to the still is vaporized, and the distillate contains 0.5% water. The vapor phase in equilibrium contains 5.5 wt % water and separates into two phases after condensation. The water, saturated with 2EH (0.1 wt %), is thrown away, and, the 2EH, saturated with water, is returned to the still.

A bench-scale unit was constructed to provide the temperature-vs-composition data in Fig. 28 and is being used to regenerate the 2EH used in development studies. By distillation, the water content in the alcohol can be readily reduced to less than 0.1 wt %. The organic system, 2EH with Paraplex G-62 surfactant, was distilled and reused for six runs with no apparent adverse effects.

3.1.3 Preparation of Thorium and Uranium-Thorium Carbide

The basic sol-gel oxide process was modified to prepare microspheroids of carbides of thorium and uranium-thorium. The procedure used is outlined in Fig. 22. It consists of 4 steps: preparation of the thorium or uranium-thorium oxide sol by the sol-gel oxide process; blending high-surface-area lyophilic carbon into the sol; forming the desired size of oxide-carbon microsphere sol drops, then setting them and drying them to gel spheroids by extracting the water; and converting the carbon-oxide to carbide spheroids by heating them in vacuum or under a slow sweep of argon at 1450 to 1800°C.

Both thorium and uranium-thorium carbide samples having C/(U + Th) atom ratios of 1 to 2.2 and U/Th atom ratios of 0.01 to 0.1 were prepared. Near perfect spheres of Th- and U-Th-oxide-carbon were formed and dried in the laboratory drying column (see Fig. 25) in batches of from 2 to 30 g (Fig. 30). These were strong enough in most cases to permit subsequent handling with little breakage. Nearly complete conversion was obtained by calcining the spheroids in vacuum at 1450 for 6 hr or 1750 to 1800°C for 1 hr. Complete conversion in that temperature-time range was not achieved in flowing argon, probably because of poor contact between argon and the spheres, but complete reaction was realized at 2000°C to 2100°C, at the reaction

PHOTO 68121

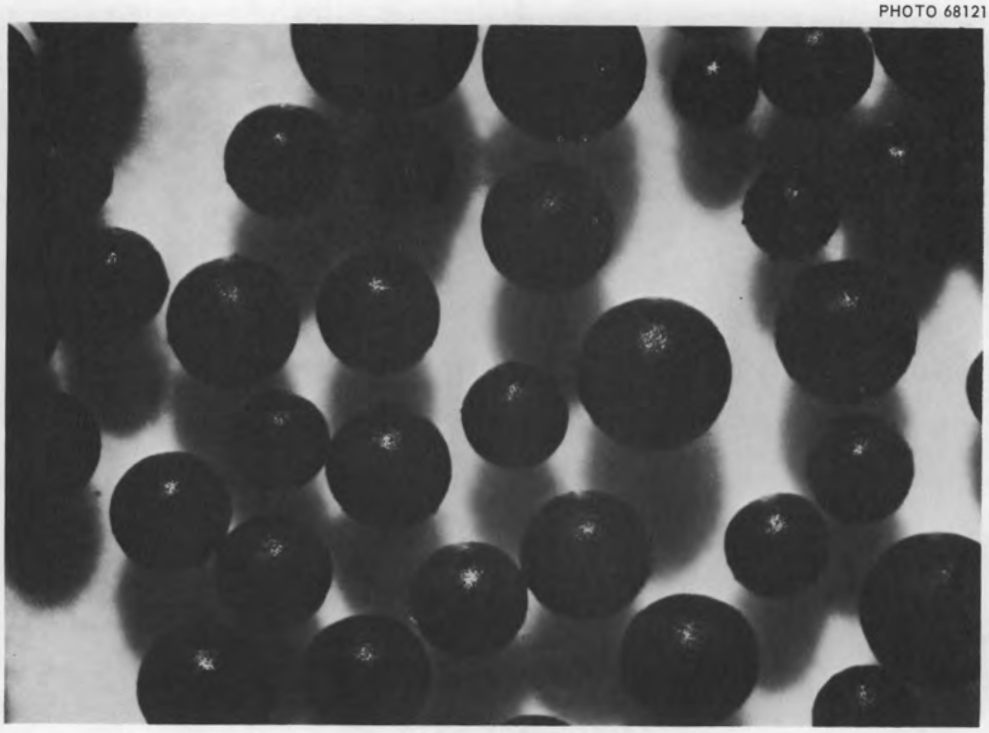

Fig. 30. Microspheres of Uranium-Thorium Oxide-Carbon Gel Prepared by the Sol-Gel Carbide Process. (320 to 580 μ diam).

Y-56029

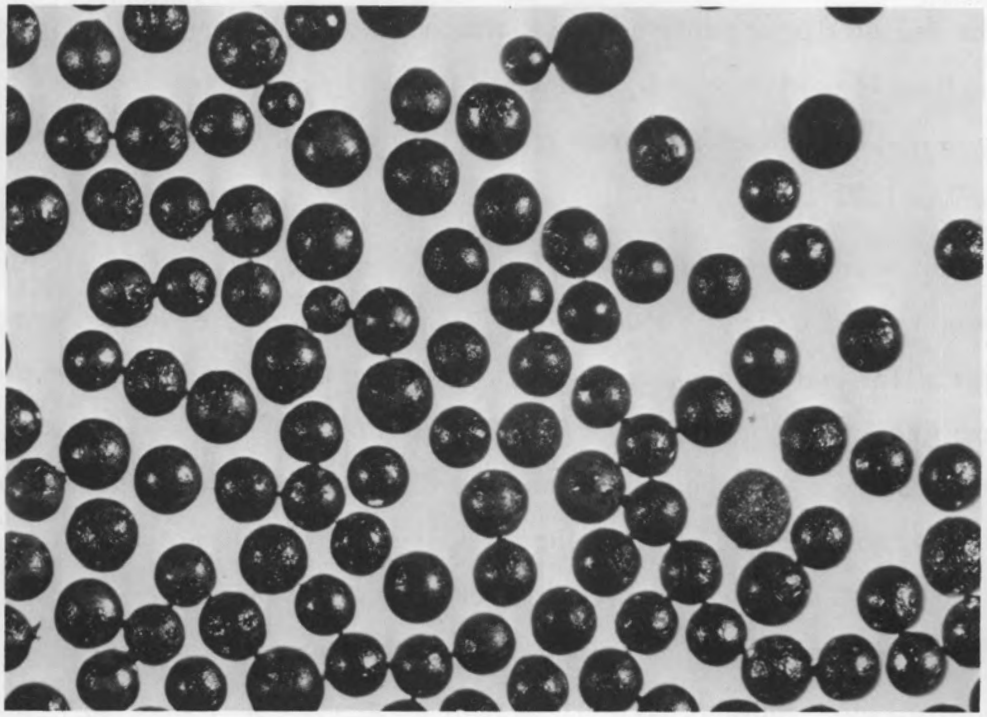

Fig. 31. Microspheres of Uranium Thorium Dicarbide Prepared by the Sol-Gel Carbide Process. (140 to 480 μ diam).

overpressure of CO in one-half to one hour. Some of the carbide spheroids were coated with pyrolytic carbon, and a sample is shown in Fig. 31. The toluene densities of the carbide products varied from 70 to 95% of theoretical density as measured by toluene or mercury displacement.

Thus, it may be stated that the feasibility of preparing carbides of thorium and uranium-thorium by the sol-gel process has been established on a laboratory scale. Future efforts will consist in optimizing each step and scaling it up to a remotely controlled operation of pilot-plant size. A more detailed study of each step will be presented in Section 4.

3.2 Effects of Irradiation on Thorium Oxide Fuels

While developing processes for preparing nuclear fuels and fabricating the fuel elements, it is essential to conduct a continuing program for testing the effects of radiation. In the thorium fuel cycle work, irradiation testing has been done on fuels packed into tubes by vibratory compaction, on pellets, and on several dispersion-type fuels composed of thorium and thoria.

3.2.1 Fuel Tubes, Containing Powdered Fuels, Vibratorily Packed

Postirradiation examination of a number of powder-compacted sol-gel and arc-fused oxide fuels has been carried out as part of the continuing program.[12]

A description of the fuel rods and a summary of the irradiation histories are given in Tables 11 and 12, and the principal results obtained from postirradiation examination are presented in Table 13. The results are presented below, grouped according to the three series of tests.

NRX and MTR. — These tests compared such variables as fuel composition, method of powder preparation, bulk density, shape of the fuel rods, heat rating, and burnup. The most severe heat rating was 426 w/cm (calculated maximum instantaneous value), in a specimen that achieved a burnup of 14,000 Mwd/metric ton (U + Th). The corresponding value calculated for $\int_{T_o}^{T_c} k d\Theta$ was 46.0 w/cm.

Table 11. Description of Vibratorily Packed ThO_2-UO_2 Fuel Rods – Postirradiation Examination Completed

Experiment	Fuel Rod Identification	Type of Oxide	Total Uranium[a] (wt %)	Cladding	Oxide Particle Size	Vibrated Density[b] (% T. D.)	Fuel Rod Dimensions (in.)		
							Length	O. D.	Wall
MTR-I	U-1	Arc-fused	3.96	304 SS	e	85.7	11.3	0.314	0.025
	Z-5	Sol-gel E	4.00	304 SS	e	86.2	11.3	0.314	0.025
NRX-I	X-1	Sol-gel A	4.31	304 SS	e	87.0	10.6	0.314	0.025
	X-8	Sol-gel A	4.31	304 SS	e	86.5	11.2	0.314	0.025
	O-3	Sol-gel B	4.39	304 SS	e	86.5	10.6	0.314	0.025
	O-5	Sol-gel B	4.39	304 SS	e	86.2	11.1	0.314	0.025
	H-3	Sol-gel B	4.39	304 SS	e	85.7	10.6	0.314	0.025
NRX-II	A-1	Arc-fused	3.96	304 SS	e	85.5	22.5	0.314	0.025
	A-2	Arc-fused	3.96	304 SS	e	85.7	22.5	0.314	0.025
	C-3	Sol-gel C	4.01	304 SS	e	83.3	22.5	0.314	0.025
	C-4	Sol-gel C	4.01	304 SS	e	82.6	22.5	0.314	0.025
ORR Loop[c]	L1A	Sol-gel 26	5.35	304 SS	f	85.2	21.5	0.460	0.015
	L1B	Sol-gel 26	5.35	Zircaloy-2	f	84.1	21.5	0.460	0.015
	L1C	Sol-gel 26	5.35	Zircaloy-2	f	84.1	21.5	0.460	0.015
ORR Poolside[d]	O3-5	Sol-gel D	2.50	304H SS	e	84.8	7.01	0.626	0.020
	O6-5	Sol-gel D	2.50	304H SS	e	85.5	7.00	0.624	0.020

[a]Fully enriched (93%) in U^{235}.
[b]Theoretical density = approx. 10.04 g/cc depending on precise composition.
[c]Three-rod bundle.
[d]Central thermocouple in each specimen.
[e]Distribution A = 60 wt % – 10 + 16 mesh
15 wt % – 70 + 140 mesh
25 wt % – 200 mesh
[f]Distribution B = 60 wt % – 6 + 16 mesh
15 wt % – 50 + 140 mesh
25 wt % – 200 mesh

ORNL DWG. 63-6401

Table 12. Irradiation History of Examined Specimens[a]

Experiment	Fuel Rod Identification	Cladding Temp. (°C)	Avg. External Pressure (psia)	Peak Linear Heat Rating		Peak Cladding Heat Flux		Maximum Burnup	
				Time Avg. (w/cm)	Max Inst. (w/cm)	Time Avg. (Btu/hr-ft^2)	Max Inst. (Btu/hr-ft^2)	$\left(\frac{\text{Mwd}}{\text{Metric Ton (U + Th)}}\right)$	$\left(\text{f/cc} \times 10^{-20}\right)$
MTR-I	U-1	100	40	299	362	381,000	461,000	12,300	2.70
	Z-5	100	40	341	426	435,000	544,000	14,000	3.08
NRX-I	X-1	100	130	116	138	147,000	175,000	13,400	2.96
	X-8	100	130	141	168	180,000	214,000	16,360	3.61
	O-3	100	130	135	162	173,000	206,000	15,690	3.46
	O-5	100	130	125	148	159,000	189,000	14,450	3.18
	H-3	100	130	86	102	110,000	130,000	10,500	2.32
NRX-II	A-1	100	130	132	138	168,000	176,000	3,170	0.69
	A-2	100	130	178	188	228,000	239,000	4,310	0.95
	C-3	100	130	200	211	255,000	268,000	4,960	1.05
	C-4	100	130	166	175	212,000	223,000	4,160	0.88
ORR Loop	L1A	260	1750	381	389	330,000	337,000	1,600	0.34
	L1B	260	1750	499	509	432,000	441,000	2,110	0.45
	L1C	260	1750	410	418	356,000	363,000	1,730	0.38
ORR Poolside	O3-5	705	315	304	337	194,000	215,000	5,220	1.13
	O6-5	540	315	275	297	175,000	189,000	4,040	0.88

[a]Assume 185 Mev/fission.

Table 13. Summary of Postirradiation Observations and Calculations

Experiment	Fuel Rod Identification	$\int_{T_o}^{T_c} k d\theta$		Kr-85 Release (%)	Diametral Change		Radial Extent of Thermal Changes		$\int k d\theta$ For Various Thermal Effects[a]	
		Time Avg. (w/cm)	Max Inst. (w/cm)		Avg. (in.)	Max (in.)	Sintering (in.)	Columnar Grain Growth (in.)	$\int_{T_o}^{T_{cg}} k d\theta$ (w/cm)	$\int_{T_o}^{T_{sin}} k d\theta$ (w/cm)
MTR-I	U-1	33.1	40.0	2.4	+0.001	+0.001	–	–	–	–
	Z-5	36.8	46.0	0.5	+0.001	+0.003	–	–	–	–
NRX-I	X-1	16.5	18.5	2.2	+0.001	+0.002	–	–	–	–
	X-8	18.8	21.3	2.8	+0.001	+0.002	–	–	–	–
	O-3	18.1	20.6	3.6	+0.001	+0.002	–	–	–	–
	O-5	17.3	19.4	2.9	+0.001	+0.002	–	–	–	–
	H-3	13.8	15.2	1.6	+0.001	+0.001	–	–	–	–
NRX-II	A-1	18.0	18.6	3.5	−0.001	−0.003	–	–	–	–
	A-2	22.2	23.1	3.3	0.000	+0.001	–	–	–	–
	C-3	24.1	25.2	4.0	0.000	+0.004	–	–	–	–
	C-4	21.0	21.3	Sample lost	+0.001	+0.004	–	–	–	–
ORR Loop	L1A	46.5	47.4	2.3	+0.001	+0.004	0.154	–	–	31.2
	L1B	57.0	58.1	Failure	0.000	+0.009	0.160	0.060	54.2	35.4
	L1C	49.6	50.6	3.9	0.000	+0.004[c]	0.130	–	–	38.2
ORR Poolside	O3-5	54.5	60.5	18.3	−0.001	−0.009	0.260	–	–	35.5
	O6-5	46.7	50.4	Gas lost	0.000	+0.002	[b]	–	–	[b]

[a]Time-averaged value.

[b]Sintering boundary could not be delineated.

[c]An indentation of 0.037-in. was observed above the Al_2O_3 disk and is believed to have resulted from disintegration of the disk.

For all rods, no bowing nor no significant changes in the dimensions were found. Little microstructural change was exhibited as a result of irradiation (see Figs. 32 and 33), and there were no marked differences between the higher- and lower-heat-rated rods. As determined by visual examination and sieve analyses (Table 14), the powder had agglomerated; however, only slight interparticle bonding had developed.

Table 14. Sieve Analyses on Low-Heat-Rated Irradiation Specimens

Screen Size	Wt % of Total Retained[a]		
	A-1	A-2	X-8
18 mesh	38.9	47.0	74.0
35 mesh	53.2	43.8	14.8
60 mesh	0.7	0.8	1.5
140 mesh	3.3	4.3	6.7
300 mesh	2.3	3.4	2.9
Pan	1.6	0.7	0.2

[a]Preirradiation particle size distribution: 60 wt % -10 +16 mesh
15 wt % -70 +100 mesh
25 wt % -200 mesh

Fission-gas retention in sol-gel oxide was comparable to that in arc-fused material (see Table 13). The variations in fission-gas release among the particular types of sol-gel oxide could be accounted for by variations in the powders themselves, especially in the surface area. Properties of all of the powders that have been tested are summarized in Table 15.

As previously reported,[13] gas diffusion through irradiated, vibratorily compacted fuel that has not sintered is sometimes poor. Out-of-pile tests at ORNL have shown that this behavior also exists prior to irradiation. This phenomenon will be investigated further as part of a waterlogging study.

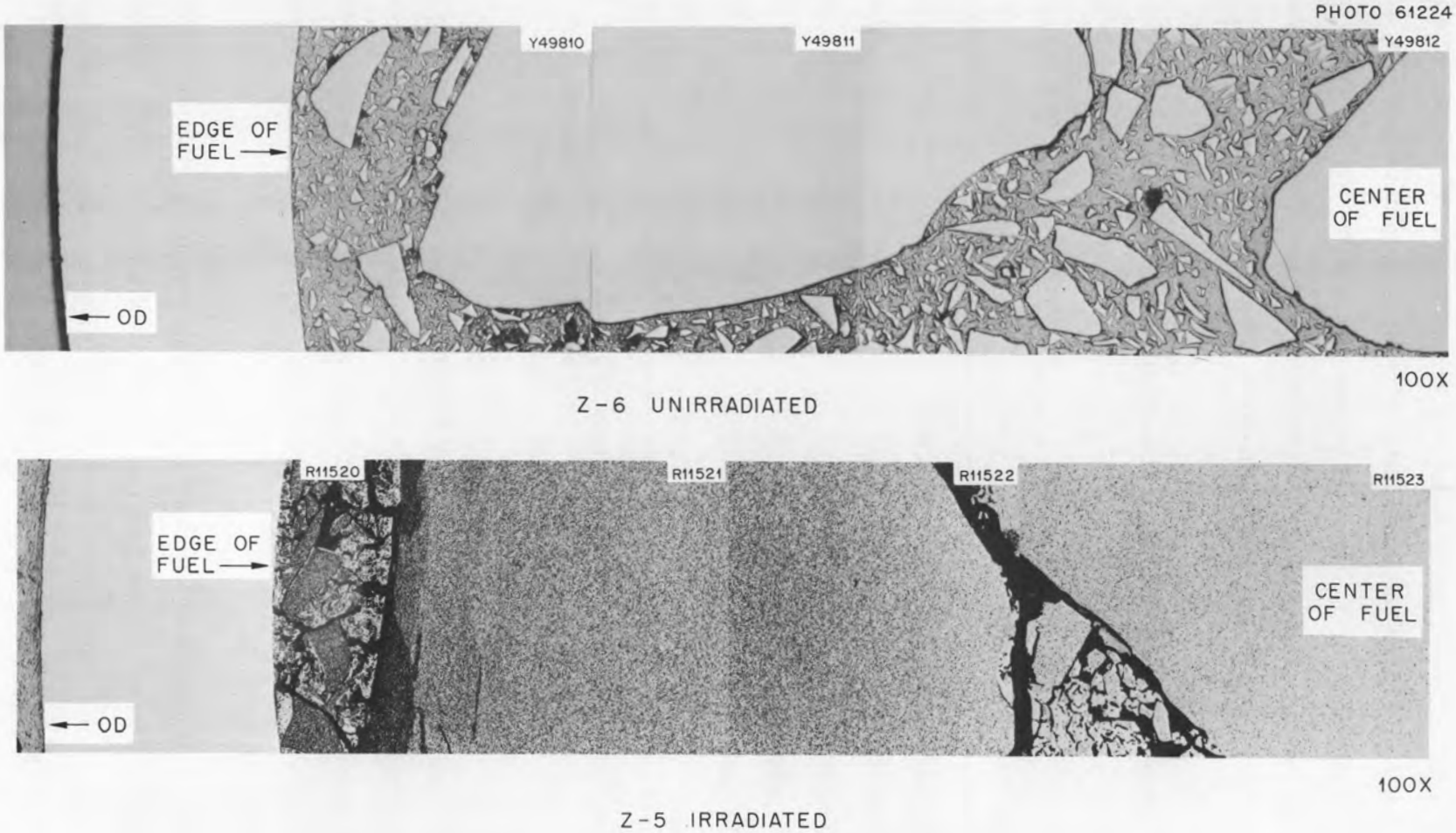

Fig. 32. Composite Photomicrograph Showing Typical Transverse Sections of Unirradiated and Irradiated Vibratory-Compacted Sol-Gel E ThO_2—4.5% UO_2. Radial area from outside diameter of the fuel as polished. 100X. Reduced 12%.

Fig. 33. Composite Photomicrograph Showing Typical Transverse Sections of Unirradiated and Irradiated Vibratory-Compacted Arc-Fused ThO_2—4.5% UO_2. Radial area from outside diameter of the fuel as polished. 100X. Reduced 23%.

Table 15. Summary of Properties of Uranium-Thorium Oxides Used in Fabrication of Completed Irradiation Specimens

	Sol-Gel A	Sol-Gel B	Sol-Gel C[a]	Sol-Gel D[a]	Sol-Gel E[a]	Arc Fused	Sol-Gel S	Sol-Gel Batch 26
Total uranium, wt %	4.31	4.39	4.01	2.50	4.00	3.96	5.00	5.35
Uranium enrichment, %	93	93	93	93	93	93	93	93
Carbon, ppm	110	100	60	40	130	120	70	40
Nitrogen, ppm	22	21	55	29	31	1130	40	13
Iron, ppm	100	50	265	140	160	130	333	215
Silicon, ppm	600	500	< 20	< 10	< 10	20	< 10	< 25
BET surface area (N_2), m^2/g	0.20	0.26	0.03	0.008	0.011	0.11	0.15	0.047
O/U ratio	2.0	2.0	2.03	2.02	2.02	2.01	2.01	2.02
Volatile matter released in vacuum at 1200°C, cc/g	0.125	0.151	0.055	0.012	0.027	0.24	0.407	0.244
Lattice parameter, A	5.591	5.592	5.593		5.593	5.594	5.594	
Crystalline size, A	2400	1700	2200				1750	
Particle density, g/cc[b]	9.94	9.92	9.76	9.97	9.92	10.11	9.86	
Packed density, g/cc[c]	8.69	8.69	8.36	8.74	8.74	8.6	8.8	

[a]Cooled in pure argon after calcination in hydrogen.

[b]Toluene intrusion, pycnometric method. Theoretical density: 10.04 g/cc.

[c]NAVCO air vibrator, 1/25-in. piston; 5/16-in.-OD × 11-in. stainless steel tube.

ORR Pressurized-Water Loop. — Examination of a Zircaloy-2 clad rod (LIB) that failed has been concluded. This rod was in a trefoil cluster irradiated in a pressurized-water loop operating at 1750 psi and 260°C. As shown in Fig. 34, the cladding was completely destroyed in the failed area, but only the outer surface of the Zircaloy-2 support sleeve (in contact with the inner surface of the cladding) had corroded. This observation suggests that internal hydriding from the evolution and reaction of volatile matter was not the cause of failure. A reaction product (Fig. 34) that appears to be hydride was observed, but it is suggested that hydriding and embrittlement did not occur as a result of normal corrosion.

Dimensional measurements revealed that this area swelled 9 mils. The change in diameter was negligible elsewhere along the rod. Some thinning of the nominally 0.015-in. thin-wall cladding to about 10 mils was observed in the vicinity of this area. For comparative purposes, a corresponding region from a similar rod (LIC) was also examined metallographically, and no signs of attack were apparent. Based on the above observations and an examination of the preirradiated cladding, it is believed that failure was initiated by a fabrication defect in the cladding, such as an inclusion or chemical inhomogeneity.

The three rods were sectioned and examined at the points of maximum burnup. Sintering and equiaxed grain growth were observed in all three rods, but columnar grains were apparent only in rod LIB. The radial extent of these changes is detailed in Table 13. The "hottest" rod, LIB, also showed evidences of lenticular void formation and perhaps the commencement of a central void. Polished cross sections of these rods are shown in Fig. 35 and radial composities of each of these rods are presented in Fig. 36. It will be observed that the changes in microstructure are analogous to those that occur in UO_2.

The $\int_{T_s}^{T_{sin}} k d\theta$ for sintering (average of three specimens) was calculated to be 17.4 w/cm ± 3.1 (34.9 w/cm ● 3.4 normalized to T_o). The $\int_{T_s}^{T_{cg}} k d\theta$ for columnar grain growth was 36.1 w/cm for rod LIB (54.2 w/cm normalized to T_o). The above are time-average values for the peak burnup region. A comparable value for nonsintered UO_2,

R-16838

AS POLISHED

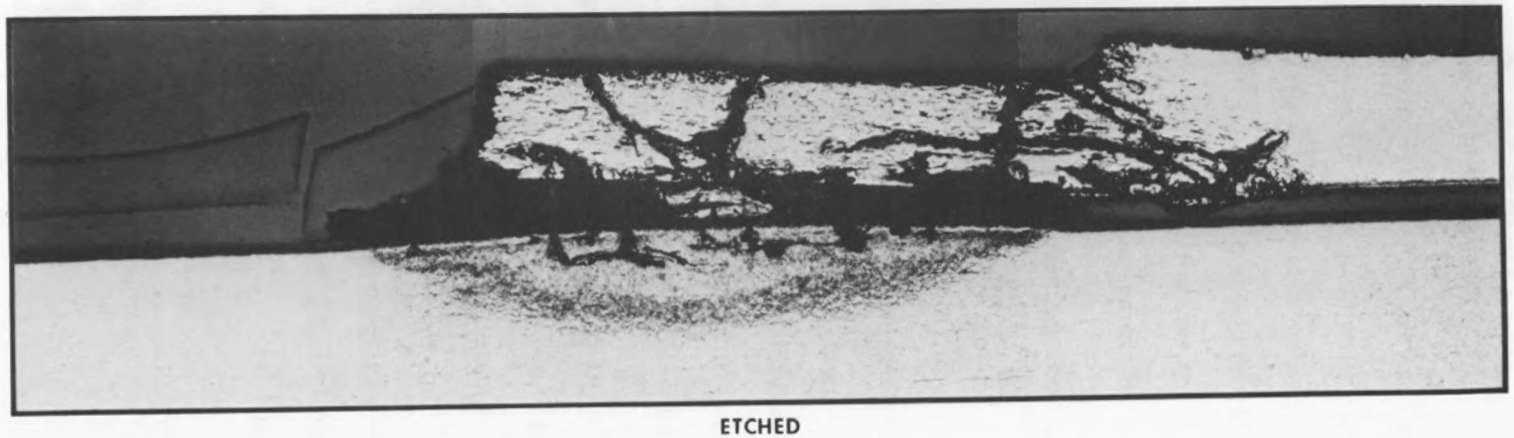

ETCHED

Fig. 34. Longitudinal Section Showing Zircaloy-2 Cladding and Support Sleeve at the Failed Region of Rod LIB. Note massive hydrides. Top: as polished; bottom: etched. 100X. Reduced 20%.

R-16881

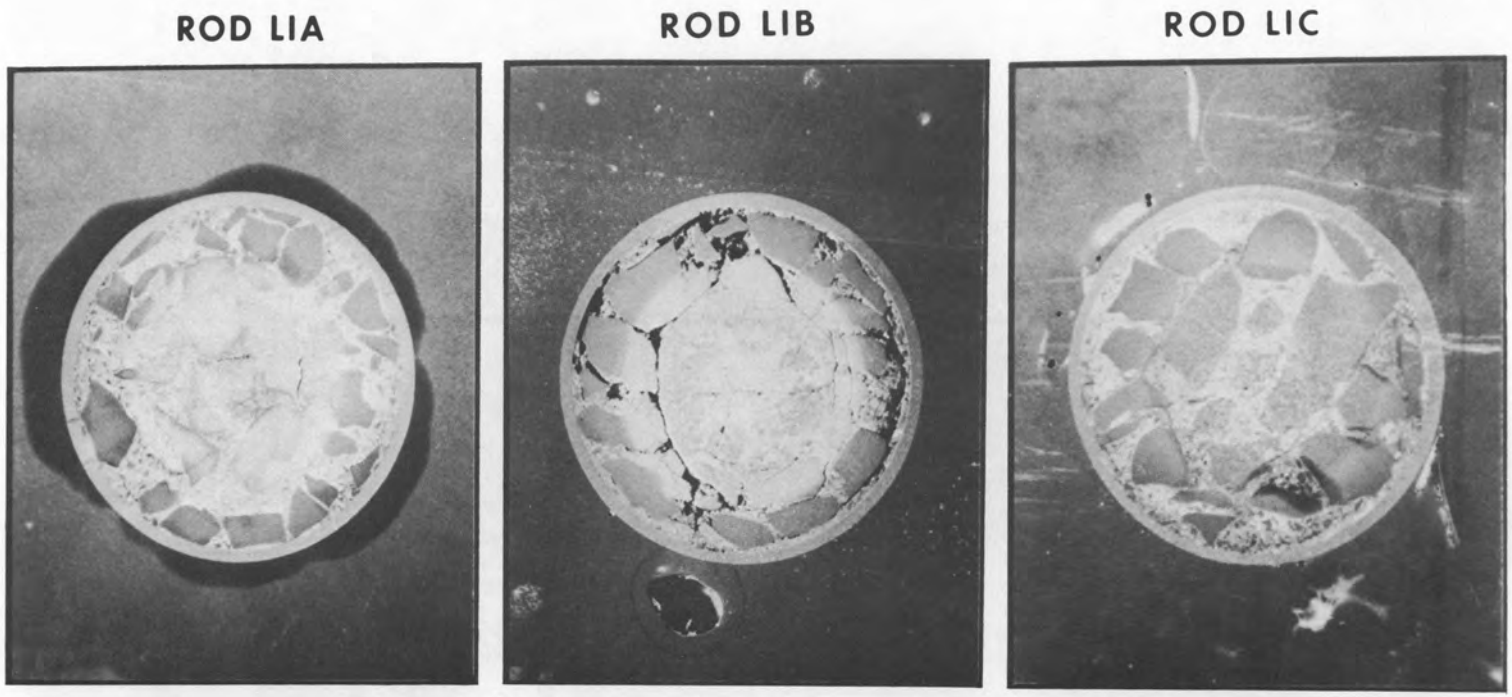

Fig. 35. Polished Cross Sections of Irradiated Fuel Rods from ORR Pressurized-Water Loop Experiment L-1, Vibratory-Compacted Sol-Gel ThO_2—6.1% UO_2. Approximately 4X. (a) Rod LIA; (b) rod LIB; (c) rod LIC. Reduced 16%.

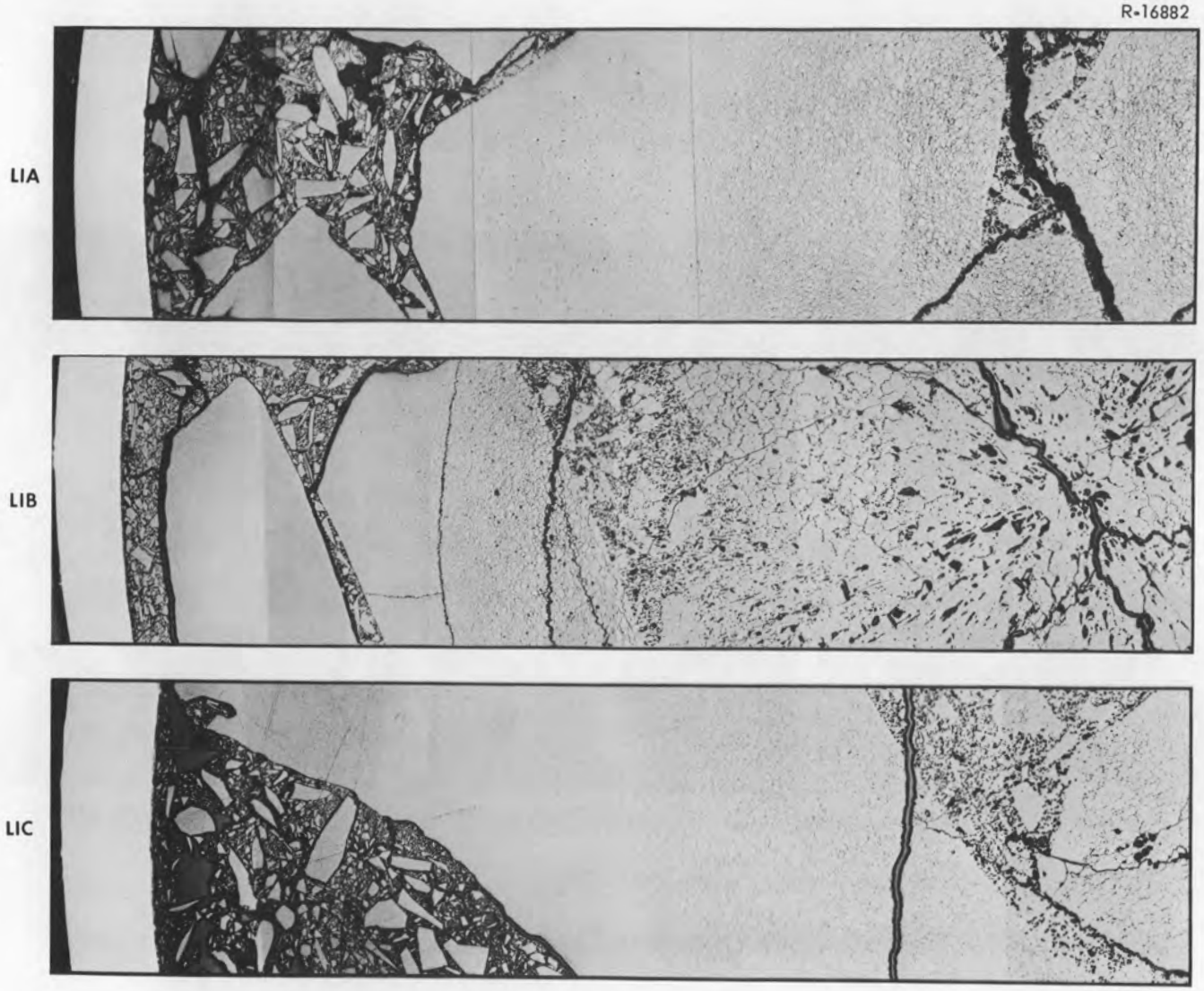

Fig. 36. Panoramas at Peak Burnup Regions of Rods LIA, LIB, and LIC. Etched. 100X. Reduced 27%.

based on the average from previous loop experiments, is $\int_{T_s}^{T_{cg}} k d\theta = 19.4$ w/cm (time-average peak value). The maximum instantaneous values are perhaps 30% closer, but this is a rather significant difference in favor of ThO_2-UO_2 and is considerably better than expected.

Instrumented ORR Poolside Capsules. — Diametral changes in the two high-surface-temperature (540 and 705°C, respectively) ORR Poolside capsules were erratic and varied from -1.7 to +2.3 mils for capsule 06-5 and from -9.4 to +3.3 mils for capsule 03-5. Both capsules decreased in length by about 0.1 in.

Initial examination revealed what was thought to be a reaction layer in the type 304H stainless steel cladding of capsule 03-5 at the fuel-cladding interface (Fig. 37); however, subsequent examination showed that the layer is merely an area of small, recrystallized grains. The precipitate in the stainless steel has the appearance of carbides.

To the extent that a grain size of 15 μ could be measured, sintering was exhibited in the specimen that operated with the lower surface temperature (540°C). The other element, which ran at a 165°C higher surface temperature and 480°C higher central temperature (1925°C), sintered across 7/8 of the radius. In addition, the grain size increased from 15 μ at the sintering periphery to about 500 μ at the center (adjacent to the axial thermowell). Radial composites of the two capsules are shown in Fig. 38.

The calculated value for the $\int_{T_o}^{T_{sin}} k d\theta$ in capsule 03-5 was 35.5 w/cm. No value could be calculated for 06-5 because the sintering boundary was not clearly delineated. Fission-gas release from the fuel in capsule 03-5 was relatively high (viz., 18.3%), but this specimen ran at a high surface temperature. Unfortunately, the gas sample from capsule 06-5 was lost.

Effective thermal conductivities have been calculated for these capsules and are listed in Table 16 with some values from the literature for pressed and sintered bodies of ThO_2 and ThO_2-10% UO_{2+x}. The ORNL values are somewhat lower than originally reported,[12] but they are still higher than initially envisioned for this type of fuel body.

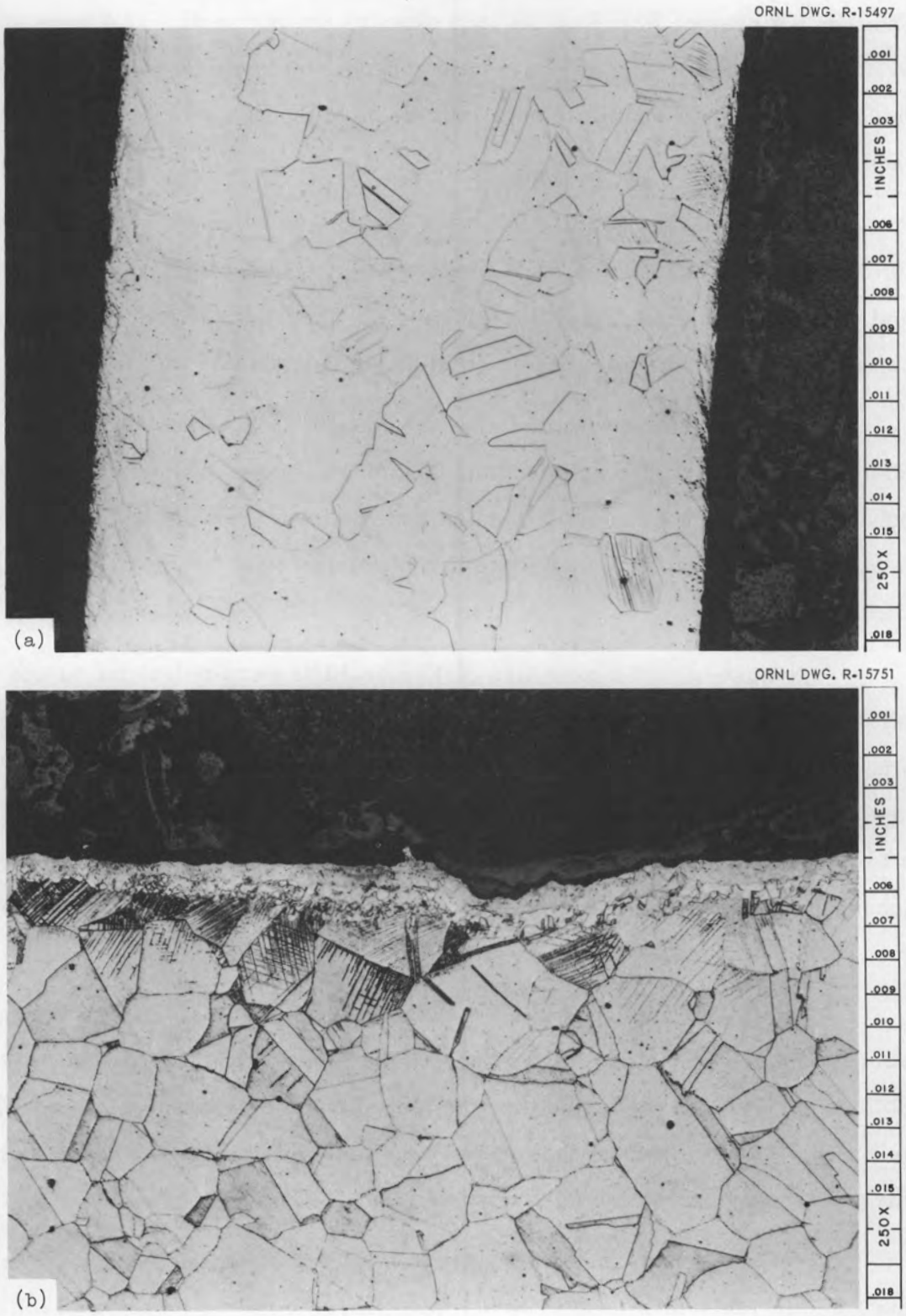

Fig. 37. Fuel Cladding Interfaces of (a) Capsule 03-5 and (b) Capsule 06-5. Etchant: glyceria regia. 250X. Reduced 29%.

R-16839

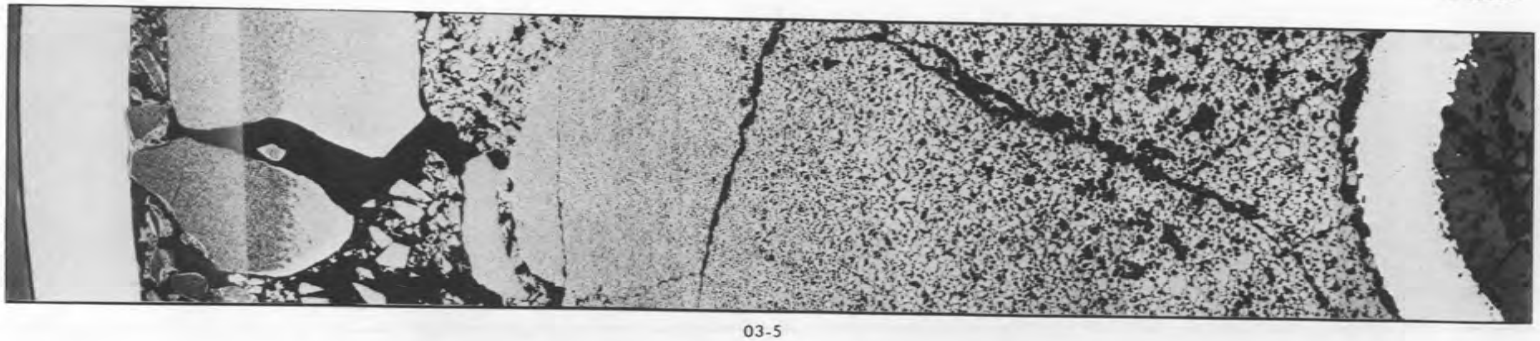

03-5

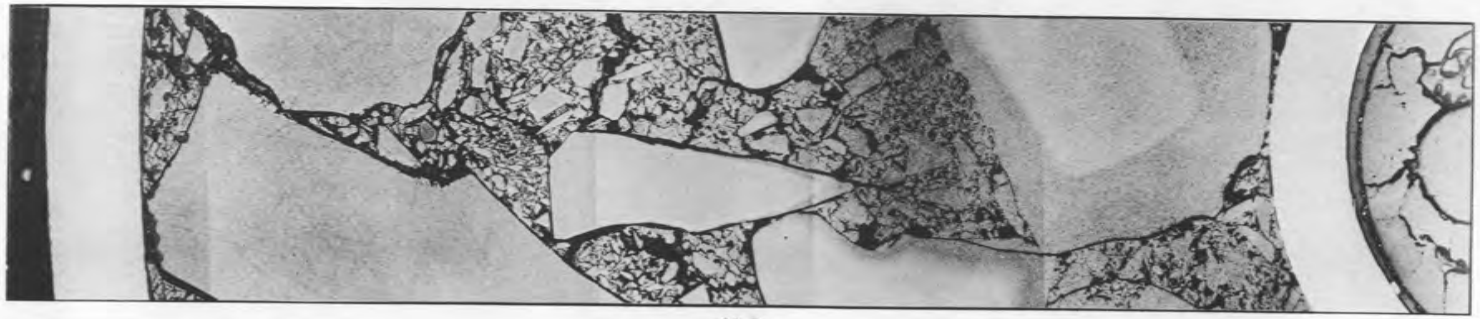

06-5

Fig. 38. Peak Burnup Regions of (a) Capsule 03-5 and (b) Capsule 06-5. Transverse areas from outside diameter of the cladding to central thermowell. Etched. 100X. Reduced 20%.

Table 16. Thermal Conductivity of Thoria-Base Fuels

Source	Composition	Average Temperature (°C)	Average Temperature (°F)	Thermal Conductivity[a] (w/cm-°C)	Thermal Conductivity[a] (Btu hr^{-1} ft^{-1} $°F^{-1}$)
ORNL (06-5)	ThO_2-2.9% UO_2	990	1815	0.021[b]	1.20
ORNL (03-5)	ThO_2-2.9% UO_2	1325	2415	0.017[b]	1.00
Kingery[c]	ThO_2	600	1112	0.046	2.66
Kingery[c]	ThO_2	800	1472	0.036	2.08
Kingery[c]	ThO_2	1000	1832	0.033	1.91
Kingery[c]	ThO_2-10% UO_{2+x}	600	1112	0.032	1.87
Kingery[c]	ThO_2-10% UO_{2+x}	800	1472	0.029	1.66
Kingery[c]	ThO_2-10% UO_{2+x}	1000	1832	0.025	1.44

[a]Data corrected to same density as vibrated ThO_2-2.9% UO_2, using the relationship $k_m = k_t(1-P)$, where P = pore volume fraction, k_m is the measured conductivity, and k_t is the value corrected to theoretical density.

[b]Based on flux calculated from burnup measurement.

[c]W. D. Kingery, J. Am. Ceram. Soc. 4 (12), 617 (1959).

3.2.2 Sol-Gel-Derived ThO_2-UO_2

It is clear from results previously reported[12] and those that have just been described that sol-gel ThO_2-UO_2 is a suitable fuel material for power reactor applications. Indeed, its irradiation behavior is comparable or superior to that of arc-fused ThO_2-UO_2 and to that of UO_2 in general. There are probably three basic reasons for this stability: (1) ThO_2 has a melting point about 500°C higher than that of UO_2, and a comparable thermal conductivity. (2) ThO_2, like UO_2, has a fluorite-type crystal structure. ThO_2 and UO_2 are mutually soluble and form a series of continuous solid solutions. (3) Sol-gel particles are dense, free of cracks, and of high purity.

It has also been observed that the thermal behavior of the mixed oxide, generally, is analogous to that of UO_2, the principal difference being that the induced microstructural changes occur at a higher heat rating for ThO_2-UO_2. Some variations were observed for the several types of sol-gel tested, variations that could be attributed to differences between the powders in composition, surface area, porosity, etc.

In addition to the typical changes described above, there are some unique and subtle microstructural features associated with sol-gel ThO_2-UO_2. One is the variation in darkness, and presumably porosity, within certain irradiated particles (Fig. 39) that had not sintered or recrystallized. This phenomenon has been observed in oxides irradiated in the MTR, NRX, and in the lower temperature ORR poolside capsule. In part, it must represent the pulling out of crystallites during metallographic polishing, which indicates a decrease in grain-boundary integrity. There is no pattern to the intraparticle density alteration.

Another interesting characteristic of irradiated sol-gel oxide is the appearance of a globular second phase in the pores (Fig. 40). It has not been possible by optical microscopy to resolve a phase in the fine porosity seen in the unirradiated fuel. This phase is not similar in appearance to the whitish inclusions that are randomly scattered in sol-gel oxide in small quantity, nor to the white second-phase precipitate found in significant quantity in arc-fused oxide. It is hoped that electron microscopy, x-ray diffraction, and selective etching will help explain these phenomena.

Still another interesting observation is the formation of equiaxed grains within individual sol-gel particles at sufficiently high heat ratings (see Fig. 36). Unirradiated sol-gel oxide appears to be an agglomeration of very fine crystallites, with minute pores throughout the particles. It has not been possible by etching to develop a grain structure in this material that is visible at 1000X. However, while the outside contours of certain individual particles remained practically unchanged by the irradiation, intraparticle recrystallization resulted in an equiaxed structure of entirely new appearance and led to an increase in grain size. There were also the usual isolation and spheroidization of pores which occur during sintering.

PHOTO 61974

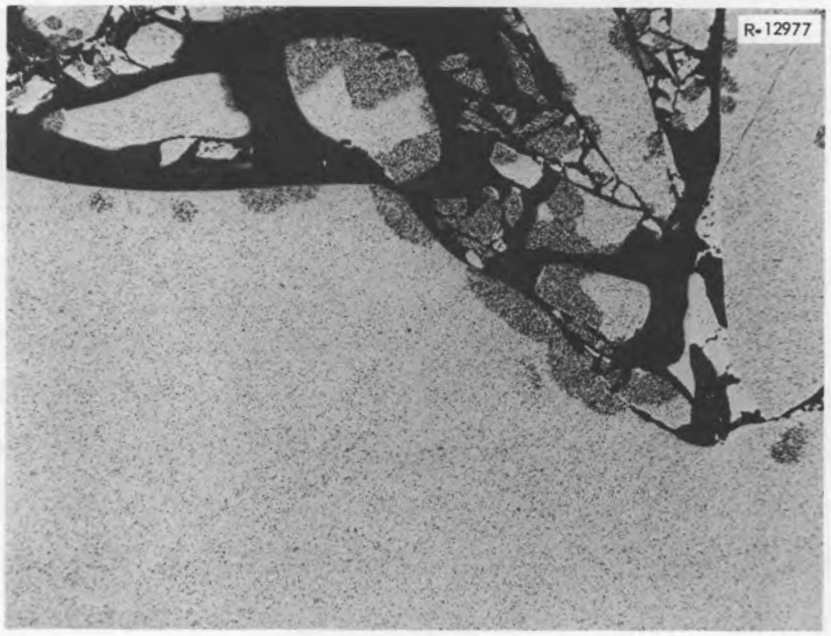

SOL-GEL A

X-1

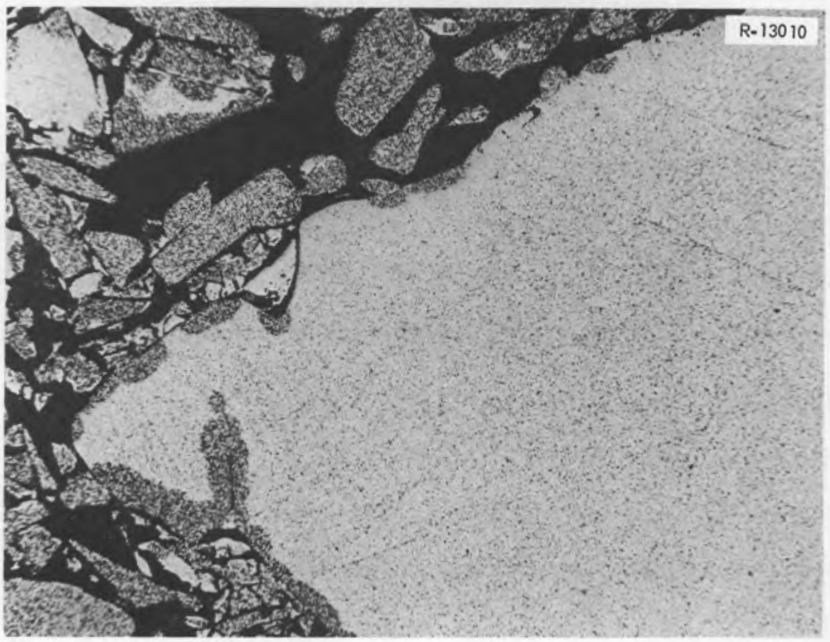

SOL-GEL B

O-3

Fig. 39. Darkened Areas in Irradiated Sol-Gel A and Sol-Gel B. As polished. 100X. Reduced 21%.

PHOTO 61564

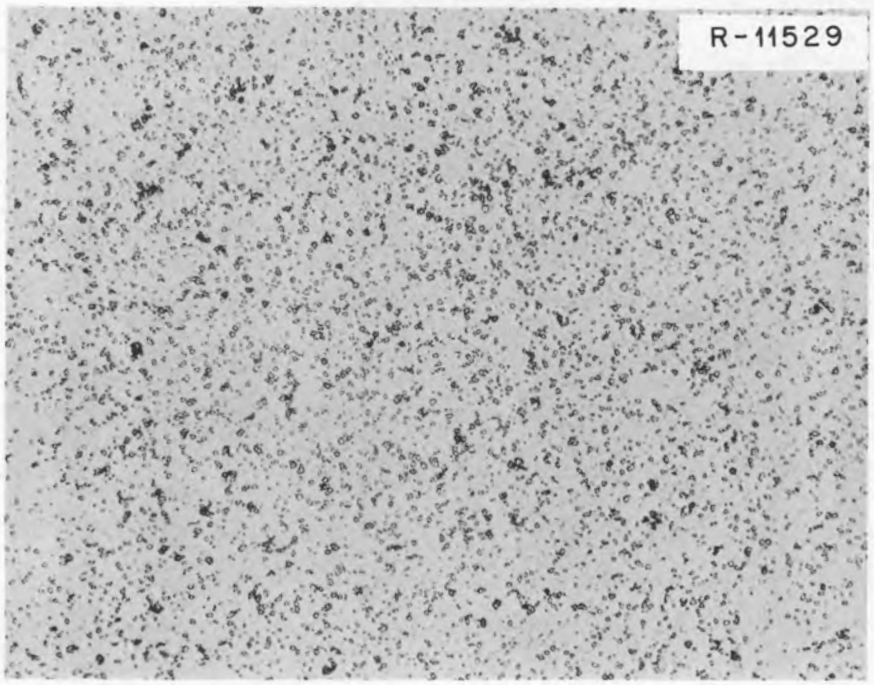

AS POLISHED, 500X

Fig. 40. Globular Second Phase in Pores of Irradiated Sol-Gel E (Capsule Z-5). Representative area at the fuel midradius.

Two other characteristics of vibratory-compacted oxide fuels are their affinity for adsorbed gases and particles embedding in the cladding. As indicated in Table 15, significant quantities of gas are sometimes present in the sized fuel. It has been found with sol-gel material that the comminuted and sized oxide releases 5 to 10 times as much of the absorbed gas as the calcined gel, but this might simply be a particle-size effect. It may be possible to reduce the quantity of gas absorbed by comminution of the gel before calcining.

With regard to the problem of embedding particles in the cladding (see Fig. 41), this is an infrequent occurrence. In thin-wall claddings, though, this could be bothersome, and adequate inspection will be required. One positive aspect of vibratory compaction, perhaps not appreciated, is that there certainly appears to be intimate contact between the fuel and cladding, which is favorable for heat-transfer.

As has been observed with UO_2, columnar grains were formed in the sol-gel ThO_2-UO_2 without any evidence of melting. MacEwan and Lawson[14] showed by means of a thermal simulation apparatus that applying a steep thermal gradient in UO_2 induced columnar grain formation at temperatures well below melting. The columnar growth is generally attributed either to the vapor deposition of material on the cold side of migrating lenticular voids or to grain boundary migration.

It can be observed from an analysis of Table 13 that there are inconsistencies in the $\int k d\theta$ values calculated for a specific physical change to occur. For example, whereas it was calculated that sintering occurs at about $\int k d\theta = 35$ w/cm, no such change was apparent in fuel rods U-1 and Z-5. It should be noted that there are inherent errors in measuring structural changes, increasing in the order: central void formation, columnar grain growth, and sintering. It is especially difficult to demarcate the radial position at which sintering begins. Another acute problem in this method arises when one normalizes the values for different experiments to $T_s = T_o = 0°C$. This is necessary for comparative purposes, but it introduces a potentially significant error when one estimates average thermal conductivities for temperatures between T_o and T_s. This is more of a problem in the case of ThO_2-UO_2

ORNL DWG. R-15744

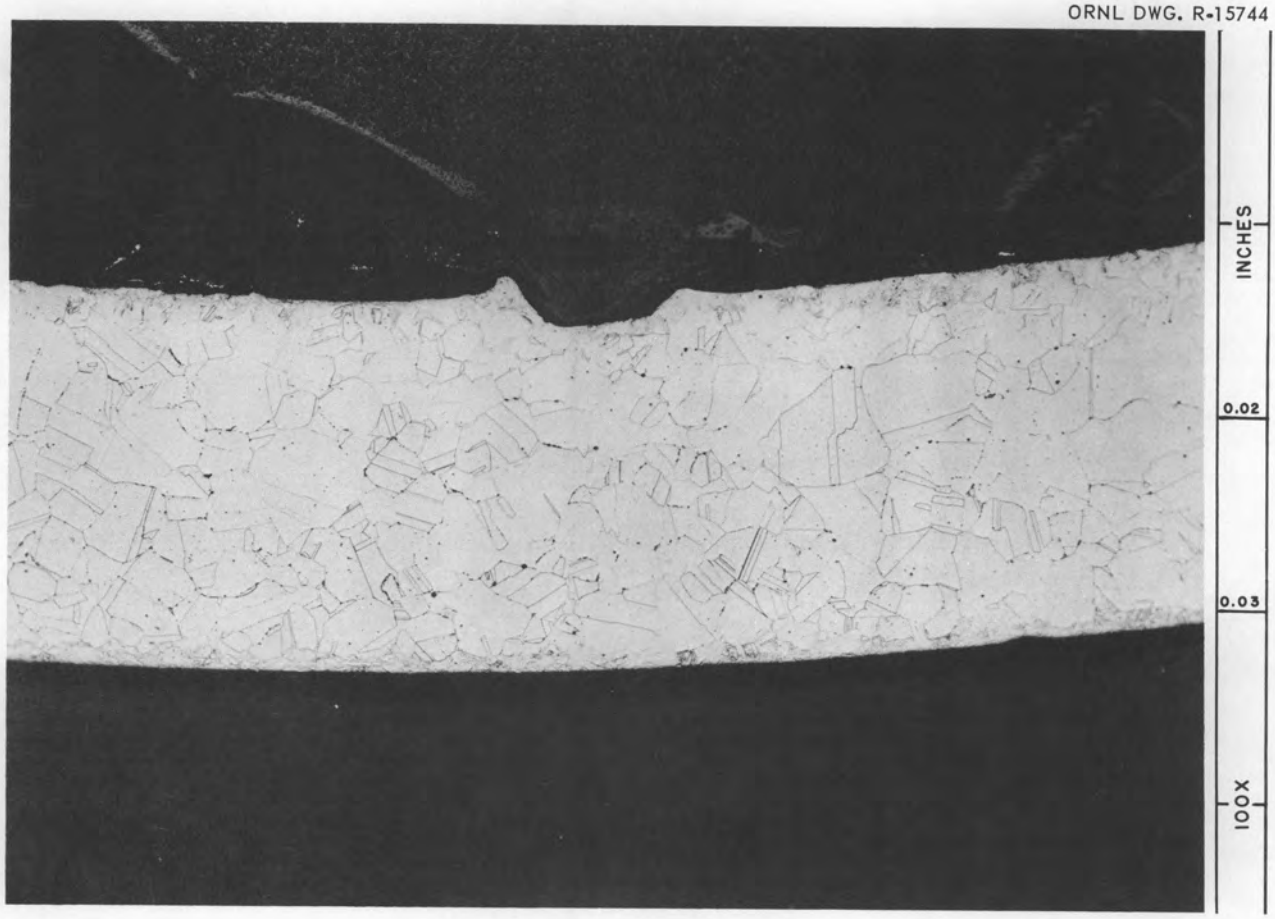

Fig. 41. Fuel Cladding Interface, Showing Particle Embedded in Cladding. Etchant: glyceria regia. 100X. Reduced 4%.

than with UO_2 because the thermal conductivity of the latter is far better documented. Still, in spite of its limitations, the parameter $\int k d\theta$ serves as an important ball-park number to indicate the thermal severity to which a fuel was exposed. In the case of the loop experiment, for example, it clearly demonstrated that ThO_2-6.1% UO_2 was more refractory than nonsintered UO_2 fuel previously irradiated in the loop.

Current Irradiation Program. — Table 17 summarizes the experiments that are in progress or that have been removed from the reactor but not examined. These test elements performed satisfactorily. The series of rods most recently inserted in the MTR and ETR are operating at heat ratings well above those heretofore examined and also will test the effects of the sol-gel calcining atmosphere on irradiation performance. Central melting is anticipated in the ETR-1 fuel rods.

3.2.3 Fuel Rods Containing Pelleted Oxide Fuel

The Power Reactor Fuel Reprocessing Irradiation Program was started several years ago at ORNL to provide irradiated fuel for dissolution studies. Subsequently, UO_2 and ThO_2—4.45% UO_2 pellet specimens have been irradiated in the MTR, ETR, and NRX to burnups at least as high as 95,000 Mwd/metric ton to metal.

At the time of inception, there was no intent to evaluate the performance of the fuel *per se*. However, in view of the interest in thorium-bearing fuels at ORNL, and in high-burnup fuels in general, it was decided to examine several of the irradiated ThO_2-UO_2 fuel rods and learn as much as possible about their behavior. Three such rods have been examined to date.

The design of a typical rod is illustrated in Fig. 42. Basic design parameters are summarized in Table 18. The fuel was ThO_2-4.45% (93.2% enriched) UO_2 pellets, clad in type 304 stainless steel. The pellets were prepared by an outside vendor. Sample pellets ranged in density from 90.8 to 93.8% of theoretical density, with an average of 92.5%.

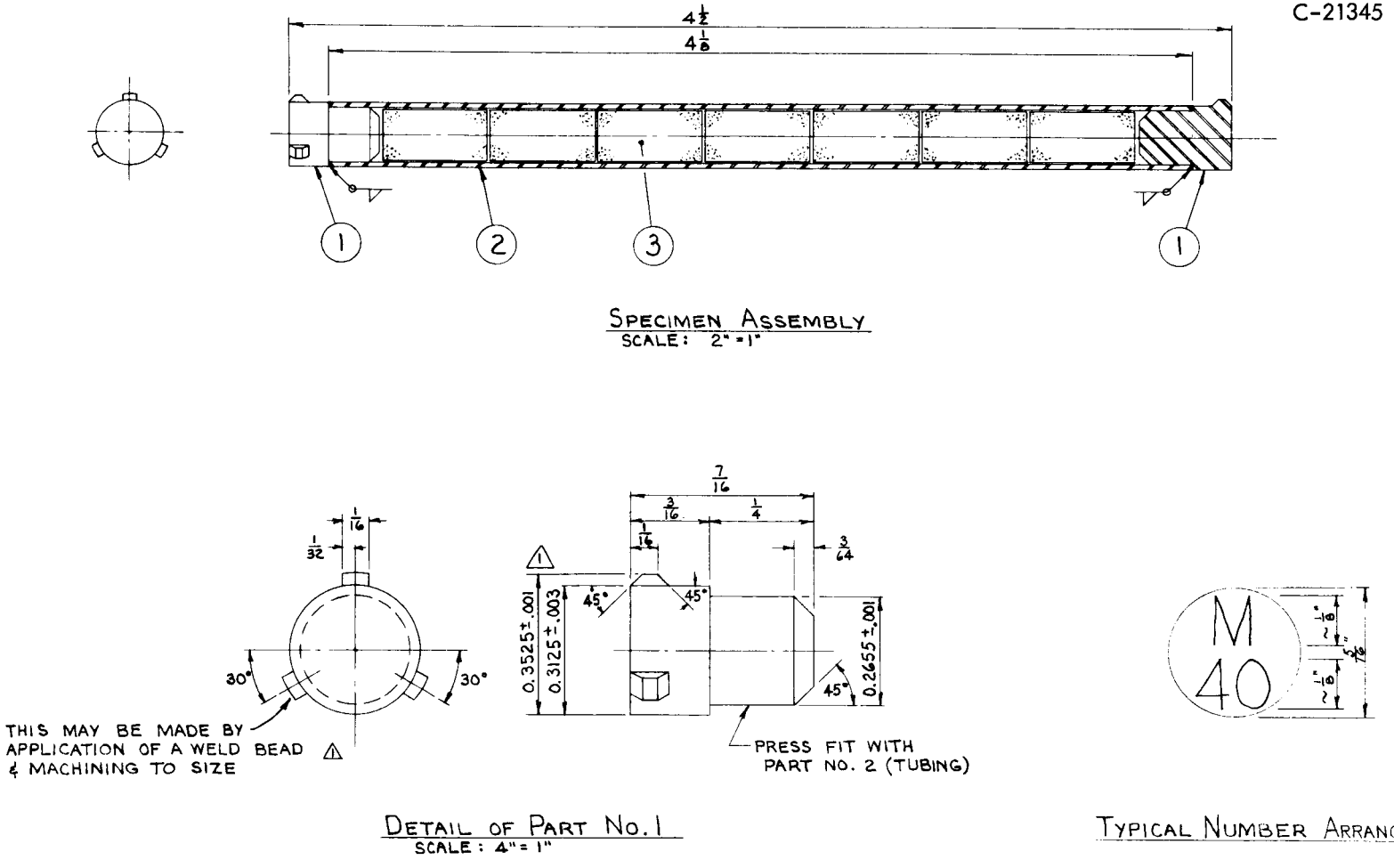

Fig. 42. PRFR Pellet Irradiation Capsule.

Table 17. Summary of Fuel Cycle Irradiations Under Examination or In-Pile[a]

Experimental Facility	No. of Capsules	Type of Oxide	Vibrated Density (% TD)	Clad Temp. (°F)	Average External Pressure (psia)	Fuel Rod Dimensions			Linear Heat Rating (Btu hr^{-1} ft^{-1})	Target Peak Burnup (Mwd/Metric Ton Metal)	Status
						Length (in.)	OD (in.)	Wall (in.)			
MTR Group I	5	Arc-fused, Sol-gel E	86 to 87	~200	40	11	0.312	0.025	45,000	35,000 to 100,000	3 in-pile 2 being examined
MTR Group II	2	Sol-gel S	88 to 89	~200	40	22	0.312	0.025	62,000	22,000 to 100,000	In 1-2-63
MTR Group III	6	Sol-gel 35 (air-fired, N_2-fired, H_2-Ar fired)	86 to 89	~200	40	12	0.438	0.025	85,000	22,000 to 100,000	4 In 10-63 2 In 12-63
ETR Group I	4	Sol-gel 35 (air-fired, N_2-fired, H_2-Ar fired)	86 to 89	~200	170	12	0.438	0.025	>100,000	22,000	In 11-63
NRX Group III	6	Sol-gel S	88 to 89	~200	130	39	0.312	0.025	28,000	23,000	Being examined
NRX Group III	3	Sol-gel ThO_2-PuO_2	74 to 76[b]	~200	130	11	0.312	0.025	27,000	22,000	Being examined

[a]Fuel = ThO_2-UO_2 except for three ThO_2-PuO_2-bearing capsules (NRX-Group III).
Cladding = Type 304 stainless steel.

[b]Packed by tamping.

Representative chemical analyses are given in Table 18. As indicated, the aluminum, silicon, and calcium contents were high, presumably present as Al_2O_3, SiO_2, and CaO, respectively. It is believed that these impurities were picked up during the ball-milling.

Table 18. Pertinent Design Specifications of Thoria-Urania Pellet Irradiation Specimens

Overall length, in.	4.5
Active length, in. (less insulating plug, if required)	3.5
Pellets per tube	7
Pellet diameter, in.	0.260
Pellet length, in.	0.500
Pellet density, % of theoretical	91-94
Tube, outer diameter, in.	0.3125
Tube wall, in.	0.025
End-plug length (each of two), in.	0.4375
Weight of fuel material per tube (no end plugs), g oxide	31

Microstructures of a ThO_2-UO_2 pellet are shown in Fig. 43. There appear to be three distinct phases: (1) the solid-solution matrix of ThO_2-UO_2; (2) a small amount of randomly dispersed, bright, metallic particles; and (3) an appreciable quantity of a glassy-like impurity phase concentrated at the grain boundaries. In addition to the secondary phases, pores may be readily observed.

Three of the fuel pins that were irradiated in MTR or ETR process water have been examined. Pertinent reactor-operating conditions and calculations are summarized in Table 19. The salient features of these experiments are that, although the cladding temperature was low, the fuel operated at heat ratings equivalent to those in power reactors, and the burnups ranged from 40,000 to 95,000 Mwd/metric ton of metal, burnups rarely obtained in in-pile exposures. The specimens performed without incident.

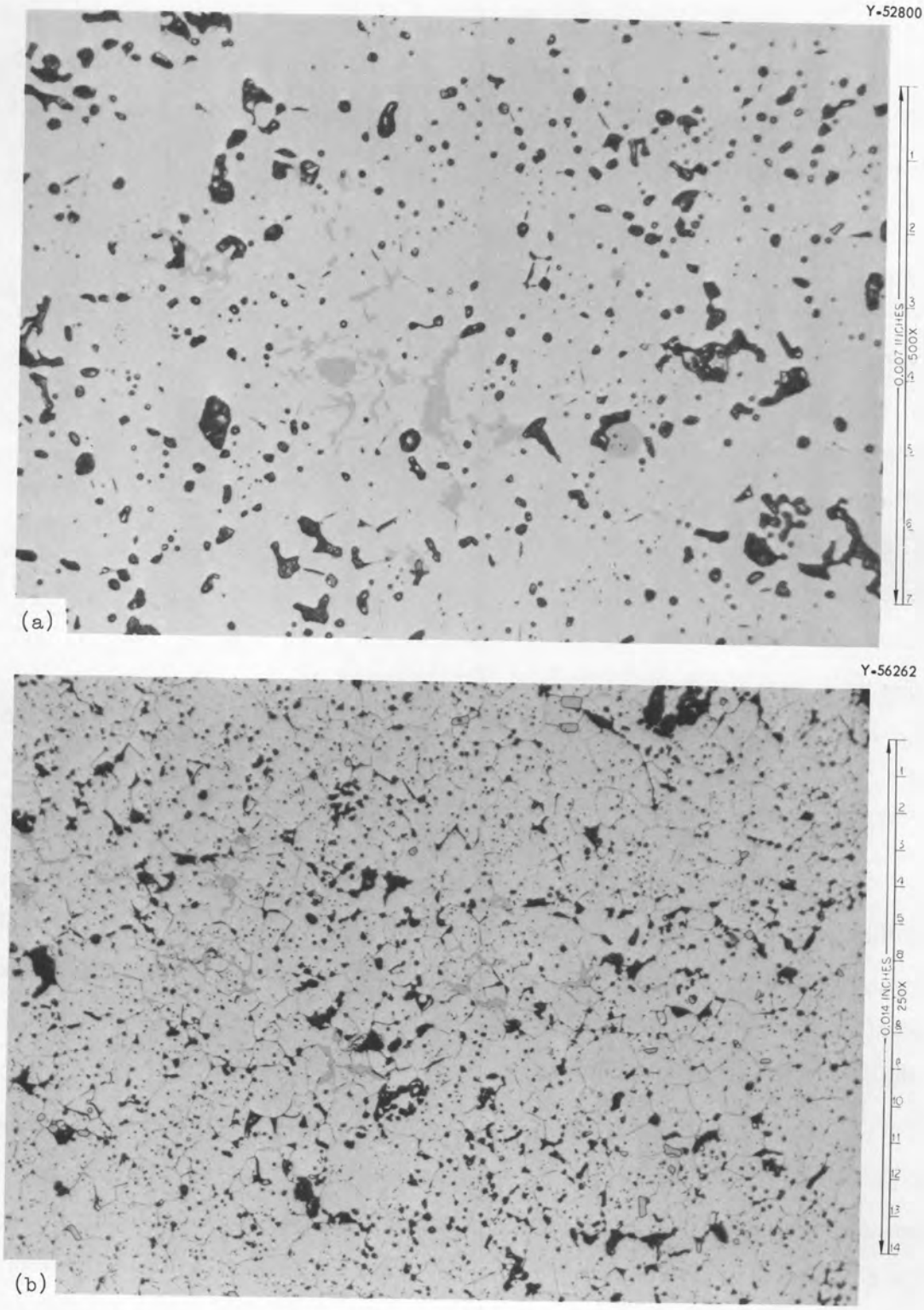

Fig. 43. (Y-52800 (a), Y-56262 (b). Unirradiated Microstructure of ThO_2-UO_2 Pellet. Note copious quantity of gray impurity phase. (a) As polished. 500X. (b) Etched. 250X. Reduced 12%.

Table 19. Results of Vendor's Chemical Analysis of Samples Taken From Pellets

U, wt %	3.93
UO_2, wt %	4.46
Th, wt %	83.64
ThO_2, wt %	95.17
Al, ppm[a]	<350
Fe, ppm	<50
Sn, ppm	50
Si, ppm	<100
Cr, ppm	40
P, ppm	<50
Ca, ppm[a]	<10

[a]Subsequent analyses at ORNL indicated that the Al and Ca contents were more probably 1000 ppm and 300 ppm, respectively.

The postirradiation evaluation is about 80% complete. Two of the pellet rods showed no degradation as a result of the irradiation; the third, fuel rod 43-44, exhibited an axial cladding defect that extended about a fourth through the cladding. Dimensional changes were insignificant for all three specimens.

Each of the rods was punctured and sampled for fission gases, but a valid sample was obtained for rod 43-40 only. Its calculated release was 15% of that theoretically generated.

Examination of the interior of the capsule revealed that no pellets were intact, and radial and transverse fractures were observed in every pellet. However, this is typical of oxide fuels. Each pellet was fractured into several pieces but did not fall out of the cladding during sectioning. No evidence of fuel-cladding reactions, central-void formation, or sintering was observed.

Table 20. Irradiation Operating Data for Pellet-Loaded Capsules 43-40, 43-41, and 43-44

	Capsules		
	MTR 43-40	MTR 43-41	ETR 43-44
Irradiation starting date	5-12-60	6-23-60	6-4-60
Irradiation discharge date	9-17-62	4-2-62	11-26-62
Reactor power, Mwd	26,400	19,874	71,078
Full-power days	660	497	406
Surface clad temperature, °F	~200	~200	~200
Maximum advertised unperturbed flux, nvt	1.13×10^{22}	7.15×10^{21}	5.88×10^{21}
Maximum burnup, Mwd/metric ton of metal	95,000	42,000	50,000
Peak linear heat rating,[a] Btu hr^{-1} ft^{-1}	47,800	28,100	41,000
Peak surface heat flux,[a] Btu hr^{-1} ft^{-2}	586,000	344,000	502,000
Peak heat-generation rate,[a] w/cc	1310	770	1120
Peak integral of $kd\theta$,[a] w/cm	36.5	21.5	31.3
Centerline temperature (assuming effective k_{fuel} = 1.7, Btu hr^{-1} ft^{-1} °F^{-1}), °F	2500	1560	2180

[a]Calculated, time-averaged value. Peak refers to maximum burnup area. Gamma heating is not included.

Metallography confirmed that there had been no columnar grain growth or void formation. It appeared that the glassy, grey phase had gone into solution toward the center of the fuel. Compatibility between the fuel and cladding was excellent. The crack in the cladding of capsule 43-44 was transgranular and appeared to contain an oxide.

Plans have been made to conduct x-ray diffraction analyses on the metallographic samples from capsules 43-40 and 43-44. This work is scheduled to be done early in 1964.

3.2.4 Thorium-Base Alloy Fuel

Irradiation testing of thermocouple-instrumented NaK-filled capsules containing Th-U-Zr alloys is in progress in General Electric Test Reactor's (GETR) radially adjustable facility tubes (RAFT). The use of RAFT positions theoretically permits close control of temperatures by movement of the capsules in a variable flux field as required. To date, a number of experimental difficulties have been encountered.

The capsules were designed and made by Advanced Technology Laboratories (ATL). A schematic of the assembled capsule is presented in Fig. 44. Each capsule contains a stack of ten 1/2-in.-diam x 1-1/2-in.-long pellets. Three alloys in two heat treatments (see Table 21) are included and are based on an alloy development program performed by ATL.[15]

Six capsules were made, consisting of three each in two groups designated as ATL-2 and ATL-3. The two series of capsules differ only insofar as the ATL-2 specimens have a thicker ZrO_2 insulation layer than the ATL-3 specimens. The ATL-2 capsules were designed to operate with a fuel-surface temperature of 650°C and an axial temperature of 760°C; the ATL-3 capsules were designed to perform with fuel-surface and central temperatures of 700 and 825°C, respectively.

The purpose of the experiment is to demonstrate whether the Th-U-Zr alloys, which possess improved elevated-temperature strength compared with Th-U alloys,[12] have sufficient resistance to radiation-induced swelling at the operating temperatures. The objective is based on the appraisal of an AEC task force[16] in 1959 that, to provide low fuel-cycle costs, Th-U alloys capable of operating at central temperatures of 835 to 1085°C were required. The range of temperature selected for the irradiation experiment is expected to straddle the threshold temperature at which swelling might occur.

Initially it was decided to irradiate the group ATL-3 capsules to burnups of 10,000, 20,000, and 30,000 Mwd/metric ton of fuel, respectively. The capsules were identified as 3-1, 3-2, and 3-3. Capsules 2-1, 2-2, and 2-3 were held in reserve. The status of the irradiations is as follows:

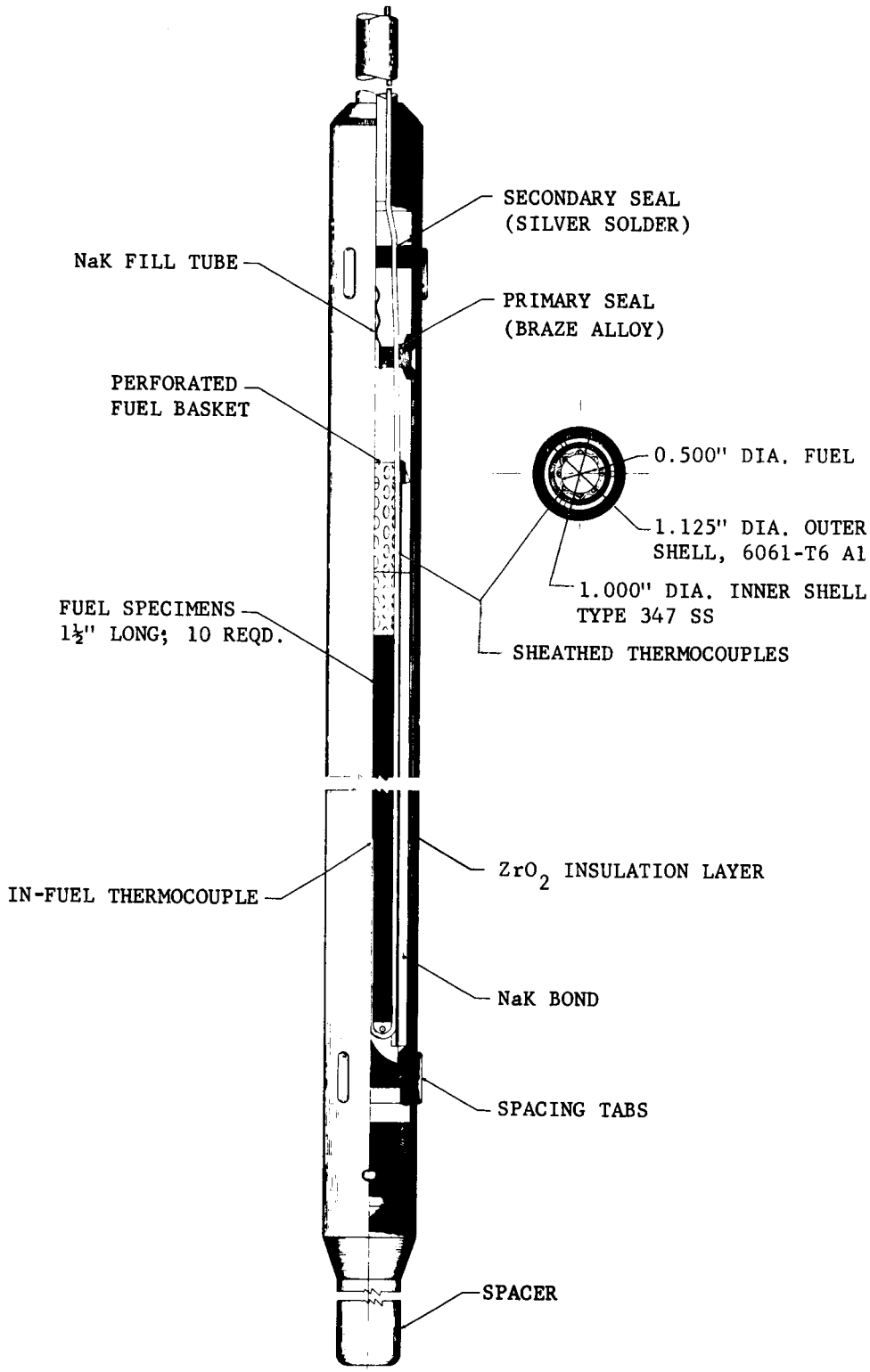

Fig. 44. ATL*-2 Irradiation Capsule. (*Capsule designed and fabricated by The Advanced Technology Laboratories Division of American Standard.)

Table 21. ATL Specimens: Composition and Heat Treatment

Specimen Code	Alloy Composition	Heat Treatment
I-A[a]	90% Th—10% U	Solution heat treated 3-1/2 hr at 1320°C, helium quenched, annealed 2 hr at 850°C
I-B[a]	90% Th—10% U	Annealed 2 hr at 850°C
II-A[b]	88% Th—10% U—2% Zr	Solution heat treated 3-1/2 hr at 1320°C, helium quenched, annealed 2 hr at 850°C
II-B[b]	88% Th—10% U—2% Zr	Annealed 2 hr at 850°C
III-A[b]	85% Th—10% U—5% Zr	Solution heat treated 3-1/2 hr at 1320°C, helium quenched, annealed 2 hr at 850°C
III-B[b]	85% Th—10% U—5% Zr	Annealed 2 hr at 850°C

[a]One specimen per capsule.

[b]Two specimens per capsule.

Capsules 3-1 and 3-3 were installed in the GETR in June 1963. Capsule 3-1 remained in-pile for about two months, at which time its irradiation was permanently terminated because most of the eight thermocouples had failed. Capsule 3-3 was irradiated for an additional two months and performed without incident until it was temporarily discharged. The capsule now is in storage in the GETR pool. The reasons for its removal from the reactor are discussed below:

Capsule 3-2 was placed in-pile toward the end of August. Its insertion had been delayed because the bottom weld was faulty and had to be repaired. The duration of exposure for this specimen was only one week, owing to a leak in the aluminum cladding. Subsequent hot-cell examination showed that the leak was caused by a crack in the top weld.

Capsule 2-2 was inserted at the same time as 3-2 in order to serve as a substitute for 3-1. This specimen was irradiated at the lower temperatures for over two months and behaved well. It was removed from the GETR simultaneously with capsule 3-3 and is in temporary storage also.

As indicated, capsules 3-1 and 3-2 were transferred from the GETR to the Radioactive Materials Laboratory for postirradiation examination. White film patterns were observed over large areas of the outside surfaces of both flow-deflector tubes. The capsules were removed from the deflectors and were found to have sustained appreciable bowing, which presumably caused them to stick to the deflectors. When this was observed, capsules 3-3 and 2-2 were indefinitely removed from the reactor until it can be ascertained whether it is safe to operate them in the bowed condition. General Electric is presently conducting tests and analyses to evaluate this.

When capsule 3-1 was disassembled, it was found that the lower portions of the fuel-pellet column, fuel-basket thermocouples, and stainless-steel containment tube had melted. The available evidence suggests that overheating had occurred because of erroneous thermocouple readings.

The interior of capsule 3-2 also was visually examined, and there were no changes apparent as a result of the one-week irradiation.

Capsules 2-1 and 2-3, which failed to pass a leak check, will be repaired so that at least one of them can be irradiated. To minimize bowing, the interior of the flow deflector will be ribbed.

3.3 Development of Vibratory-Compaction Method

A major problem in obtaining high bulk-fuel densities in powder-packed rods is in optimizing the vibration energy delivered to the fuel tube. A study was initiated to find generalized rules that will lead to a simple prescription for vibratorily packing oxide fuels to high bulk densities. Some of the initial results obtained for fused and ground UO_2 packed into type 304 stainless steel tubes (42 in. long x 0.5 in. OD x 0.035 in. wall) are presented below.

For these initial experiments, the vibration energy sources were an MB electrodynamic shaker and a Branford variable-impact vibrator (VIV). The electrodynamic shaker generates a pure sine wave over a frequency range of 0 to 3000 cps and is limited to a maximum acceleration of 100 g. On the other hand, the VIV produces a mechanical pulse exceeding acceleration levels of 20,000 g. The pulse-repetition rate is variable between approximately 1 to 400 impacts per minute, and the pulse width at half maximum is approximately 25 μsec.

3.3.1 Results of Experiments

The experimental approach followed in this study was first to optimize the procedures for packing with the electrodynamic shaker and then to compare the electrodynamic shaker with the Branford VIV. Several basic modes of operation are available with the electrodynamic shaker. These are: (1) constant frequency and constant acceleration level, (2) continuously varying frequency and constant acceleration level, and (3) continuously varying frequency and varying acceleration level. The mode of operation in (3) is difficult to reduce to a simple prescription and depends greatly on the operator's attention to several controls. This mode is also most likely to result in damage to the shaker and therefore was discarded early in the program because the results did not warrant further study.

Some of the results obtained for operation in mode (1) are shown in Figs. 45 and 46. The plots in Fig. 45 show that bulk density is a slowly varying function of acceleration level and that there is a small frequency dependency. The data obtained in Fig. 46 show the frequency dependency at a fixed acceleration level of 60 g and a small time dependence. This mode of operation is not considered to be optimum because the maximum bulk density obtainable was only 85% of theoretical.

Figure 47 shows the results for operation in mode (2). The frequency sweep is automatically performed and is relatively simple to set into the equipment. This plot shows that the maximum bulk density was obtained by cycling the frequency between 300 and 1000 cps for 10 min while maintaining the acceleration level constant at 60 g. It was also found that the bulk density was not sensitive to the total time (5 to 15 min)

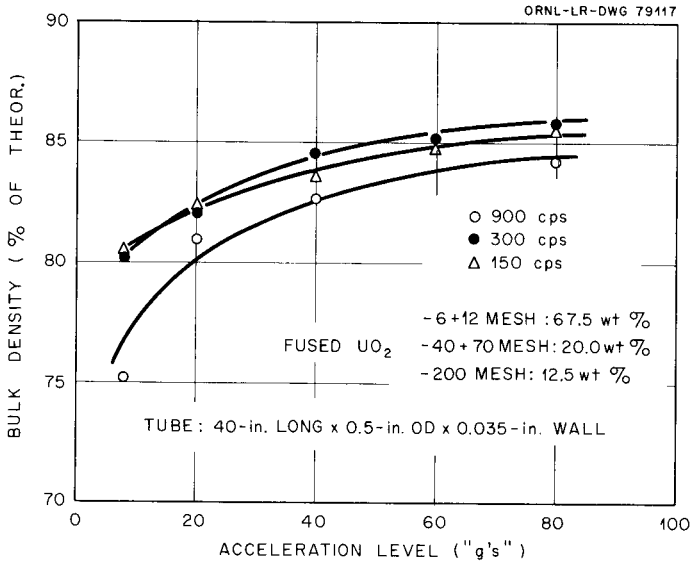

Fig. 45. Effect of Acceleration on the Bulk Density of Fused and Ground UO_2.

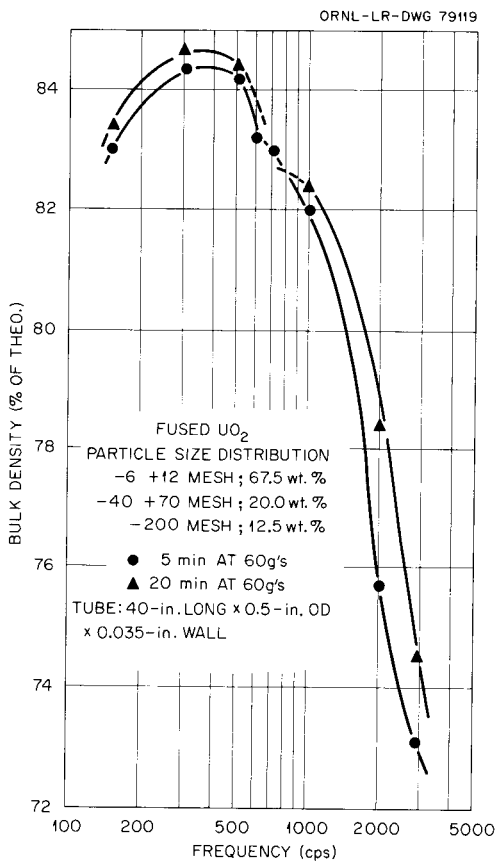

Fig. 46. Effect of Frequency at Fixed Acceleration on Bulk Density of Fused, Ground UO_2.

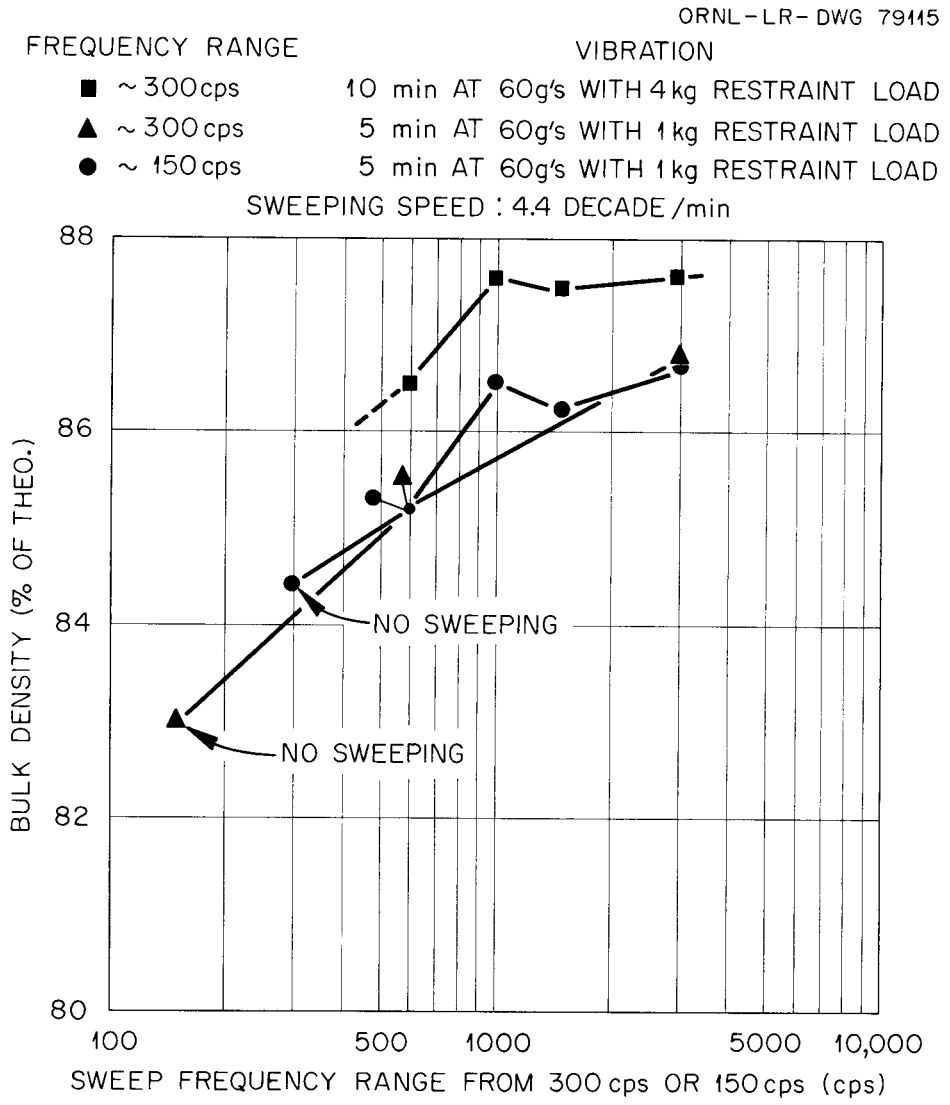

Fig. 47. Effect of Sweep Frequency Range at Constant Acceleration on Bulk Density.

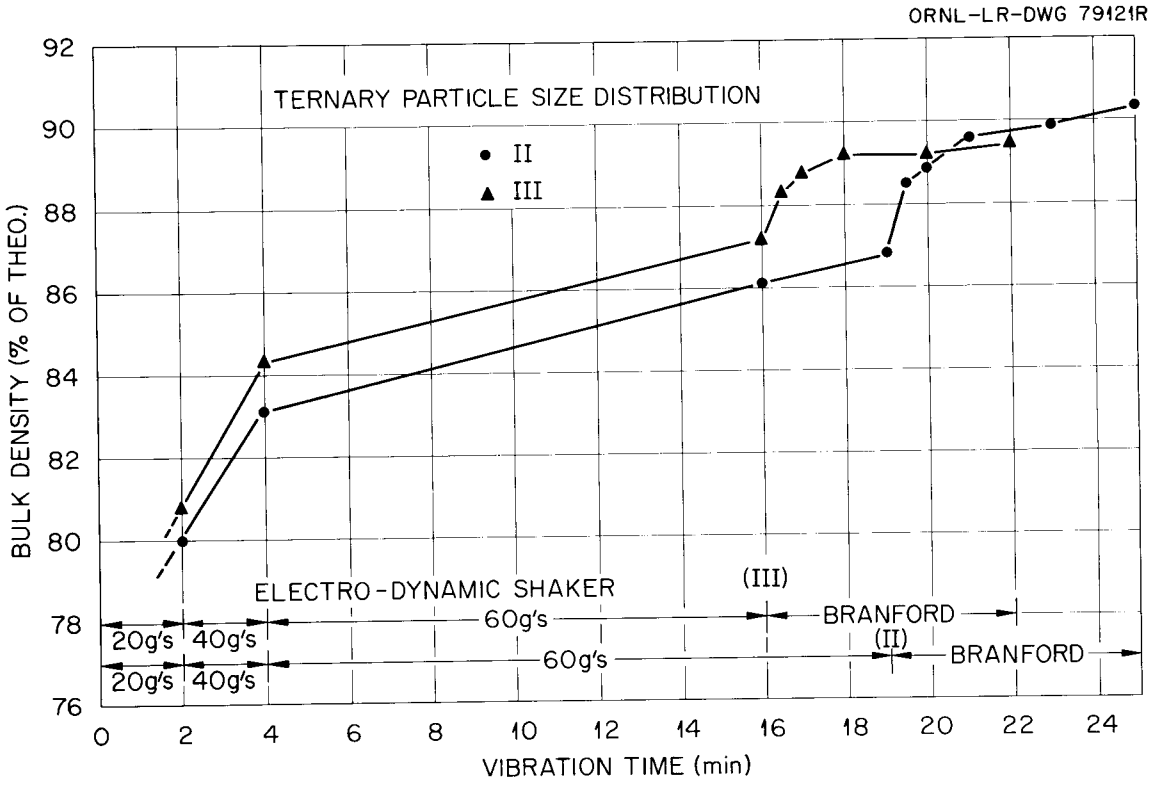

Fig. 48. Density Change with Vibration Time Using Continuously Varying Frequency and Constant Acceleration.

or to the sweeping range, provided that the resonance frequency of the loaded tube is included in the range. Fast sweep rates yield higher bulk densities than slow ones because the slower rates allow a longer resonance excitation which leads to de-densification. The resonance frequency for the 42-in.-long tube used in these experiments is about 650 cps.

3.3.2 Method Adopted

The compaction procedure derived from the above experiments is summarized below:

1. Load tube with material at 8 g and 300 cps.
2. Vibrate at 20 g and 300 cps for 2 min.
3. Sweep between 300 and 2800 cps at 40 g for 2 min.
4. Increase acceleration level to 60 g and continue for additional 12 min. This procedure was used in the comparison experiments with the Branford VIV, which was operated at 40-psi chamber pressure and 370 impacts a minute.

Figure 48 shows the results of packing ternary particle-size distributions first on the electrodynamic shaker and then on the Branford VIV.

Separate experiments with only the Branford VIV showed that the same end results could be achieved for the same time the Branford VIV was applied as indicated in Fig. 48. That is, the data points in Fig. 48, for the Branford VIV are independent of the prior compaction obtained on the electrodynamic shaker.

From these experiments it appears that energetic mechanical pulses yield higher packed densities than the low-energy pure sine wave. This information is being used to develop low-cost shakers operated pneumatically.

3.4 Permeability of Vibratorily Compacted Fuels: Waterlogging

The vibratory packing of loose oxide fuels into suitably dense systems within fuel rods, and the adaptability of the process to remote operation, make the method attractive for making thorium-based fuels. Reported in-reactor failure of a few fuel

compacts,[13] presumably caused by the entrance of water through a cladding defect during zero or low-power operation followed by expansion of the water upon increasing reactor power, showed that the mechanism of this type of failure must be adequately understood in order to minimize or eliminate such failures. (Water imbibition in a fuel is known as waterlogging.)

The permeability of these fuels is of interest because of its relationship to waterlogging. High permeability and low void volume in the compact facilitate the release of water from a waterlogged fuel element during reactor startup. Conversely, if the fuel were impermeable with no accessible voids, waterlogging could not occur.

Present studies are concerned with the quantitative relationship of surface area, degree of approach to theoretical density, and permeability of the fuel to waterlogging susceptibility of Kilorod type fuel elements.

3.4.1 Results of Experiments

The measurement of permeability consists in measuring the flow through a porous permeable sample under controlled conditions. The resulting data are reported in the form of a permeability coefficient:

$$\text{permeability coefficient} = k = \text{flow rate} \; \frac{(\text{viscosity})}{(\text{area}) \; \frac{\text{pressure}}{\text{length}}} \; ,$$

applicable to incompressible fluids. Suitable corrections allow for the compressibility of gases as working fluids, but, in high-density compacts, data points at several pressures must be taken to eliminate slip-flow effects.

In the absence of any surface interaction between the fluid and compact, the same calculated coefficient will be obtained, whether the working fluid is a liquid or a gas, if the data are taken in the viscous flow region.

To obtain the data, experimental permeabilities were obtained for tubular samples of compacted sol-gel oxides by measuring the flow rate of gases (argon and air) and liquids (water, methanol, benzene) under known pressure gradients at various

temperatures. The pressure gradient for liquid flow was provided by regulated air pressure applied to a calibrated pipette containing the liquid. Flow rate was calculated from the displacement-time plot. Gas-flow measurements were taken with the gas pressure as the driving force, and the flow rate was calculated from the time required to replace a known liquid volume with the exhausted gas at room pressure. This value was then corrected to the mean pressure within the sample and plotted as shown in Fig. 49 from data in Table 22.

Two sets of samples were prepared for the experiments reported here. Six samples were sol-gel oxide packed into 7/16-in.-OD stainless steel tubes from two sieve fractions; the packed length was about 15 cm. Table 22 contains the initial results from these samples.

Table 22. Observed Permeabilities for Samples of the Same Mixture at Various Packed Densities

Sample Code[a]	Packed Density[b]	Water	Air	Later Values - Water (Subscript indicates order)	
1	88.3	0.24×10^{-3}	1.99×10^{-3}		
2	88.0	0.30×10^{-3}	1.54×10^{-3}	$0.62 \times 10^{-3}_{2}$	
3	88.4	0.46×10^{-3}	4.38×10^{-3}	$0.37 \times 10^{-3}_{2}$	
4	84.6	0.45×10^{-3}	15.8×10^{-3}	$0.95 \times 10^{-3}_{2}$	$1.6 \times 10^{-3}_{3}$
5	85.3	0.59×10^{-3}	11.7×10^{-3}	$3.83 \times 10^{-3}_{2}$	
6[d]	84.6	0.70×10^{-3}	-		

[a]All samples from sol-gel oxide (65%, 6/16 mesh; 35%, -200 mesh)

[b]% of theoretical

[c]Values in Darcy (multiply by $\sim 10^{-8}$ for cgs units)

[d]BET surface area = 0.26 m^2/g; similar measurements not available on other samples.

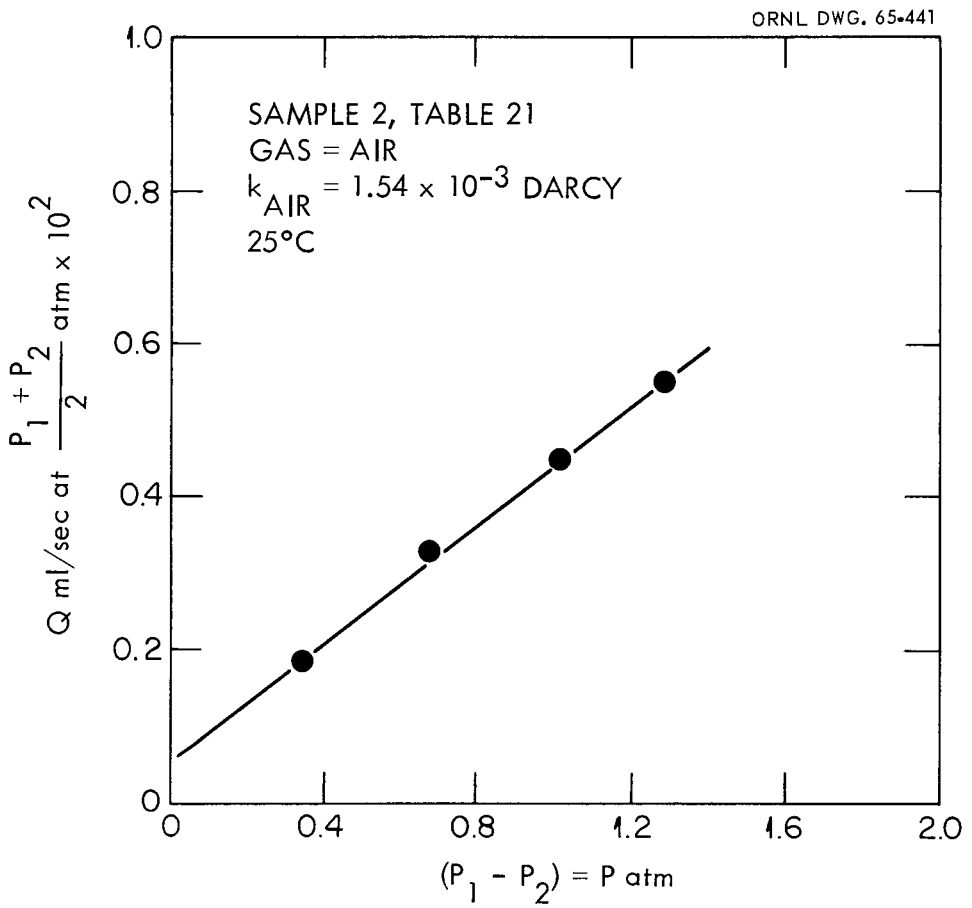

Fig. 49. Typical Gas Permeability Data.

Five other samples were prepared in 0.43-in.-ID stainless steel tubes that contained a porous, sintered filter at one end. These samples had a packed length of about 14 cm and were prepared from various size fractions of sol-gel oxide. Table 23 summarizes data from these samples.

Table 23. Gas Permeabilities for Various Size Fractions and Packed Densities

Sample Code	Packed[a] Density	Gas Permeability (Darcy)	Surface Area (BET) (m^2/g)	Size Fraction
A	89.6	[b]2.84×10^{-4}	0.37	45% 6/16 mesh 25% 16/50
B	90.6	[b]3.82×10^{-4}	0.42	15% 50/140 15% - 140
C	~87	[b]4.43×10^{-3}	0.28	65% 6/16 mesh 35% - 200 mesh
D	82.9	[c]6.5×10^{-2}	(d)	No fines Smaller than 325 mesh
E	86.5	[a]5.16×10^{-3}	(d)	No fines Smaller than 325 mesh

[a]% of theoretical

[b]Argon

[c]Air

[d]Not yet available

The large differences between liquid and gas permeabilities recorded in Table 22 were unexpected; however, later data indicate that probably two mechanisms are responsible.

The fact that the system is heterogeneous (mixed size fractions) allows many interstitial volumes, and the packing is not as dense as the bulk density indicates. The fine particles from these volumes are transported by the flowing liquid to nearby crevices where they pack to a higher density and restrict the flow. The result is a smaller value for apparent permeability. This effect is not observed with gas flow since the low-density gas will not transport the fines.

The second mechanism results from the surface properties of the oxide. The highly charged surface and small flow passages cause a streaming potential which appears as a backpressure phenomenon. This appears as a lower apparent permeability to liquid flow. The low dielectric constant of gases keeps this effect minimal.

Evidence supporting the second mechanism is shown in Table 24 and Fig. 50. These data were collected in a continuous set. That is, after initial saturation of the compact, it remained full of liquid. Water was the initial fluid, followed by methanol and benzene. It was felt that this approach would minimize further transport of the fines after initial saturation. In general, these data demonstrate the probability of a surface effect, since the apparent permeability increases with decreasing dielectric strength at constant temperature. The decrease in apparent permeability with temperature may be due to the increased combined specific conductance of the liquid and surface of the porous medium. This is suggested by an equation developed by Scheidegger[17] for a simple capillaric model. This evidence is not unequivocal but seems too specific to be entirely fortuitous.

Evidence for the first mechanism is more specific. Gas-permeability values are the same for a sample when taken before liquid saturation and after subsequent drying of the sample, whether by vacuum drying at 100°C or merely by passing room-temperature air through the sample. The indicated surface area of the material (according to Carman's technique[18]) is much lower than the surface area determined by the nitrogen adsorption method. This may be assumed to be due to bridging of the larger particles, which makes the fines noncontributors to the gas permeability. The final evidence for fines transport is the inability to reproduce a liquid permeability

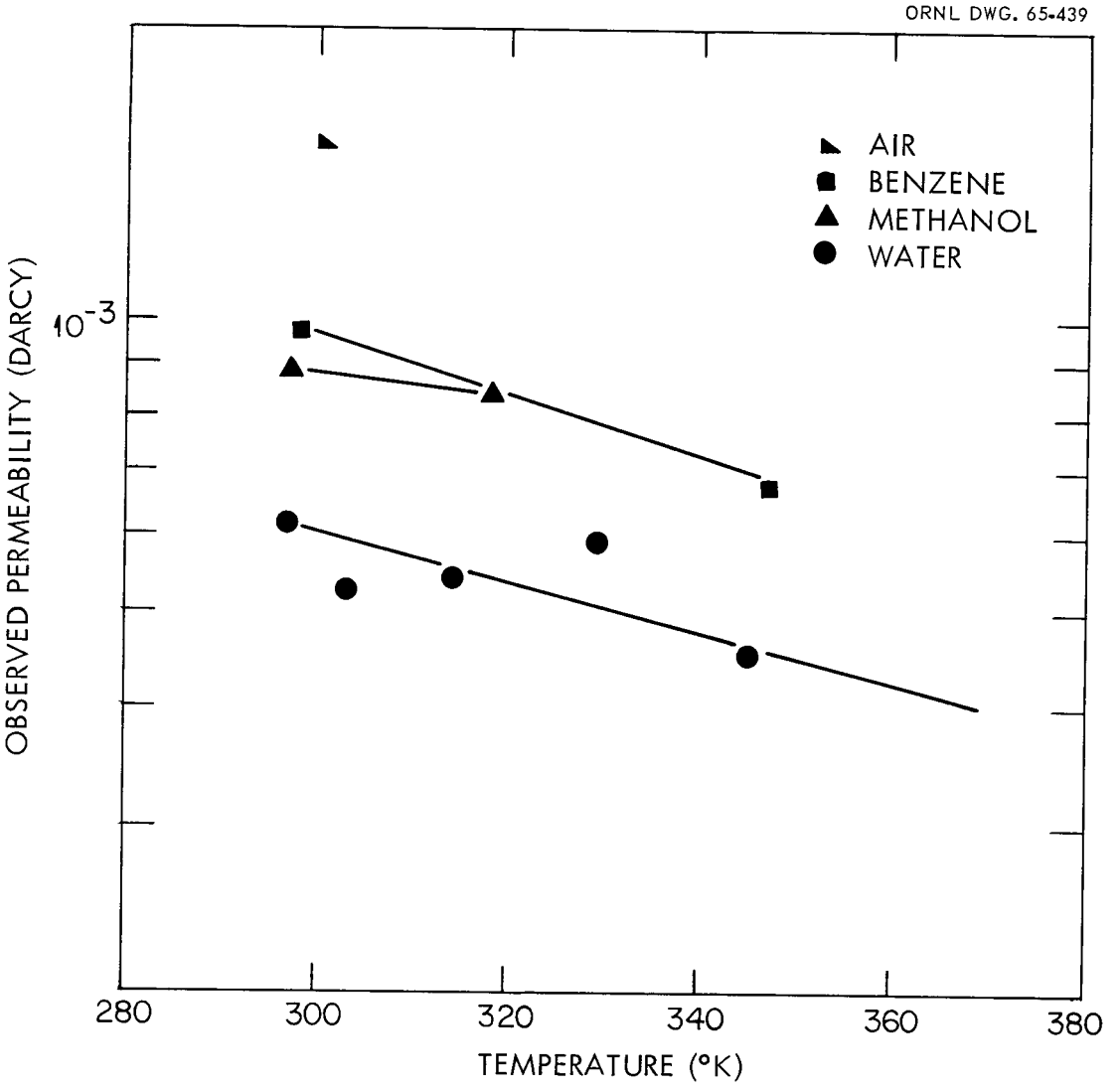

Fig. 50. The Effect of Fluid and Temperature on Observed Permeability.

value on a sample that has been adequately dried, although the reproducibility is fairly good as long as the sample remains wet.

Table 24. Effect of Dielectric Constant and Temperature on Observed Permeability

All data from Sample 2, Table 1

Fluid	Permeability Observed (Darcy)	Dielectric (Nominal)	Constant Temperature (°C)
Water	6×10^{-4}	80	25
Methanol	9×10^{-4}	33	24
Benzene	10×10^{-4}	3	25
Air	15×10^{-4}	1	25
Water	4.5×10^{-4}		73
Benzene	7×10^{-4}		74

3.4.2 Conclusions

The evidence for fines transport plus the fact that all samples examined thus far are in the intermediate range of permeability for water indicate that waterlogging upon failure of the cladding would present a problem under reactor conditions. Continuing studies will attempt to derive the quantitative relationship between permeability, surface area, and void fraction to waterlogging susceptibility and failure and to develop techniques to minimize such failure.

3.5 Pellet Fabrication

Powders prepared from calcined gel oxides are poorly suited to standard ceramic fabrication methods. Pellets made from this material result in structures

having poor strength and low density due to the high density and low surface activity of the individual powder particles. Sintering characteristics of the calcined gel oxide would be greatly improved by an extreme reduction in particle size (to approximately 1 to 2 μ), by blending lubricants and binders into the powders, and by using high forming pressures. These practices, however, are not well suited to remote fabrication. In another approach, a study was started on fabricating the gel in the uncalcined or low-temperature-calcined state. Pellets have been made from materials calcined at temperatures ranging from 150 to 700°C. Bulk densities of the pellets, up to 92% of theoretical, have been obtained when sintered at 1450°C, but they do not press well. The hard, abrasive particles dragging on the die wall during forming cause a patchy skin formation of uneven densities, which are reflected in surface-shrinkage tears during sintering. In addition, the evolution of large amounts of gases causes gross cracking. Efforts to improve the quality of these pellets are based on micronizing the gel oxides, using isostatic forming methods, and carefully controlling the heating rates during sintering.

3.6 Thorium Metal Fuels

In addition to the studies based on the sol-gel process for thorium oxide fuel preparation, a continuing effort has been carried on in thorium metallurgy. The principal effort has been on a study of ways to increase the high temperature strength of thorium metal.

During the past year, effort has been devoted to increasing the strength of thorium metal at elevated temperatures by dispersion hardening. In dispersion hardening, a finely divided refractory, nonreactive material such as a metal, a fine oxide, or other compound which will be stable, that is, one that will not go into solution or agglomerate into larger particles, is added to a metal. An example is the dispersion of Al_2O_3 in aluminum, which has been found to increase the creep strength of aluminum, even at temperatures approaching its melting point, to a greater extent than does alloying.

In order to achieve dispersion hardening in thorium, it is necessary to develop methods for making a fine thorium metal powder having an average particle size of less than 1 μ. The finely divided metal may then be blended with an equally fine refractory powder such as ThO_2. Two approaches were studied to produce the finely divided thorium metal. One was the conversion of thorium metal to thorium hydride, which is a friable compound that can be ground to a fine powder and then converted to the metal. The other was the grinding of calcium-reduced metal powder using various grinding aids. As reported previously,[19] the effects of length of ball-milling time of thorium hydride on particle size and the hot-hardness of hot-pressed compacts containing Th-10 vol % ThO_2 were studied. The compacts were extruded and hot-hardness tests indicated that a milling time of 24 days gave the highest hardness at all temperatures. Subsequent stress-rupture tests at 800°C on the extruded Th-10 vol % ThO_2 compact milled for 24 days indicated that the creep rate for dispersion-hardened thorium is from 3 to 6 times smaller than that reported for the strongest arc-melted alloy[20] at the same stress levels and temperatures.

Efforts were made to convert commercial calcium-reduced thorium powder directly to a fine powder to eliminate the hydriding and dehydriding operations. Ball milling of the powder alone was not successful because of the tendency of thorium to weld to itself. The use of grinding aids such as alcohol, heptane, and stearic and oleic acids did yield fine powders. However, because of the extreme reactivity of thorium, the aids reacted with the metal to form thorium carbide and other compounds. With alcohol, an unstable compound was formed, exploding violently upon being disturbed. Because of these adverse results, no further work was undertaken on the grinding of metal powders.

The strengthening of thorium by a combination of alloying and dispersion hardening was attempted by the addition of 10 vol % ThO_2 to alloys containing 2 and 5 wt % Zr. The alloys were prepared by ball milling thorium and zirconium hydrides for 24 days, hot pressing, and extruding. Hot-tensile-strength test results shown in Table 25 indicate that additions of ThO_2 to the thorium-zirconium alloys caused a decrease in strength rather than an increase.

Table 25. Thorium-Zirconium Alloy Tensile-Strength Tests at 800°C

Alloy	Ultimate Tensile Strength (psi)	Yield Strength (psi)	Elongation (%)
Th-2 wt % Zr	5300	4245	55
Th-2 wt % Zr—10 vol % ThO_2	5190	4810	16.5
Th-5 wt % Zr[a]	4570	No yield	0.4
Th-5 wt % Zr-10 vol % ThO_2	2385	2210	5.0

[a]Average of two tests

Another alloying element that has shown promise in strengthening thorium is indium. However, both arc and induction melting of thorium-indium alloys into forms suitable for fabrication has been difficult because of the high volatility of the indium. To alleviate this, powder-metallurgy procedures were used to prepare a series of alloys containing 2, 3, 4, and 5 wt % In. The indium, although very malleable, was converted to powder by ball milling in alcohol. It was then blended with calcium-reduced thorium powder. The mixture was hot pressed under a partial pressure of argon, homogenized at 1000°C and extruded at 900°C. Table 26 gives the results of tensile-strength tests at 800°C on the alloys.

From these tests it is seen that both strength and ductility of the alloys are optimum at 5 wt % indium—the highest indium content studied.

In order to determine the optimum oxide content for dispersion hardening of thorium, a series of mixtures containing 4, 7, 10, and 13 vol % ThO_2 were prepared by milling thorium hydride and ultrafine ThO_2 for 24 days. The powders were blended, hot pressed, and extruded. The results are given in Table 27. Thirteen vol % ThO_2, the highest content studied, imparted the highest strength to thorium.

However, its effect is not as great as the addition of 5 wt % In, as indicated in Table 26.

Table 26. Thorium-Indium Alloy Tensile-Strength Tests at 800°C

Alloy	Ultimate Tensile Strength (psi)	Yield Strength (psi)	Elongation (%)
Th-2 wt % In	6475	5550	10.0
Th-3 wt % In	7315	6330	6.0
Th-4 wt % In	6940	6120	5.5
Th-5 wt % In	7810	7130	20.0

Table 27. Th-ThO_2 Alloy Tensile-Strength Tests at 800°C

Alloy	Ultimate Tensile Strength (psi)	Yield Strength (psi)	Elongation (%)
Th-4 vol % ThO_2	6425	5360	11.0
Th-7 vol % ThO_2	4835	4530	33.0
Th-10 vol % ThO_2	4245	3415	15.5
Th-13 vol % ThO_2	7010	6265	23.5

The best alloys containing ThO_2, zirconium, and indium, based on the tensile-strength results, will be tested for stress-rupture properties in order to determine the optimum alloying conditions.

4. BASIC STUDIES

4.1 Preparation of Thorium Carbide and Uranium-Thorium Carbide by the Sol-Gel Process

The primary objectives of this work are to obtain uniform gel spheres of thoria-carbon and thoria-urania-carbon which will calcine to dense, uniform microspheres of dicarbides. The objective of a dense dicarbide sphere has been reached only in a qualified sense. Dicarbide microspheres having a density of about 80% of theoretical density have been prepared, but higher densities appear difficult to attain by the present approach. This problem is one for further study.

A flowsheet for the preparation of dicarbides of thorium and uranium-thorium by the sol-gel process was presented and discussed in Section 3.1.3. The steps in the process will be discussed in this section.

4.1.1 First Step: Preparation of Thoria and Thoria-Urania-Carbon Sols

First, thorium- or thorium-uranium oxide sols are prepared by the basic sol-gel process.[21] Then, a proprietary lyophilic carbon, Columbian Carbon Company or Cabot Corporation channel black, is added as the dry powder to the sol. The mixture is heated and agitated for 1 hr at 50 to 55°C. The carbon must have an acidic reaction with water to yield a pH of 3 to 4.5 and a high specific surface-area (100 to 1300 m^2/g).

Properties of Carbons Used for Preparing Sols. — Channel blacks are colloidal carbons, prepared by impinging a hydrocarbon-fueled (largely methane) flame, burning with excess oxygen, on a water-cooled surface. The carbon particle sizes range from 10 to 1000 A, and specific surface areas from 100 to 1400 m^2/g.

The properties of the carbons selected for use in this study are presented in Table 28. The more actively adsorbing carbons have a high content of volatile matter, a significant fraction of which is evolved as oxygen-containing gases (i.e., CO and CO_2) when the carbon is heated at 1000°C in argon.

Table 28. Properties of Carbons Used for Preparing Oxide-Carbon Sols[22,23]

Channel blacks: high surface area, lyophilic, high percentage volatile matter, acid reaction in water

Designation of Carbon Black	Particle Size (A)[c]	Specific Surface Area[d] (m^2/g)	Volatile Matter Content[e] (% by wt)	pH of 5 M Slurry in H_2O	DPG Adsorption Index[f]
Neo Spectra Mark I[a]	110	1390	16.2	3.0	100
Neo Spectra Mark II[a]	130	1000	14.7	3.3	98
Carbolac[b]	90	950	16.0	3.0	100
Black Pearls 46[b]	120	800	14.0	3.0	75
Supercarbovar[b]	140	400	5.0	5.0	20
Black Pearls 71[b]	160	380	5.0	5.0	17
Spheron 9[b]	290	105	5.0	4.5	20

[a]Columbian Carbon Company, New York, data sheet.

[b]Cabot Corporation, Boston, data sheet.

[c]Measured from electron micrographs.

[d]Nitrogen adsorption, B.E.T. method.

[e]Loss in weight at 1000°C in argon.

[f]Chemisorption of diphenyl guanidine relative to "inert" carbon—an indication of readily available acid groups on the carbon surface, in terms of an arbitrary relative scale.

The channel blacks listed in Table 28 are wetted by water, producing an acid suspension, the acidity of which increases with the amount and oxygen content of the volatile matter. These carbons are described by several workers[24,25] as a semi-amorphous material in which regular layers of graphite are stacked randomly to form 10- to 40-A crystallites. These crystallites are held together by otherwise unorganized

carbon to form moderately strong aggregates as open networks. Oxygen is chemisorbed onto the surface to form functional groups analogous to ethers, phenols, quinones, lactones, hydroquinones, peroxides, and carboxylic acids. In addition to chemisorbed oxygen, the carbon adsorbs hydroxyl ions preferentially into its highly porous structure from water, alkali, or salt solutions, leaving the solutions more acid. This acidity may be titrated with dilute KOH, but inflections are poorly defined, and there may be several. It is likely that carboxylic acid groups and phenolic groups contribute to the acidity. In water or alkaline solution and in the presence of a dispersing agent, the carbons can be dispersed by high-shear agitation to produce stable sols at a 5- to 6-M carbon concentration. The sols are flocculated by dilute acids or by an excess of alkali. Carbon aqua sols are electronegative, with particle mobilities being comparable to those of metal sols. At a pH of 3 or greater, positive ions and positive colloidal particles are sorbed by the carbon.

Interaction Between Surfaces of Colloidal Thoria and Carbon. — Colloidal thoria prepared by the steam denitration of thorium nitrate reacts with water to form basic hydroxyl surface sites that can be titrated with acid. For example, a plot of the conductivity of a ThO_2 sol against the number of micromoles of dilute HNO_3 added per square meter of surface gave a linear plot of near-zero slope up to a value of 5.3 micromoles/m^2. An abrupt increase in conductance at this point with additional HNO_3 gave a second linear plot having a slope equal to the increase in conductivity commensurate with increased HNO_3 concentration. Thus, the capacity of the ThO_2 surface for acid equivalents is 5.3 micromoles/m^2 (ref 26) (or between 0.07 and 0.08 mole of HNO_3 added per mole of ThO_2).

Similarly, a mixture of 4.4 moles of Neo Spectra Mark II (Table 28) carbon and 1 mole of ThO_2, prepared by steam denitration of thorium nitrate, in 1 liter of water was titrated with dilute HNO_3 (Fig. 51). A similar effect was shown for the same NO_3^-/ThO_2 mole ratio except that the transition in conductance for the mixture was a smoother curve rather than a break shown in the titration curve for pure ThO_2. The reason for the gradual, rather than sharp, change in slope is believed to be that the active surface groups on the carbon are weak acids which buffer the titration of the ThO_2 suspension with HNO_3.

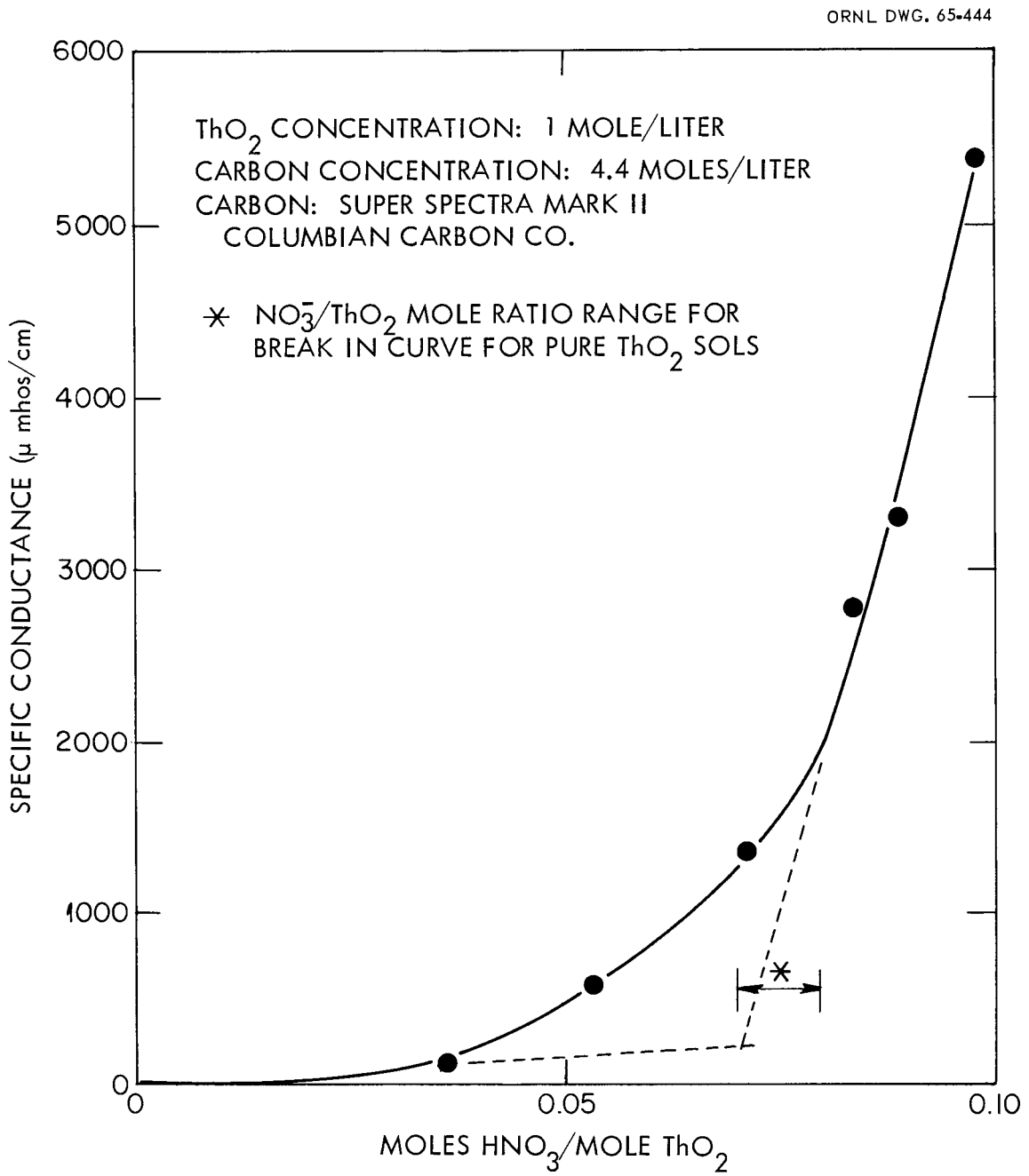

Fig. 51. The Specific Conductance of a Thoria-Carbon Sol at Various NO_3^-/ThO_2 Mole Ratios.

The weak-acid character of the carbon surface is further demonstrated by the plot of a conductimetric titration of Neo Spectra Mark II carbon-H_2O sol with dilute NaOH. As shown in Fig. 52, the conductance of the sol increases sharply at a value of 5.6 millimoles of NaOH per mole of carbon. This corresponds to a value of 2.12 micromoles of NaOH per square meter of carbon surface. The acid (HNO_3) equivalence of thoria (derived from steam denitration) in the stable sol form is 119.0 millimoles per mole. The carbon equivalent of thoria is therefore 21.2 moles of C per mole of ThO_2. The reaction between weak-acid sites of carbon and basic sites of ThO_2 can account for the adsorption of carbon on thoria if probable steric effects are taken into account. The electron micrograph (Fig. 53) of an evaporated thoria-carbon sol shows that the particles consist of crystallites or very small aggregates of thoria (opaque particles), each completely coated by the more nearly transparent (to electrons) carbon.

Stability of Thoria-Carbon and Thorium-Uranium Oxide-Carbon Sols. — When high-surface-area channel black (e.g., Columbian Neo Spectra Mark I, surface area = 1300 m^2/g) is agitated (without shearing) for 1 hr with well-dispersed thoria sol at 50°C, a fairly stable suspension results. If evaporated immediately to gel, the fine and coarse particles of gel which result have the same C/ThO_2 mole ratio, within 3%, and that all samples of the gel are fairly uniform in composition. However, if the same sols are allowed to stand for 72 hr, settling occurs. The distribution of ThO_2 and carbon between supernatant and settled phases is a function of the initial C/ThO_2 mole ratio. Table 30 shows the results of settling in a series of sols that had varying C/ThO_2 ratios. The C/ThO_2 ratio in the settled phase tends to be at equilibrium at 8.6 for the components used in this experiment, regardless of the initial ratio.

Since at the pH of thoria-sol stability the ionization of the carbon surface sites is suppressed, chemical means of dispersion are unlikely to be as effective for carbon as for thoria. Mechanical dispersion of the carbon aggregates is therefore important. Sols prepared by high shear dispersion were more stable, but they were highly thixotropic and plastic. But, thixotropy and plasticity interfere with the formation of small-diameter jet streams of sol, rendering sphere formation by the present spray system impossible.

Table 30. Distribution of Carbon and Thoria in Settled Sols

Settling time, 72 hr; composition, 0.92 M ThO_2, with various amounts of Columbian Neo Spectra Mark I carbon added

	Supernatant Phase			Settled Phase		
C/Th Atom Ratio of Sol as Prepared	C/Th Atom Ratio	ThO_2 Content (mg/ml)	Carbon Content (mg/ml)	C/Th Atom Ratio	Solids (C + ThO_2) (wt %) of Total in Suspension	Percent by Volume of Total Suspension
3	0.25	135	1.5	7.4	66.0	34.0
4	0.5	106	2.5	8.6	78	43.0
5	1.0	88	4.0	8.6	84	52.6
6	2.6	86	10.5	8.6	86.2	58.2

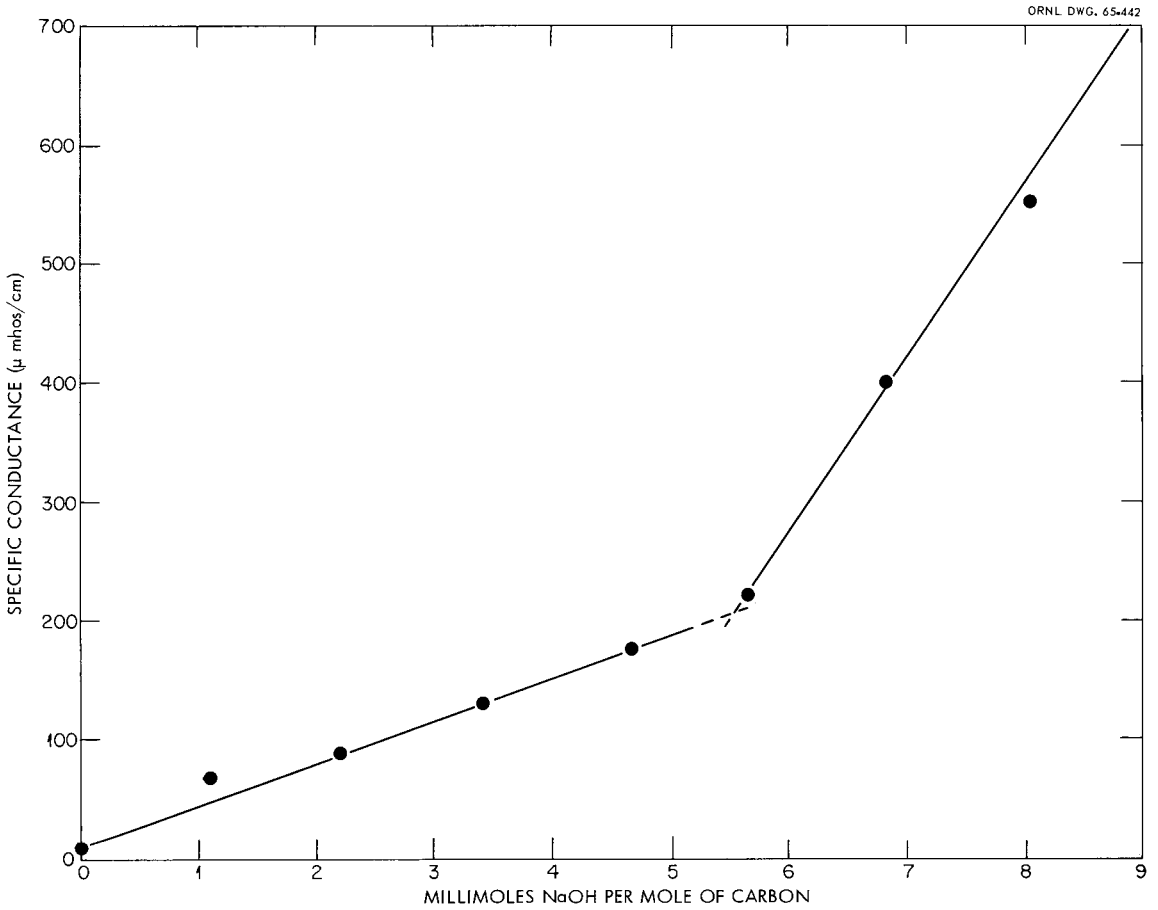

Fig. 52. Conductimetric Titration of Neo Spectra Mark II Carbon with NaOH.

PHOTO 68120

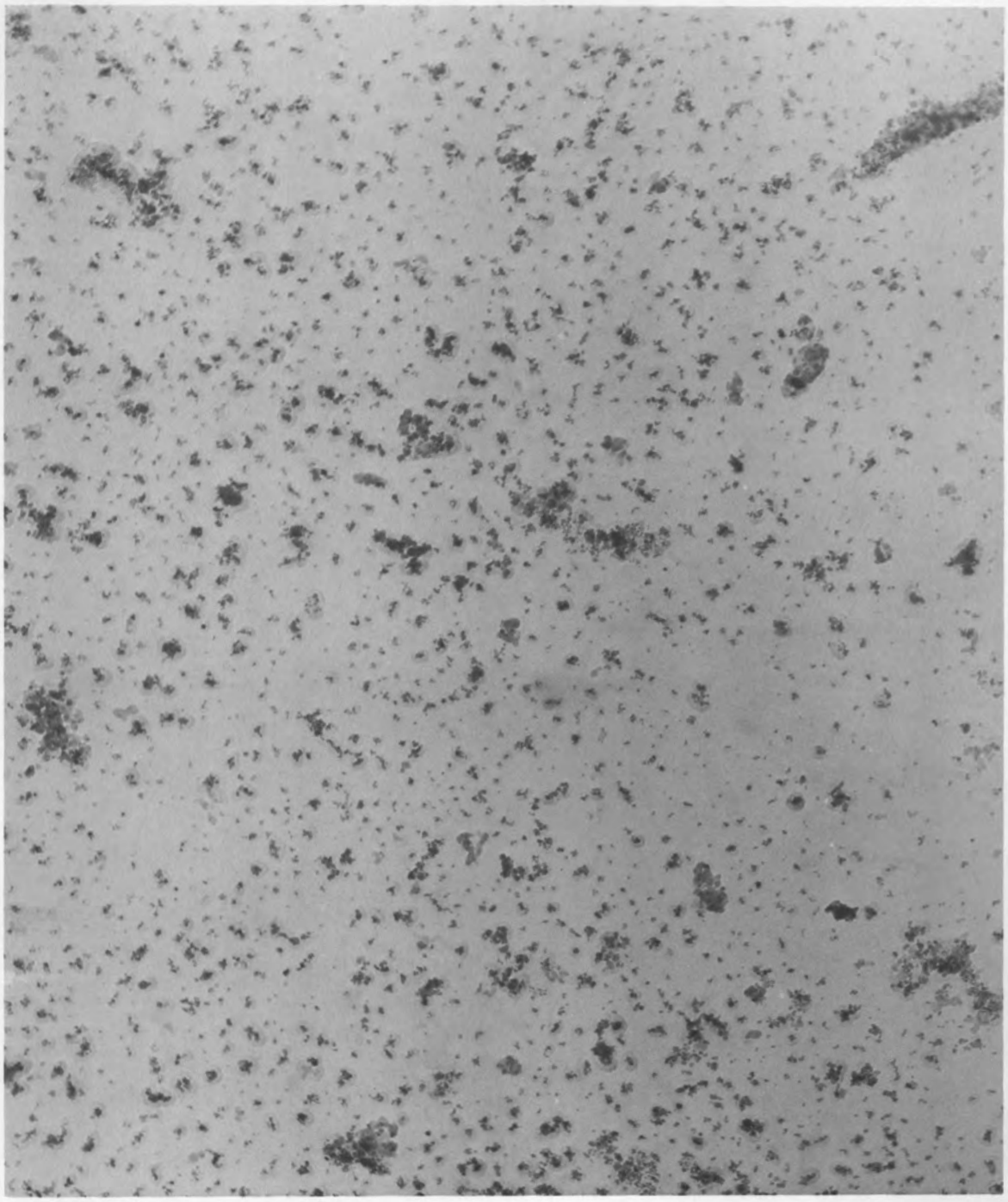

Fig. 53. Electron Micrograph of an Evaporated Thoria-Carbon Sol. ThO_2 concentration, 1 M; carbon concentration, 4.4 M; carbon, Columbian Neo Spectra Mark II Channel Black (68000X).

In order to study the effects of carbon activity on the stability of the sols, a series of thoria-urania-carbon sols was prepared, using carbons of widely differing surface activities. The sols were agitated at moderately high rates of shear, and nitrate/thoria mole ratios were maintained as low as possible (about 0.07) while still ensuring the stability of the sol. After one to two weeks of aging, the sols were formed into microspheres without further agitation. The properties of the carbons, sols, and gels are summarized in Table 31. The S-9 carbon (the lowest-surface-area carbon studied) appeared to give sols showing the least segregation of carbon and oxide, and also yielded gel spheres having the highest tap density. All the sols were more stable and uniform than those presented in Table 30. We suspect however that complete dispersion of carbon was not obtained in any of the above sols, and that the carbon was held to the ThO_2 surface as crystalline aggregates.

A uniform urania-thoria-carbon sol was prepared that had a U/Th atom ratio of 0.2 and sufficient carbon to convert both metal oxides to dicarbides. In preparation, the uranium was sorbed onto the carbon from a uranyl nitrate solution. This mixture was heated to 500°C (under argon) to remove nitrate, cooled, and then added to a stable thoria sol, using a wetting agent. The resulting sol was stable (did not settle) for longer than a week.

4.1.2 Second Step: Preparation of Gel Microspheres from Thoria-Carbon and Thorium-Uranium Oxide-Carbon Sols

In the second operation, microspheres of thoria-carbon and uranium oxide-thorium oxide—carbon having 10 to 1000 μ in diameter and 0 to 10 mole % in uranium were prepared by forming, suspending, and drying sol drops in organic liquids that were immiscible with the sols at room temperature (see Section 3.1.2). The organic liquids have small capacities for water (0.5 to 5% by weight) and extract water and HNO_3 slowly enough to gel the sol droplets without cracking them. The criteria for good microspheres are: near perfect sphericity, freedom from cracks or pits, highly reflective surface, high density with low porosity, and high strength. Laboratory studies were made to optimize the system for fulfilling the above criteria, and then to project the procedure to greater production.

Table 31. Properties of the Carbons,[a] Sols, and Gels

	Lot Designation		
	S-9	BP-71	BP-46
Specific surface, m^2/g (BET, N_2)	103	459	752
Volatile matter of the carbon[b]	5%	5%	14%
Volatile matter of the carbon[c]	8.5%	8.7%	27%
Sol U/Th atom ratio, nominal	0.0326	0.0326	0.0326
Gel U/Th atom ratio[c]	0.0325	0.0328	0.0339
Sol C/metal atom ratio, nominal	4.10	4.10	3.60
Gel C/metal atom ratio[c]	4.23	3.25	5.04
Tap densities, g/cm^3[d]	1.88	1.68	1.38

[a]Carbon blacks are a product of Cabot Corporation.

[b]From data provided by the manufacturer.

[c]From analysis at ORNL.

[d]Determined for formed and dried gel microspheres.

The column system (Sec 3.1.2) has been selected for the engineering development of the system for forming microspheres, so optimization studies were also carried out in a column system. Two small laboratory columns were built for studying the effects of variables in sol, extractant, and surfactant on the gel spheres.

Optimization of Extractant. — Sol droplets were formed by pumping a stream of extractant in laminar flow at right angles to a fine stream of sol injected into the extractant by a syringe. Several undesirable effects were observed as the sol microspheres fell through the column countercurrent to an upflow of extractant. These were: coalescence of droplets and sticking of the sol to the wall of the column, sphere deformation (tear drops, fishtails, and other nonspherical shapes), clustering, cracking, pitting, extraction of carbon, and extraction of thorium. Means of correcting some of the above effects have been found. Coalescence and wall adherence are thought to be due to excessive interfacial tension between sol and extractant. At present, the upper limit beyond which sphere coalescence and sticking to the column wall occurs is thought to be about 15 dynes/cm. Sphere deformation occurs at low interfacial tension and also when high residual water is present in the gel product. For oxide and oxide-carbon sols, the minimum interfacial tension for good sphere formation appears to be about 4 dynes/cm. Clustering of droplets is not well understood. Cracking is characteristic of large droplets in extractants having a high capacity for water (5 to 7 wt %) or of gel microspheres having a high residual water content. Pitting is thought to be due to uneven drying of the droplet. Extraction of either carbon or thoria causes the microsphere to crumble or to be porous and very weak. It is related to chemical reaction between sol and extractant but is not well understood. A problem commonly observed in forming carbon-containing sols is the "shedding" of carbon into the extractant, which leaves the spheres with a matte surface.

Fourteen water extractants were examined, and of these, 2-ethyl-1-hexanol (2-EH) was the most suitable for setting both oxide and oxide-carbon sols to gel microspheres. The properties of 2-EH that appear to be significant are:

viscosity, 25°C	10 to 13 centipoises
water solubility in 2-EH, 25°C	2.6 wt %
solubility of 2-EH in water	<0.1 wt %
interfacial tension with water, 25°C	15 dynes/cm in equilibrium with water
flash point	185°F
minimum-boiling azeotrope with water at 98°C	25% H_2O in azeotrope
chemically neutral to sol	no acid, base, or oxidizing agent

A higher viscosity (about 100 cp) would be better for forming microspheres of 100 to 500 μ diameter because it would permit higher extractant velocities in the column while still retaining laminar flow. Laminar flow is important in minimizing collisons between the spheres. The high flash point is desirable for safety, particularly if azeotropic distillation is to be used for separating water from the extractant. The formation of a low-boiling azeotrope makes possible the recovery of extractant below its flash point.

Other primary alcohols were marginally useful — 1-hexanol, 1-heptanol, 1-octanol, and 2-methyl—1-pentanol. Cyclohexanol, a secondary and cyclic alcohol has too low an interfacial tension with the sols. Ketones are too soluble in the sols.

Selection of Surfactants. — Surfactants control the interfacial tension, preventing or minimizing many of the undesirable effects listed above. In forming sol spheres, surfactants which are more soluble in extractant than in sol, yet very slightly soluble in the sol, are the most successful.

Cationic surfactants have been the most effective with oxide sols containing no carbon. The Armour "Ethomeens" and the Geigy "Amines" and "Altosperse" surfactants are preferred, and were effective at concentrations of 0.5 to 1.0 vol % of the extractant. All evidence to date shows that these surfactants recycle without serious deterioration through the distillation step for removal of water from the 2-EH. Anionic surfactants enhance extraction of thoria into the organic phase. Non-ionic surfactants (polyethylene glycol esters of fatty acids and fatty acid-amides) have been effective

only if they have a relatively large number of hydroxyl groups in their molecules and are objectionable because they lower interfacial tension too much, distorting the microspheres.

For sols containing carbon, the carbon itself may be a sufficiently active surfactant to prevent coalescence and wall-sticking. Anionic and cationic surfactants enhance thorium and carbon extraction, respectively, and weaken the gel structure. Carbowax esters of oleic and ricinoleic acids at 1 to 2% concentration suppressed carbon shedding.

4.1.3 Materials and Experimental Equipment

The formed and dried gel microsphere of thorium oxide—carbon or uranium-thorium oxide—carbon were converted to the corresponding carbides by induction heating in a vacuum or a current of inert gas, such as argon. Nearly complete conversion of the oxides to carbides was attained in 1 to 6 hr in the temperature range of 1450 to 1750°C. In another heating procedure, argon at 1 atm was passed through the furnace up to the initiation of the reaction. The argon was then turned off, and the system was sealed to retain reactant gases. Under such conditions completion of the reaction required about 6 hr at 1900°C, or 1 hr at 2100°C.

Calculations from thermodynamic data (Fig. 54) for the reaction

$$ThO_{2(c)} + 4C_{(c)} \rightleftharpoons ThC_{2(c)} + 2CO_{(g)}$$

show that conversion of thorium oxide to thorium dicarbide at 1500°C will give an equilibrium vapor pressure of CO of about 6000 μ Hg under the conditions for which the data were obtained. For the conversion runs conducted in vacuum, the total pressure of the evolved gases (assumed to be CO) varied from 10 to 1000 μ. Assuming good contact between the reactants, if the system pressure is maintained below the equilibrium pressure of CO, the reaction should proceed until one of the reactants is consumed. The intimate contact achieved between reactants by mixing them as colloidal dispersions, as in the sol-gel process, probably accounts for the completeness of the reaction achieved in this system.

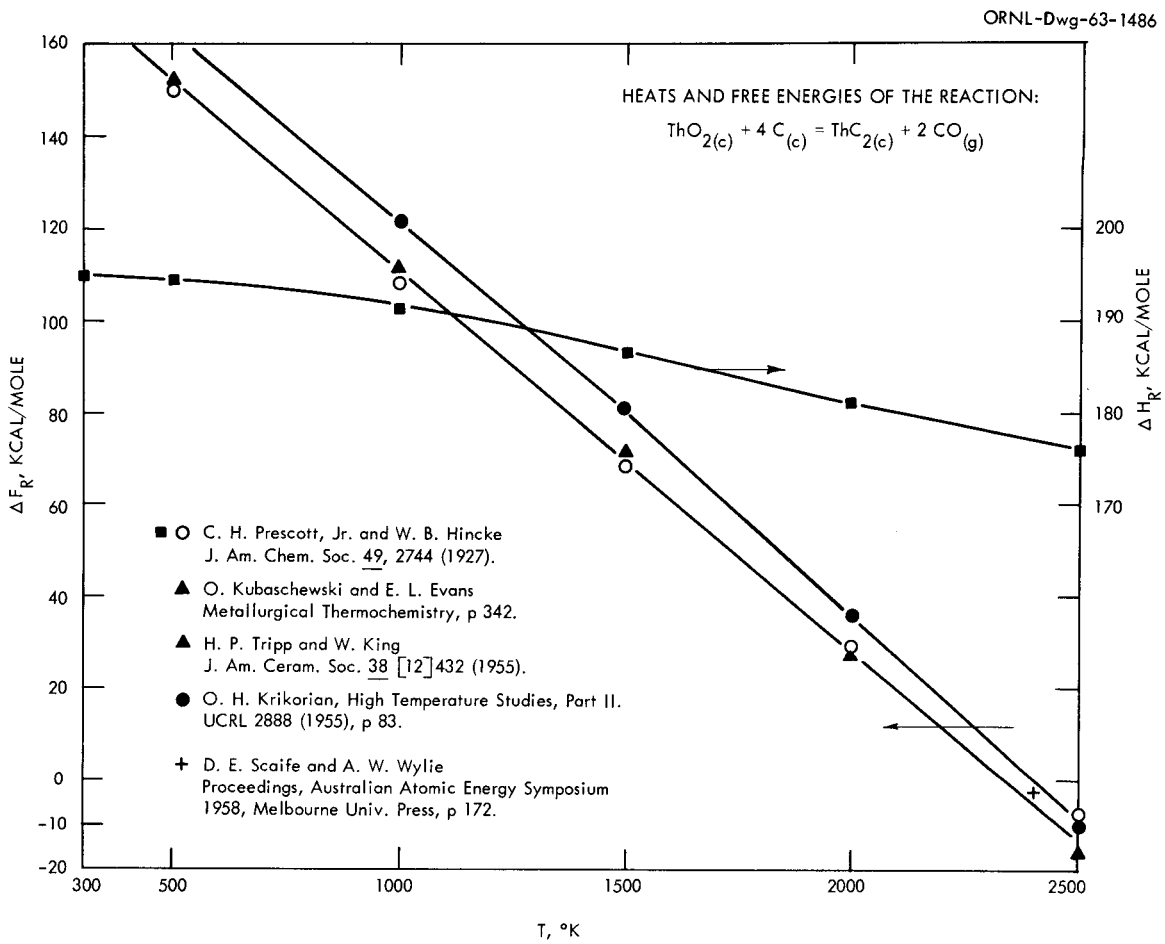

Fig. 54. Enthalpies and Free Energies for the Conversion of ThO_2 to ThC_2.

The kinetics of the oxide-carbon reactions taking place in vacuum and at temperatures from 1445 to 1750°C were investigated. A drawing of the apparatus is shown in Fig. 55. The reaction took place in an inductively heated graphite cylinder suspended in an evacuated quartz envelope. The vacuum pump operated throughout the run, and the vacuum varied from 1000 μ at the start to about 10 μ at the finish. The pump exhausted the evolved carbon monoxide to a volumetric gas meter. The volume of carbon monoxide evolved was plotted against time (Figs. 56 and 57) to give kinetic information on the reaction. The reaction rate was proportional to the amount of unconverted ThO_2 and fits the first equation:

$$\frac{-d\,(ThO_2)}{dt} = k(ThO_2) \quad .$$

In integrated form,

$$-\ln\,(1 - X) = kt + \text{constant}$$

where

(ThO_2) = fraction of ThO_2 unreacted,
X = the fraction of ThO_2, reacted,
t = time, hr,
k = specific reaction rate, hr^{-1}.

The linearity of the plot of $-\ln\,(1 - X)$ vs t (Fig. 57) confirms the pseudo first-order nature of the reaction system up to about 86% conversion. In Fig. 57 reaction rate data at 1615°C are presented. At 1445°C, the reaction rate constant was 0.586 hr^{-1} and at 1615°C, 5.69 hr^{-1}, as calculated from the slopes of the plots of $-\ln\,(1 - X)$ vs time.

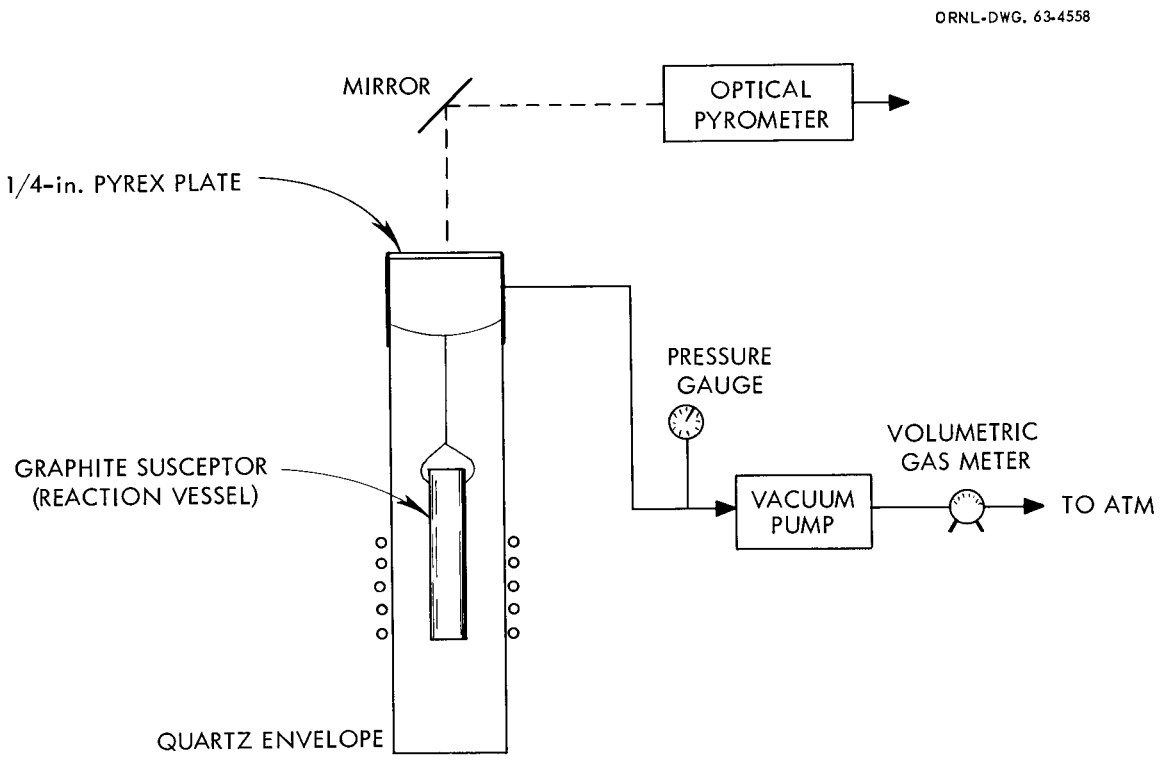

Fig. 55. Schematic Representation of the Apparatus Used for the Study of the Kinetics of Conversion of ThO_2 to ThC_2.

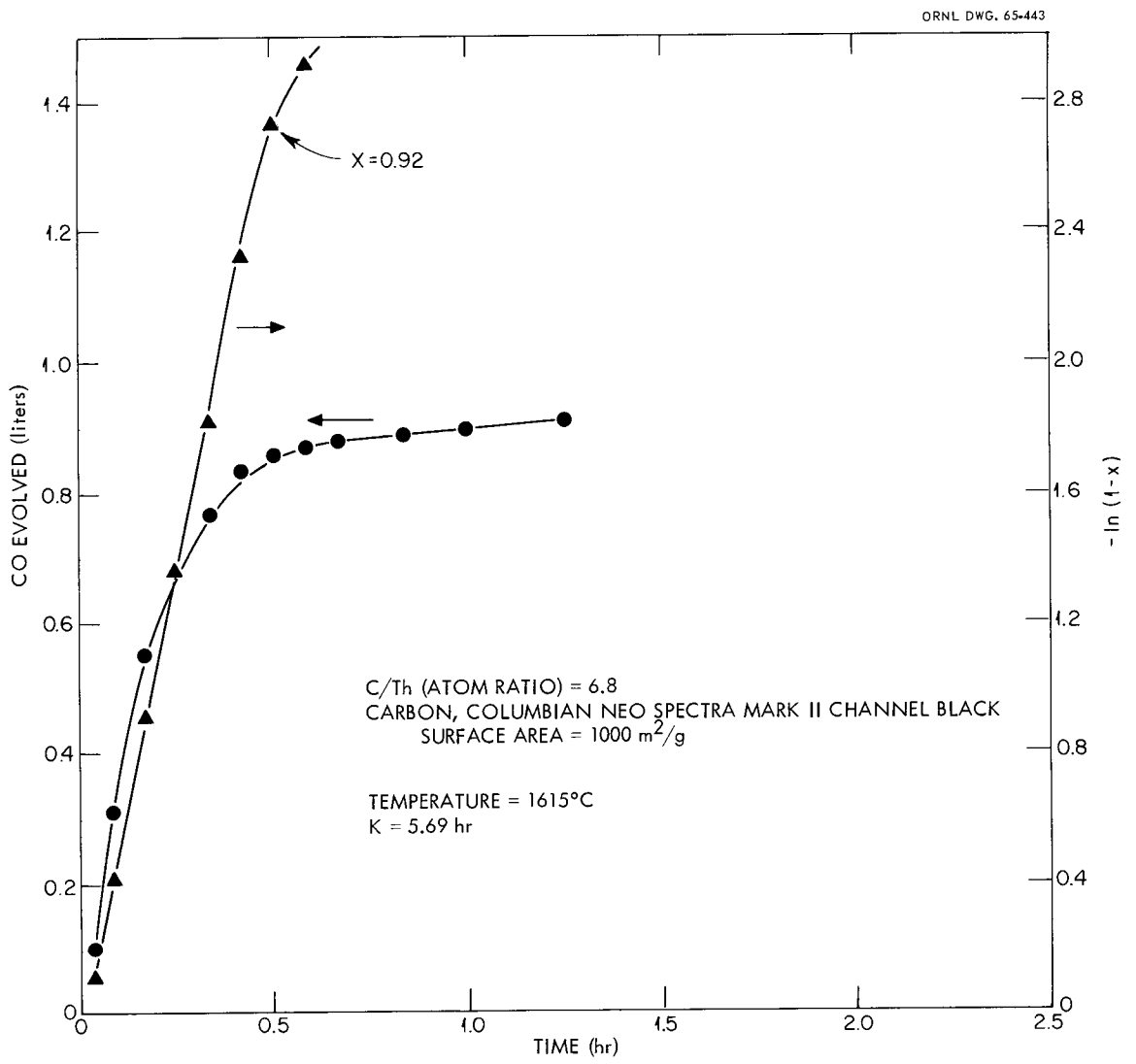

Fig. 56. Evolution of Carbon Monoxide as a Function of Time from the Reaction at 1445°C of ThO_2 with Columbian Neo Spectra Mark II Channel Black having a Specific Surface Area of 1000 m^2/g.

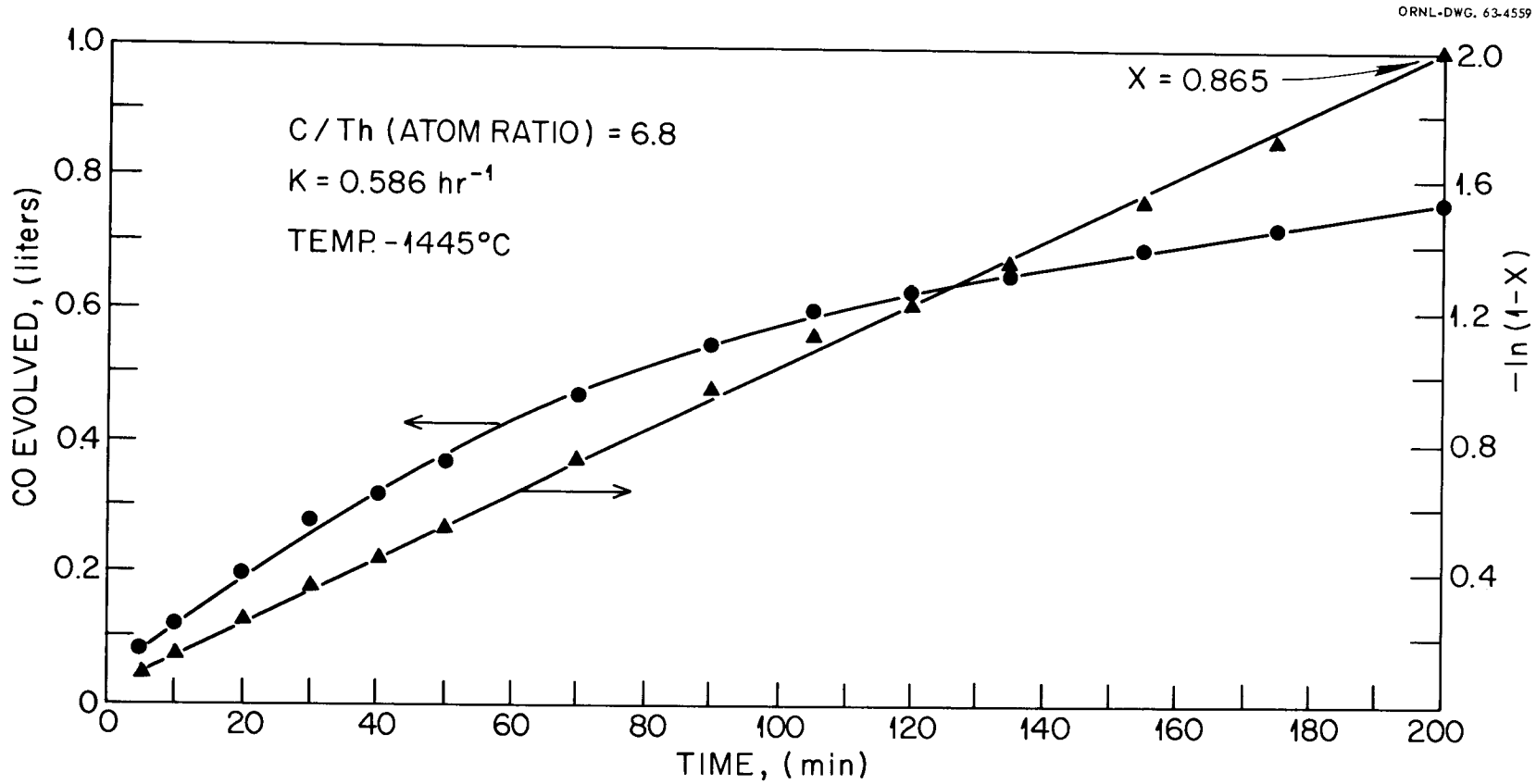

Fig. 57. Evolution of Carbon Monoxide as a Function of Time from the Reaction at 1615°C of ThO_2 with Columbian Neo Spectra Mark II Channel Black having a Specific Surface Area of 1000 m^2/g.

In Fig. 58, the reaction rate constants for conversion of thoria and of ThO_2—5% UO_2 to the corresponding dicarbides are plotted against the reciprocals of absolute temperatures between 1718 and 2023°K. Carbon-to-metal atom ratios from 4.3 to 6.8 are also represented. The activation energy for the oxide-dicarbide conversion was about 112 kcal per g-mole of ThO_2. Variations in the uranium content (0 to 5 at. %) and amounts of carbon as much as 170% in excess of the stoichiometric requirement for the formation of ThC_2 produced no significant effects on the reaction rates.

4.1.4 Properties of the Carbide Products

Particles of thorium- and uranium (0 to 5 at. %)-thorium dicarbide formed from irregularly shaped gel fragments contained 2 to 22 wt % of free carbon, had densities of approximately 2.74 to 8.58 g/cc, and contained surface-connected porosities of 6.9 to 48.3 vol % as measured by Hg porosimetry. The gel fragments had been preheated in argon to 1000°C before finally firing to about 1800°C in vacuum.

Spheroids formed in carbon tetrachloride—15% isopropyl alcohol shrank about 30% in diameter when calcined in a way similar to that just described for the irregularly shaped pieces. The density of the product was decreased and porosity was increased in direct relation to the amount of free carbon. There was some indication that the preparations calcined at higher temperatures and for longer times had higher densities and lower porosities.

The particle densities and porosities were measured by pycnometric toluene immersion and mercury porosimetry. Neither method has been refined to the point where completely reliable density and porosity data can be obtained for carbides because the wettability of the product by toluene and by mercury are not known accurately. The particle-density values are to be considered only as good approximations.

Figure 59 is a plot of pore volume vs pore diameter calculated (on the assumption of cylindrical pores) from data obtained by the mercury porosimetry of cracked, irregularly fragmented particles of the dicarbides. Several populations of pore diameters

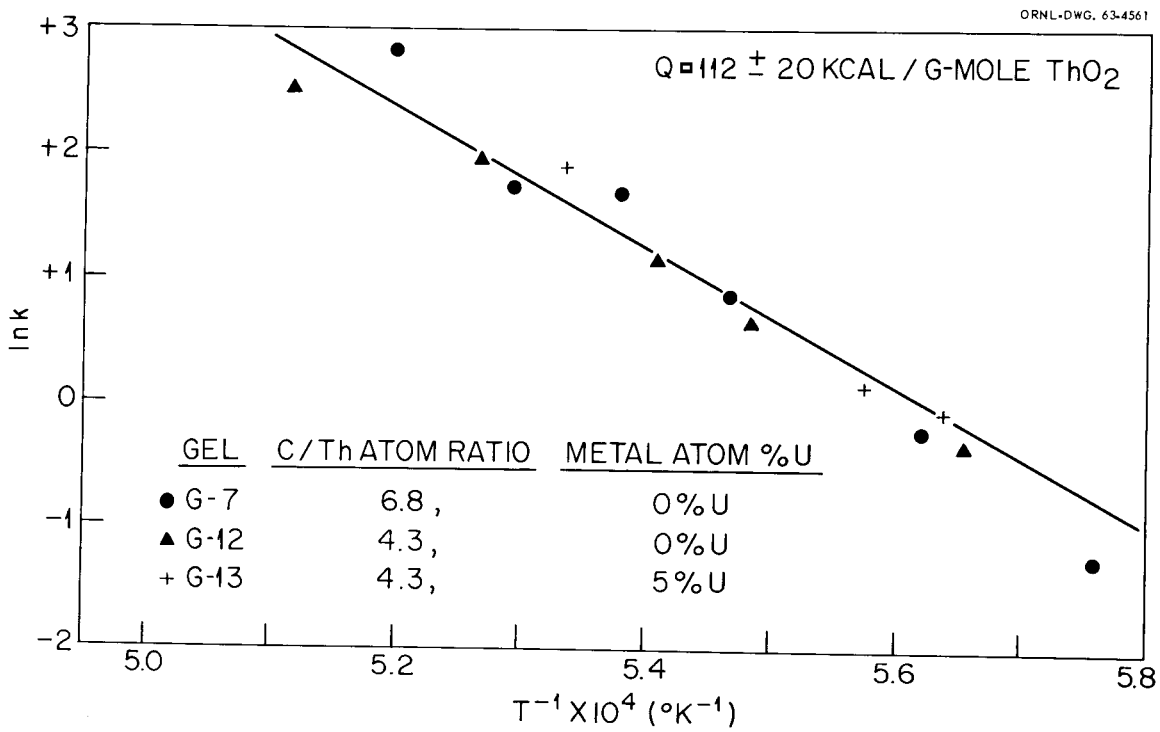

Fig. 58. Arrhenius Plot of Specific Reaction Rates for the Conversion of ThO_2 to ThC_2.

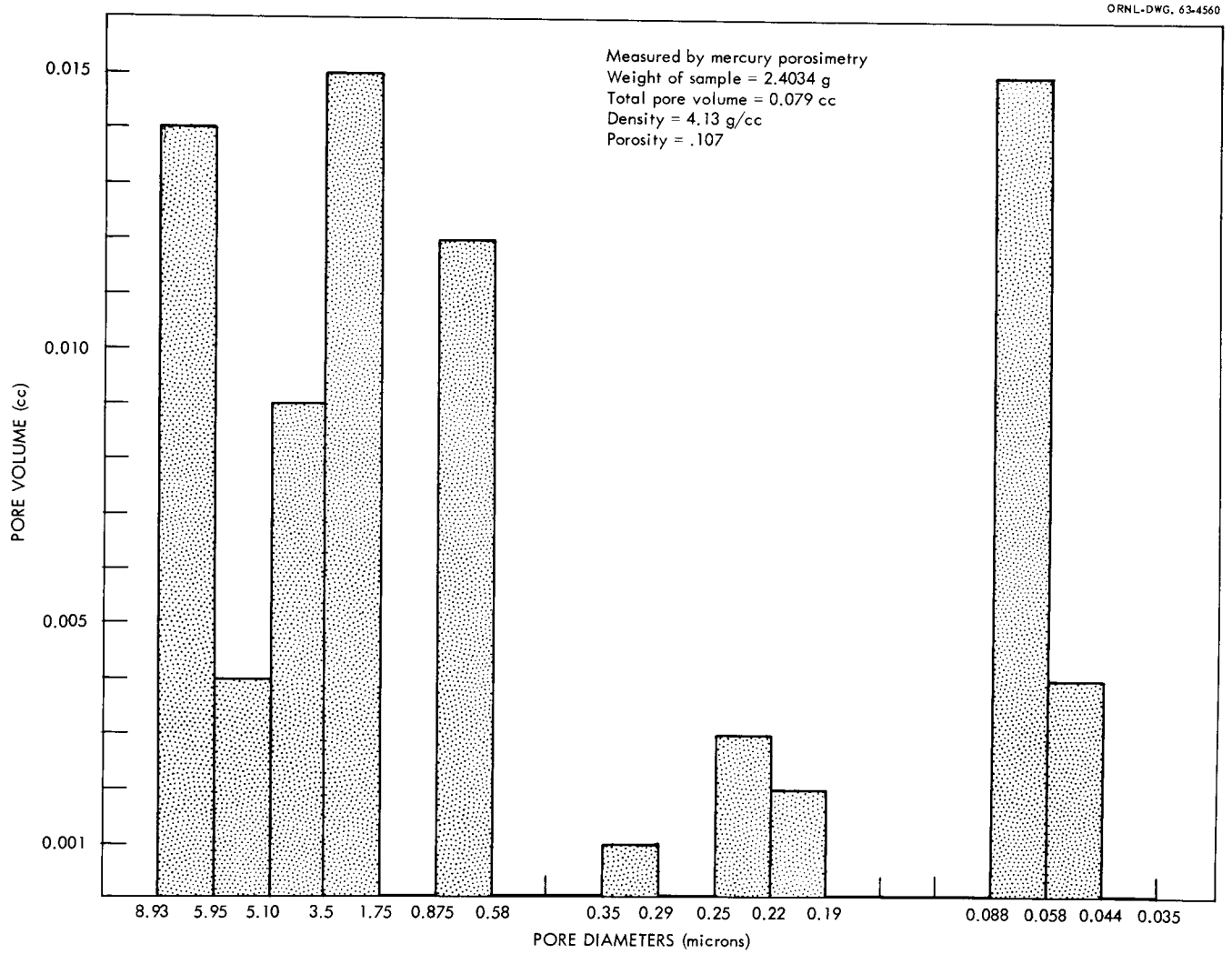

Fig. 59. Pore Volume Distribution of a Thorium—5% Uranium Dicarbide Sample Prepared from Irregularly Shaped Gel Fragments.

are present in these dicarbides. The pore volume of the group having the largest pores was at least 50% of the total pore volume in nearly all the dicarbide products of the various oxide-carbon sols studied, regardless of their C/Th atom ratio. From visual observation, it appears that the large pores may be due to cracks generated in the gel fragments during the drying step. Apparently the larger pores were eliminated from the particles when they were spheroidized in 2-EH.

A series of spheroidal carbide products was prepared from thoria sols containing about 3 at. % uranium oxide and one of four channel blacks. The spheroids were formed in 2-EH (see Sec 4.1.2), dried at 100°C, and converted to carbides in a static atmosphere of argon, with CO increasing as the reaction progressed at 2100°C. The properties of the sols, gels, and carbides at the various stages of preparation are presented in Table 32. The gel spheres containing carbons having the low specific surface areas (100 to 400 vs 800 m^2/g) have higher densities (2.7 vs 2.1 g/cc) and lower porosities (0.09 and 0.08 vs 0.11 and 0.13 cc of pores/cc of solid) than those containing carbons having high specific surface areas. There is some indication that the gels of higher density calcine to carbides of higher density. An increase in uncombined carbon content appears to decrease the density of the product.

The percentage conversion of oxide to carbide appears to be related to the amount of excess carbon, the final calcination temperature, and the calcination time. The accuracy of the percentage conversion data is subject to some doubt. Contact with moisture or air converts a part of the carbide to oxide, and the conversion is based on the residual ThO_2 found by analysis. The stoichiometric ratio of combined carbon to thoria for the dicarbide is 1.96[27], therefore, the theoretical weight percentage of carbon in dicarbide should be 9.18%.

Spheroids of thoria-carbon gel and of urania-thoria-carbon have proved to be strong enough to permit handling with no special care. Oxide-carbon gel spheroids have been subjected to rapid heatup from room to reaction temperature (25 to 2100°C) in 10 min with little observed breakage. Some interparticle sintering was observed in firings at 2100°C for 1 hr, but none at 1750° for 1 hr.

Table 32. Properties of Sol-Gel Carbide Preparations at Successive Stages

Conversion conducted by heating rapidly to 2100°C and holding for 1 hr in a static atmosphere of argon, except where noted

	Sol				
Preparation No.	S-9	BP-71	BP-46	79 SC[a]	
U/Th atom ratio	0.0325	0.0328	0.0339	0.0330	
C/metal atom ratio	4.23	3.25	5.04	5.20	
Surface area of carbon, m^2/g	105	380	800	400	
	Gel Spheroid (formed in 2-EH and dried at 100°C)				
Densities, g/cc					
tap	1.80	1.68	1.38	1.35	
pore-free solid	3.04	2.83	2.24	2.37	
geometric sphere	2.78	2.63	2.02	2.09	
Porosity $\frac{\text{vol of pores}}{\text{vol of pore-free solid}}$	0.091	0.079	0.114	0.133	
	Carbide Product				
U/Th mole ratio	0.0317	0.0328	0.0336	0.0337	0.0327
Total carbon, wt %	8.93	7.29	10.6	9.24	8.65
Free carbon, wt %	0.17	0.08	1.74	0.35	0.18
Combined carbon, wt %[b]	8.76	7.21	8.86	8.89	8.47
Density, g/cc[c]					
By toluene immersion	-	9.1	8.3	-	-
By Hg porosimetry	-	-	7.9	-	-
Conversion, % of initial oxide to carbide	97.4	94.5	92.4[d]	98.28	94.7
% conversion to dicarbide	91.2	56.4	-	93.6	87.8
% conversion to monocarbide	6.2	38.1	-	4.6	6.9

[a]Single sol preparation fired in two batches.

[b]The theoretical percentage of carbon in thorium dicarbide ($ThC_{1.95}$) is 9.18 wt %; for ThC, 4.92 wt %.

[c]Theoretical density for ThC_2 is 9.6 g/cc.

[d]Conversion carried out in argon for 1 hr at 1875°C after having been fired at 600°C for 1 hr.

4.2 Rates and Mechanisms of Fission-Gas Release from Thoria-Urania Fuels

The kinetics and mechanisms responsible for fission-gas release from nuclear fuels have been under intensive investigation for many years. However, the rapid bursts of the noble fission gases released during temperature rises has not been explained. In an attempt to explain, it was reasoned that since dislocation movement is greatly accelerated by temperature increases, moving dislocations might well be the means by which noble gases are carried through a structure.

Experiments designed to investigate the interrelation of dislocation movement and fission-gas bursts seemed warranted and have been carried out. Preliminary results are presented here.

Application of a stress can cause dislocations to move at constant temperature. The experiment consists in applying and removing a known load to irradiated fuel pellets and measuring the ^{133}Xe released. The pellets consisted of ThO_2 containing 2 wt % highly enriched UO_2. These were irradiated for a length of time resulting in 1.85×10^{15} fissions/cm^3 and stored for a week to allow decay of the short-lived isotopes. Specimens were brought to a selected temperature and the fission-gas release rate was determined. A compressive stress was applied and the change in release rate was measured.

In these experiments, as has been observed in many others, there was an initial burst of radioactivity when the temperature was increased. After a steady-state condition was achieved, stress was applied,and there was again a burst of radioactivity. The magnitude of this release varied from an amount similar to that released during the temperature change to 50% more than the radioactivity measured during the temperature change. The stress-induced burst releases of activity could be increased by increasing either temperature or load. After the initial burst, the steady-state release rate was markedly higher from stressed specimens than for specimens tested at the same temperature with no applied stress. When the applied stress was removed, the rate of fission-gas release decreased to about the rate observed before applying the load.

There is a qualitative similarity between the characteristics of stress-induced release of ^{133}Xe and the creep behavior exhibited by thoria. Proportionately, the magnitude of the burst and the higher release rates at steady state under stress are similar to the magnitude of creep deformation expected under these conditions. Thus, there seems to be a strong correspondence between the motion of dislocations and the release of fission gas. However, some definitive tests are required before the mechanism by which dislocations transport the fission gas and the role of temperature changes on fission-gas release can be proposed.

4.3 Volatilization of Protactinium from Irradiated Thoria Fuels: Use of Chloride Melts

The prompt separation of protactinium from reactor-irradiated thorium would minimize neutron losses and result ultimately in the formation of ^{233}U of high isotopic purity. Separation processes could be facilitated by handling the thorium and/or the protactinium as a volatile material. Low-melting salt compositions should be attractive for this purpose. Volatilization techniques have been suggested for the separation.

An interesting separation has been reported in a patent;[28] $AlCl_3$ was heated with irradiated finely divided thoria in a sealed tube, after which aluminum and protactinium chlorides were volatilized at 75 to 150°C and condensed in a cool region, leaving behind thorium and uranium chlorides. Since the information in the patent is sparse, the elaboration of any such processes requires a detailed study of the phase and separation chemistry of the chloride salt systems. Knowledge of the vapor pressures, phase relationships, chemical complexes possibly existing in various phases, and the general thermodynamic characterization of the protactinium salts are desirable.

A preliminary study of the phase relationships of the $ThCl_4$-$AlCl_3$ system has been made. In addition, a study of the ability of $ZrCl_4$ to increase the mutual solubility of the components of this system has been attempted by investigating the $AlCl_3$—$ZrCl_4$ and $ThCl_4$—$ZrCl_4$ systems.

4.3.1 Materials and Experimental Equipment

Since work on the phase behavior of these salt systems has suffered from the lack of availability of components of adequate purity, considerable attention was devoted to the preparation of suitable starting materials. Aluminum chloride was made[29] from the elements by using high purity analytical-reference aluminum metal; thorium chloride was resublimed from material originally prepared by Dean and Chandler.[30] Commercial $ZrCl_4$ specified as "reactor grade" was resublimed prior to use. Materials were characterized by chemical, thermal, spectrochemical, and x-ray analyses.

Table 33 summarizes the results of chemical analyses. The empirical formulae shown are all slightly below stoichiometric values for chloride. Based on the sharpness and accuracy of melting point determination of the pure substances, the purity of the salts was deemed adequate for the phase studies.

Table 33. Properties of Chloride Salts

	$ThCl_4$	$AlCl_3$	$ZrCl_4$
Melting point °C, observed	760-765	192	436
(Literature)	(770)	(192.4)	(437)
Chemical analyses, wt %			
Cation, observed	61.74	20.31	39.16
(Theor.)	(62.07)	(20.23)	(39.14)
Chloride, observed	36.4	79.60	58.3
(Theor.)	(37.93)	(79.77)	(60.86)
H_2O, observed	0.50	0.27	0.07
Empirical formula	$ThCl_{3.86}(H_2O)_{0.10}$	$AlCl_{2.98}(H_2O)_{0.02}$	$ZrCl_{3.83}(H_2O)_{0.01}$

The hygroscopicity and volatility of the salts required the use of a dry box. All exposed operations were done in an argon atmosphere having a water content in the range 10 to 20 ppm. The chloride mixtures were confined in fused quartz capillaries or welded nickel or Inconel capsules fitted with thermocouple wells. These containers

were designed to withstand the substantial pressures associated with $AlCl_3$ and the corrosive attack of the chloride salts.

Thermal studies were made by heating and cooling the specimens at a predetermined rate of 1 to 2°C/min and observing the time-temperature relationship. In most cases the temperature of a reference capsule identical geometrically to the specimen and similarly filled, but with inert Al_2O_3, was compared with the specimen-capsule temperature. This was done by the sol-called differential thermal analysis (DTA) method. The availability of a semiautomatic DTA apparatus permitted parallel runs and more efficient production of data.

In order to detect and identify subtle phase changes and to confirm evidence of supercooling observed, direct visual studies with quartz capillaries heated in transparent alkali nitrate salt baths were attempted.[31] Uniformity of temperature, ease of observation, and control of experimental conditions were excellent.

4.3.2 Experimental Observations

$AlCl_3$-$ThCl_4$ System. — Observations were made at 10 mole % and at 90 mole % $ThCl_4$, using metal capsules in the temperature range of 100 to 800°C. After several thermal cycles, leaks developed at the upper temperature in each case. Inspection of the capsule showed no visible internal corrosive attack but did indicate defective welding to be the cause of the ruptures. Observations before the leaks are taken as valid. Temperature halts at 190 to 200°C, corresponding to the $AlCl_3$ triple point (reported as 192.6° at 171.5 cm Hg), were observed at both compositions. A rather broad transition was noted between 740 and 770°C (mp of $ThCl_4$ is variously reported between 750 to 770°C). Considerable supercooling was observed for both transition temperatures.

Direct observations of heating and cooling cycles (up to 350°C) were made by sealing various compositions in 1-mm-ID, 3-mm-OD quartz capillary tubes. A range of concentrations including 1, 0.9, 0.75, 0.5, 0.25, 0.10, and 0 mole fraction of $ThCl_4$ in $AlCl_3$ were observed. In the low $ThCl_4$ concentration region, it was visually observed that a phase change occurred at about the triple point of pure $AlCl_3$. No

interaction of the liquid $AlCl_3$ with the $ThCl_4$ was evident during repeated thermal cycling of the mixtures over a period of several days. At high $ThCl_4$ concentrations, similar observations were made but were less conclusive in part because of the masking effect of the presence of relatively large amounts of $ThCl_4$. Russian work, reported by B. G. Korshunov[32] indicates that the mutual solubility of $AlCl_3$ and $ThCl_4$ is low. Our work indicates that the solubility of $ThCl_4$ in $AlCl_3$ will be much below 10 mole %. Techniques other than thermal analysis will be used to determine this solubility.

$AlCl_3$-$ZrCl_4$ System. — A number of compositions in this system have been studied by differential thermal analysis. Transition temperatures, as estimated from differential temperature vs absolute temperature data, are listed in Table 34. The upper and lower temperature halts during heatup are presumed to be liquidus and eutectic temperatures. Corresponding observations during cooldown indicate substantial supercooling of the $AlCl_3$-rich compositions.

A combination of visual observations of several salt mixtures of 5 and 14 mole % $ZrCl_4$ in $AlCl_3$, using 1-mm-ID quartz capillary and thermal analysis, clearly show a transition from liquid to solid on cooling at about 120 to 130°C. By thermal analysis, melting starts at about 160°C, which corresponds to the presumed eutectic melting temperature.

I. S. Morozov and L. Tsegledi reported[33] a eutectic at 17 mole % $ZrCl_4$ for the $AlCl_3$-$ZrCl_4$ system at 116°C, another transition at about 127°C, and indicate the presence of two liquid phases at intermediate compositions above 127°C. None of these were observed in this study. The transition at 127°C observed by the Russian workers may be related to our observation of supercooling at the $AlCl_3$-rich end of the composition range.

From our observations indicated above, we find no present necessity of inferring any phenomena other than a eutectic in the 5 to 14 mole % $ZrCl_4$ region, at about 160°C. An effort will be made to locate this more precisely.

$ThCl_4$-$ZrCl_4$.— Observations of temperature halts for compositions 0.0, 0.25, 0.5, 0.75, 1.0 mole fraction of $ZrCl_4$ in $ThCl_4$ up to a temperature of 550°C show only a single differential temperature peak. This corresponded closely to the melting point of the pure $ZrCl_4$. Although study of the properties of ternary mixtures of these salts would be required to completely investigate the possibilities of $ZrCl_4$ for acting as a "bridging solvent", the evidence developed so far for the $ThCl_4$-$ZrCl_4$ system indicates little mutual solubility. A few further measurements are planned in the ternary system.

Table 34. Summary of $AlCl_3$-$ZrCl_4$ Thermal-Analysis Data

Composition (Mole %[a] $ZrCl_4$ in $AlCl_3$-$ZrCl_4$ Mixture)	Temperature Halts (°C)			
	Heatup		Cooldown	
	Liquidus	Eutectic	Liquidus	Eutectic
0	192	-	170	-
0	192	-	172	-
5	-	176	-	136
5	-	166	-	139
5	195[b]	166	-	132
5	185[c]	157	-	126
14	194	161	-	125
14	192	161	-	123
14	189	158	-	128
33	-[c]	182	314[d]	144
50	-[c]	167	366	143
50	372	161	366	140
50	372	162	367	145
67	402	162	397	146
67	399	161	397	142
67	398	162	394	143
100	436[e]	-	438[e]	

[a] As $AlCl_3$ monomer.

[b] Supercooling clearly indicated in several cases in this column.

[c] Very vague liquidus.

[d] Capsule leaked.

[e] Run using thermal curves, non-DTA from precision potentiometer with well defined sharp temperature halt.

APPENDIX

Table A1. Summary of Sol-Gel Operating and Control Data for Campaign 1

Over-all campaign ratio: $\frac{^{233}U}{^{233}U + Th} = \frac{3.196}{3.196 + 104.693} = \frac{3.196}{107.889} = 0.0296 = 2.96\%$

Campaign No.	BNL Carrier Shipment No.	Sol-Gel Run No.	$\frac{^{233}U^{a}}{^{233}U + Th}$ Ratio	Uranium-233		Thorium Charged		Product Prepared: $UO_2 + ThO_2$ (kg)
				SX[b] Batch No.	Quantity Processed (kg)	As Denitrator Product: ThO_2 (kg)	As Thorium Metal (kg)	
1	1	1	2.92	HJ-1	0.2615	10.010	8.629	9.025
1	1	2	3.02	HJ-1	0.2615	10.010	8.629	9.975
1	1	3	2.99	HJ-1	0.2612	10.010	8.619	9.700
1	1	4	3.04	HJ-1	0.2616	10.010	8.623	9.195
1	1	5	2.91	HJ-1	0.2721	10.510	9.026	10.275
1	1	6	2.94	HJ-1	0.2736	10.479	9.026	10.155
1	1	7	2.95	HJ-1	0.2736	10.479	9.026	10.580
1	1	8	2.92	HJ-1	0.2613	10.010	8.623	9.837
1	1	9	3.00	HJ-1	0.2669	10.010	8.623	9.920
1	1	10	3.12	HJ-1	0.2694	10.010	8.623	10.036
1	1	11	2.92	HJ-1	0.2667	10.010	8.623	9.850
1	1	12	2.92	HJ-1	0.2667	10.010	8.623	10.064
				TOTALS	3.196	121.558	104.693	118.562

[a]Ratio specification: $\frac{100\ ^{233}U}{^{233}U + Th} = 3.00 \pm 0.05$; however, product falling within the 2.90 to 3.10 ratio may be blended to obtain the desired ratio.

[b]SX = solvent extraction.

Table A2. Summary of Sol-Gel Operating and Control Data for Campaign 2

Over-all campaign ratio: $\frac{^{233}U}{^{233}U + Th} = \frac{4.255}{4.255 + 137.162} = 0.03008 = 3.01\%$

Campaign No.	BNL Carrier Shipment No.	Sol-Gel Run No.	$\frac{^{233}U}{^{233}U + Th}$ Ratio	Uranium-233 SX Batch No.	Uranium-233 Quantity Processed (kg)	Thorium Charged As Denitrator Product: ThO_2 (kg)	Thorium Charged As Thorium Metal (kg)	Product Prepared: $UO_2 + ThO_2$ (kg)
2	1	13	2.98	HJ-2	0.265	10.003	8.573	8.816
2	1	14	3.02	HJ-2	0.267	10.003	8.573	9.922
2	1	15	3.03	HJ-2	0.267	10.014	8.582	9.242
2	1	16	3.03	HJ-2	0.267	10.003	8.573	11.028
2	1	17	3.01	HJ-2	0.267	10.014	8.582	10.178
2	1	18	3.03	HJ-2	0.270	10.003	8.573	10.376
2	2	19	3.08	HJ-2	0.270	10.003	8.573	9.895
2	2	20	3.07	HJ-2	0.270	10.003	8.573	10.149
2	2	21	3.00	HJ-2	0.262	10.003	8.573	10.517
2	2	22	2.94	HJ-2	0.260	10.003	8.573	10.348
2	2	23	2.99	HJ-2	0.265	10.003	8.569	10.150
2	2	24	3.01	HJ-2	0.265	10.003	8.569	10.007
2	2	25	3.04	HJ-2	0.265	10.003	8.569	9.979
2	2	26	3.03	HJ-2	0.265	10.003	8.569	10.008
2	2	27	3.02	HJ-2	0.265	10.003	8.569	10.262
2	2	28	3.03	HJ-2	0.265	10.003	8.569	10.063
				TOTALS	4.255	160.070	137.162	160.940

Table A3. Summary of Sol-Gel Operating and Control Data for Campaign 3

Over-all campaign ratio: $\frac{^{233}U}{^{233}U + Th} = \frac{3.166}{3.166 + 102.468} = 0.02997 = 3.00\%$

Campaign No.	BNL Carrier Shipment No.	Sol-Gel Run No.	$\frac{^{233}U}{^{233}U + Th}$ Ratio	Uranium-233 SX Batch No.	Uranium-233 Quantity Processed (kg)	Thorium Charged As Denitrator Product: ThO_2 (kg)	Thorium Charged As Thorium Metal (kg)	Product Prepared: $UO_2 + ThO_2$ (kg)
3	2	29	3.00	HJ-2	0.265	10.008	8.573	9.215
3	3	30	3.06	HJ-3	0.265	10.008	8.573	9.798
3	3	31	3.02	HJ-3	0.265	10.008	8.558	9.830
3	3	32	2.95	HJ-3	0.259	10.008	8.528	9.995
3	3	33	3.01	HJ-3	0.264	10.023	8.540	10.050
3	3	34	2.99	HJ-3	0.264	10.008	8.528	9.985
3	3	35	3.00	HJ-3	0.264	10.008	8.528	9.970
3	3	36	3.01	HJ-3	0.264	10.008	8.528	10.075
3	3	37	2.96	HJ-3	0.264	10.008	8.528	9.810
3	3	38	2.98	HJ-3	0.264	10.008	8.528	9.960
3	3	39	3.06	HJ-3	0.264	10.008	8.528	10.095
3	4	40	3.00	HJ-3	0.264	10.008	8.528	9.685
			TOTALS		3.166	120.111	102.468	118.468[a]

[a] 7.115 kg of material from SGO-1,5,8,10,12 dumped with this oxide. Already accounted for in Campaign 1, not included in total.

Table A4. Summary of Sol-Gel Operating and Control Data for Campaign 4

Over-all campaign ratio: $\frac{^{233}U}{^{233}U + Th} = \frac{3.450}{3.450 + 110.724} = 0.03021 = 3.02\%$

Campaign No.	BNL Carrier Shipment No.	Sol-Gel Run No.	$\frac{^{233}U}{^{233}U + Th}$ Ratio	Uranium-233 SX Batch No.	Uranium-233 Quantity Processed (kg)	Thorium As Denitrator Product: ThO_2 (kg)	Thorium As Thorium Metal (kg)	Product Prepared: $UO_2 + ThO_2$ (kg)
4	4	41	2.94	DC-1	0.262	10.006	8.484	9.370
4	4	42	3.01	DC-1	0.267	10.006	8.484	9.825
4	4	43	3.02	DC-1	0.267	10.006	8.484	10.185
4	4	44	2.98	DC-1	0.265	10.006	8.484	9.935
4	4	45	3.01	DC-1	0.266	10.006	8.484	9.895
4	4	46	2.95	DC-1	0.265	10.006	8.484	9.900
4	4	47	3.01	DC-1	0.266	9.966	8.450	10.015
4	4	48	2.96	DC-1	0.266	10.006	8.598	9.955
4	4	49	3.05	DC-1	0.266	10.006	8.598	9.965
4	4	50	2.99	DC-1	0.269	10.006	8.598	10.040
4	5	51	3.02	DC-1	0.266	10.006	8.598	9.880
4	5	52	2.98	DC-1	0.266	10.006	8.598	9.720[a]
4	4	53	3.07	DC-1	0.259	9.752	8.380	10.055
				TOTALS	3.450	129.784	110.724	128.740

[a] 1.455 kg unused analytical samples were added to this batch. Not included in total.

Table A5. Summary of Sol-Gel Operating and Control Data for Campaign 5

Over-all campaign ratio: $\frac{^{233}U}{^{233}U + Th} = \frac{6.056}{6.056 + 195.530} = 0.0300 = 3.00\%$

Campaign No.	BNL Carrier Shipment No.	Sol-Gel Run No.	$\frac{^{233}U}{^{233}U + Th}$ Ratio	Uranium-233 SX Batch No.	Uranium-233 Quantity Processed (kg)	Thorium As Denitrator Product: ThO_2 (kg)	Thorium As Thorium Metal (kg)	Product Prepared: $UO_2 + ThO_2$ (kg)
5	5	54	3.02	DC-3	0.266	10.002	8.595	9.150
5	5	55	2.95	DC-3	0.258	9.774	8.343	9.780
5	5	56	2.96	DC-3	0.258	9.774	8.343	9.975
5	5	57	2.99	DC-3	0.258	9.776	8.343	9.675
5	5	58	3.00	DC-4	0.264	9.999	8.534	10.060
5	5	59	3.01	DC-4	0.264	10.000	8.534	9.905
5	5	60	2.99	DC-4	0.266	10.000	8.534	9.845
5	5	61	3.01	DC-4	0.261	9.900	8.449	9.765
5	5	62	2.91	DC-4	0.264	10.000	8.534	9.925
5	5	63	2.96	DC-4	0.262	10.000	8.463	9.995
5	6	64	2.97	DC-4	0.262	10.000	8.463	9.810
5	6	65	3.00	DC-4	0.264	10.000	8.463	9.840
5	6	66	3.00	DC-4	0.264	10.000	8.463	10.030
5	6	67	2.96	DC-4	0.262	10.000	8.463	9.920
5	6	68	3.00	DC-4	0.264	10.000	8.463	9.720
5	6	69	3.01	DC-4	0.262	9.950	8.421	10.030
5	6	70	3.00	DC-4	0.266	10.000	8.595	9.825
5	6	71	3.05	DC-4	0.266	10.000	8.595	9.990
5	6	72	3.02	DC-4	0.266	10.000	8.595	10.025
5	6	73	3.04	DC-4	0.266	10.000	8.595	9.850
5	6	74	2.99	DC-4	0.264	10.000	8.595	9.900
5	6	75	3.04	DC-4	0.264	10.000	8.595	9.905
5	6	76	3.00	DC-4	0.265	9.950	8.552	9.925
				TOTALS	6.056	229.125	195.530	226.845

REFERENCES

1. Status and Progress Report for Thorium Fuel Cycle Development for Period Ending December 31, 1962, compiled by D. E. Ferguson, ORNL-3385, pp 73-89.

2. J. D. Sease, A. L. Lotts, and F. C. Davis, "New Remote Facility and Equipment at the Oak Ridge National Laboratory for Fabrication of Fuel Rods Bearing ^{233}U and Thorium Oxide," Proceedings of the 11th Conference on Hot Laboratories and Equipment, ANS Winter Meeting, Nov. 18-21, 1963, New York.

3. J. D. Sease, A. L. Lotts, and F. C. Davis, Thorium-^{233}U Oxide (Kilorod) Facility - Rod Fabrication Process and Equipment, ORNL-3539 (in press).

4. J. E. Van Cleve and A. L. Lotts, "Operation of a Lightly Shielded Facility at the Oak Ridge National Laboratory for Fabrication of Fuel Rods Bearing ^{233}U and Thorium Oxide," paper presented at the Powder Filled UO_2 Symposium, Worcester, Mass., Nov. 5, 1963 (to be published in Proceedings).

5. A. R. Irvine and A. L. Lotts, Criteria for the Design of the Thorium Fuel Cycle Development Facility, ORNL TM-149 (Mar. 2, 1962).

6. A. R. Irvine and A. L. Lotts, "The Thorium Fuel Cycle Development Facility Conceptual Design," Proceedings of the Thorium Fuel Cycle Symposium, Gatlinburg, Tennessee, December 5-7, 1962, TID-7650, Book 1, pp 330-350.

7. O. C. Dean et al., "The Sol-Gel Process for Thoria Base Fuels," Proceedings of the Thorium Fuel Cycle Symposium, TID-7650, pp 519-42.

8. D. E. Ferguson et al., Preparation and Fabrication of Thoria Fuels, ORNL-3225 (June 5, 1962).

9. W. Ernst, personal communication, Jan. 1964.

10. Status and Progress Report for Thorium Fuel Cycle Development for Period Ending December 31, 1962, compiled by D. E. Ferguson, ORNL-3385, p 9 et seq.

11. A. D. Merrington and E. G. Richardson, "The Breakup of Liquid Jets," Proc. of Physical Soc. (London) 59, 1-13 (1947).

12. Status and Progress Report for Thorium Fuel Cycle Development for Period Ending December 31, 1962, compiled by D. E. Ferguson, ORNL-3385, pp 102-128.

13. J. Belle, Uranium Dioxide, Properties and Nuclear Applications, p 638, Naval Reactors, Division of Reactor Development, USAEC.

14. J. R. MacEwan and V. B. Lawson, J. Am. Ceram. Soc. 45 (1), pp 42-46 (Jan. 1962).

15. R. H. Cole and L. G. Wilkinson, Development of High-Strength Ternary and Quaternary Thorium-Uranium-Base Alloys Final Report, ATL-A-128 (Nov. 1, 1961).

16. Report on Civilian Reactor Fuel Elements, TID-8505, p 4.3.6 (June 1959).

17. A. E. Scheidegger, The Physics of Flow Through Porous Media, p 191, MacMillan, New York, 1960.

18. F. C. Carman, Flow of Gases Through Porous Media, p 88, Butterworths, London, 1956.

19. Status and Progress Report for Thorium Fuel Cycle Development for Period Ending December 31, 1962, compiled by D. E. Ferguson, ORNL-3385, p 136.

20. R. H. Cole and L. G. Wilkinson, Development of High-Strength Ternary and Quaternary Thorium-Uranium-Base Alloys Final Report, ATL-A-128, p 138.

21. Status and Progress Report for Thorium Fuel Cycle Development for Period Ending December 31, 1962, compiled by D. E. Ferguson, ORNL-3385, p 6 et seq.

22. C. W. Swertzer, L. J. Venuto, and R. R. Estelow, Colloidal Carbon, Its Properties and Uses, Columbian Carbon Co., New York, Vol. XI (3). Reprinted from Paint, Oil, and Chemical Review 115 (8), (April 1952).

23. Cabot Corporation, Data Sheet.

24. V. A. Garten and D. E. Weiss, "The Ion- and Electron-Exchange Properties of Activated Carbon in Relation to its Behavior as a Catalyst and Adsorbant," Reviews of Pure and Applied Chemistry 7, 69-122 (1957).

25. J. Biscoe and B. E. Warren, "An X-ray Study of Carbon Black," J. of Applied Phys. 13, 364-71 (June 1942).

26. Status and Progress Report for Thorium Fuel Cycle Development for Period Ending December 31, 1962, compiled by D. E. Ferguson, ORNL-3385, p 36.

27. M. J. Bradley and L. M. Ferris, "Hydrolysis Between 25 and 100°C of Thorium Monocarbide Thorium Dicarbide and Mixtures of the Carbides," (to be published in Jour. Inorg. and Nuclear Chem.).

28. J. G. Malm and S. Fried, "Separation of Protactinium from Contaminants," U.S. Patent 2,893,825, July 7, 1959; USAEC application, April 11, 1951.

29. Work performed by D. E. Lavalle and R. B. Quincy, Jr., Inorganic Preparation Group, ORNL Analytical Chemistry Division.

30. O. C. Dean and J. M. Chandler, "The Preparation of Anhydrous $ThCl_4$," Nuclear Sci. and Eng. 2, 57-72 (1957).

31. C. J. Barton, G. M. Hebert, and W. L. Marshall, "Aqueous Systems at High Temperature," Jour. Inorg. and Nuclear Chem. 21, 141-151 (1961).

32. B. G. Korshunov et al., "Investigation of the Interaction of Thorium Chloride with Chlorides of Magnesium, Calcium, Cerium, Aluminum, Iron, Niobium and Tantalum and with Niobium Oxychloride upon Fusion," Izvest. Vyshikh. Ucheb. Zavedenii, Tsvetnaya Met. (6), 114-118 (1960). (Also CA 55: 18519g).

33. I. S. Morozov and L. Tsegledi, "Thermal and Tensimetric Study of the Systems $ZrCl_4$-$AlCl_3$-KCl and $ZrCl_4$-$FeCl_3$-KCl," Zh. Neorgan. Khim. 6, 2766-75 (1961). See also N. K. Druzhinina, "Thermal and Tensimetric Study of the Systems $ZrCl_4$-$AlCl_3$-NaCl," Tr. Vses. Nauchii - Issled. Alyumin-Magnievyi Inst. 1963 (50), 143-6; (als0 CA 59: 9382h).

ORNL-3611
UC-25 – Metals, Ceramics, and Materials
TID-4500 (41st ed.)

INTERNAL DISTRIBUTION

1. Biology Library
2-4. Central Research Library
5. Reactor Division Library
6-7. ORNL – Y-12 Technical Library
Document Reference Section
8-27. Laboratory Records Department
28. Laboratory Records, ORNL R.C.
29. J. W. Anderson
30. S. E. Beall
31. R. E. Blanco
32. A. L. Boch
33. W. D. Bond
34. G. E. Boyd
35. R. E. Brooksbank
36. K. B. Brown
37. F. R. Bruce
38. W. D. Burch
39. J. A. Burka
40. J. M. Chandler
41. S. D. Clinton
42. E. L. Compere
43. F. L. Culler
44. J. E. Cunningham
45. H. P. Danforth
46. F. C. Davis
47. D. A. Douglas, Jr.
48. W. S. Ernst, Jr.
49. D. E. Ferguson
50. L. M. Ferris
51. R. B. Fitts
52. H. A. Friedman
53. J. H Frye, Jr.
54. T. A. Gens
55. H. E. Goeller
56. A. T. Gresky
57. J. C. Griess
58. W. R. Grimes
59. P. A. Haas
60. W. O. Harms
61. C. C. Haws
62. M. R. Hill
63. F. J. Hurst
64. A. R. Irvine
65. M. T. Kelley
66. M. J. Kelly
67. A. T. Kleinsteuber
68. C. E. Larson
69. R. E. Leuze
70. A. L. Lotts
71. H. G. MacPherson
72. J. L. Matherne
73. J. P. McBride
74. K. H. McCorkle
75. H. F. McDuffie
76. J. R. McWherter
77. A. B. Meservey
78. F. W. Miles
79. E. C. Miller
80. C. S. Morgan
81. E. L. Nicholson
82. A. R. Olson
83. F. L. Peishel
84. J. T. Roberts
85. M. W. Rosenthal
86. J. L. Scott
87. H. E. Seagren
88. J. D. Sease
89. R. J. Shannon
90. W. A. Shannon
91. A. J. Shor
92. M. J. Skinner
93. J. W. Snider
94. A. J. Taylor
95. D. B. Trauger
96. J. W. Ullmann
97. J. E. Van Cleve, Jr.
98. J. T. Venard
99. A. M. Weinberg

100. W. J. Werner
101. M. E. Whatley
102. R. G. Wymer
103. G. Young
104. P. H. Emmett (consultant)
105. J. J. Katz (consultant)
106. C. W. J. Wende (consultant)
107. C. E. Winters (consultant)
108. M. B. Bever (consultant)
109. A. A. Burr (consultant)
110. J. R. Johnson (consultant)
111. A. R. Kaufmann (consultant)

EXTERNAL DISTRIBUTION

112. W. J. Larkin, USAEC, ORO
113. R. E. Pahler, USAEC, Washington, D.C.
114. Research and Development Division, AEC, ORO

115-662. Given distribution as shown in TID-4500 (41st ed.) under Metals, Ceramics, and Materials category (75 copies – CFSTI)